ELUCIDATING THE ROLE OF POLYBROMO-1 IN TARGETING THE PBAF COMPLEX UNDER STRESS

by

Elizabeth Grace Porter

Dissertation

Submitted to the Faculty of Purdue University

In Partial Fulfillment of the Requirements for the degree of

Doctor of Philosophy

Department of Medicinal Chemistry and Molecular Pharmacology

West Lafayette, Indiana

May 2019

THE PURDUE UNIVERSITY GRADUATE SCHOOL
STATEMENT OF COMMITTEE APPROVAL

Dr. Emily C. Dykhuizen, Chair
Department of Medicinal Chemistry and Molecular Pharmacology
Dr. Stephen F. Konieczny
Department of Biology
Dr. Joseph Ogas
Department of Biochemistry
Dr. Vikki M. Weake
Department of Biochemistry

Approved by:
Dr. Andy Hudmon
Head of the Graduate Program

Dedication

To Adam Bonner and Mrs. D'Amico

ACKNOWLEDGMENTS

I would first like to thank my PhD advisor, Dr. Emily Dykhuizen. Thank you for taking me into your lab and for your constant encouragement and mentoring, as well as for all the pep talks over the years. You've been an amazing mentor and advisor and I aspire to be like you one day. I would also like to thank my thesis committee, Dr. Stephen Konieczny, Dr. Joe Ogas, and Dr. Vikki Weake. I appreciate the productive conversations and for continually challenging me.

Thank you to the Dykhuizen lab. I am so grateful to have been surrounded by amazing colleagues whom I can also call my friends. I can't wait to see where the future takes you all. A special thanks to Dr. Katelyn Connelly. I can't imagine going through graduate school without you. Thank you for being one of my best friends and always being there through the ups and downs of every aspect of my life. I'm looking forward to being lifelong friends and collaborating in the future. I would also like to share my gratitude for Dr. Alisha Dhiman and the soon-to-be Dr. Aktan Alpsoy. I highly value both your scientific insight and friendship.

I would not have been able to make it through graduate school without the love and support of my family. Thank you to my parents, Scott and Drue Porter, for supporting me and teaching me to always strive for excellence. I am also grateful for my siblings Scott, Maggie, Katie, Joe, David, and Emily. I wouldn't have grown up any other way. I can't express how meaningful it was to have you all at my defense.

Thank you to all my Lafayette friends. I am so blessed to have so many close friends that were constantly there to remind me to get out of the lab and enjoy life. I would especially like to mention Lizzie, Elizabeth, Maria, Emily, Jenna, and Anna.

Finally, thank you to the love of my life, best friend, biggest supporter, and fiancé, John Hausman. Thank you for being my partner and believing in me and always encouraging me to follow my dreams.

Thank you to my funding sources: The Borch Endowment Graduate Fellowship and the Bilsland Dissertation Fellowship.

TABLE OF CONTENTS

TABLE OF CONTENTS 6

LIST OF FIGURES 12

ABSTRACT 14

CHAPTER 1. INTRODUCTION 16

1.1 Introduction 16

1.2 BAF in Cancer 18

1.3 SWI/SNF 18

1.4 Composition of Human BAF 19

1.5 PBRM1 domains 20

1.6 Distinct functions of BAF and PBAF 21

1.7 PBRM1 in DNA damage response 22

1.8 PBRM1 in renal clear cell carcinoma 22

1.9 PBAF in immune therapy response 23

1.10 Conclusion 24

CHAPTER 2. PBRM1 REGULATES THE EXPRESSION OF GENES INVOLVED IN METABOLISM AND CELL ADHESION IN RENAL CLEAR CELL CARCINOMA 25

2.1 Introduction 25

2.2 Materials and Methods 26

2.2.1 Cell culture 26

2.2.2 Constructs 26

2.2.3 Lentiviral Infection 27

2.2.4 Sulforhodamine B assays 27

2.2.5 RNA isolation 27

2.2.6 Library Construction and Sequencing 27

2.2.7 Transcriptome Analysis 28
2.2.8 Real-time polymerase chain reaction (RT-PCR) 28
2.2.9 Immunoblot Analysis 29
2.2.10 Cell cycle distribution assays 29
2.2.11 Apoptotic assay 30
2.2.12 Exposure to Hypoxia 30
2.2.13 Glucose Uptake Assay 30
2.2.14 Imaging of actin cytoskeleton 30
2.2.15 *In vitro* Scratch Test 31
2.2.16 Cholesteryl ester (CE) fingerprinting by mass spectrometry 31
2.3 Results & Discussion 32
2.3.1 PBRM1 expression in RCCs 32
2.3.2 Generation of Isogenic cell lines for controlled studies of PBRM1 function. 32
2.3.3 Effect of PBRM1 expression on cell proliferation 35
2.3.4 Differentially expressed genes upon PBRM1 re-expression in Caki-2 35
2.3.5 PBRM1 in cell cycle and apoptosis 39
2.3.6 PBRM1 in hypoxia 39
2.3.1 PBRM1 in glycolysis and cholesterol homeostasis 41
2.3.2 PBRM1 in cell adhesion 43
2.3.3 Differentially expressed genes in PBRM1 mutant tumors derived from patient samples 45
2.4 Conclusion 45
CHAPTER 3. POLYBROMO-1 CONTRIBUTE TO CHROMATIN ASSOCIATION AND TUMOR SUPPRESSION IN CLEAR CELL RENAL CARCINOMA 48
3.1 Introduction 48
3.2 Materials and Methods 50
3.2.1 Recombinant Protein Expression 50
3.2.2 Thermal Shift Assay 51
3.2.3 Cell Culture 51
3.2.4 Constructs for Mammalian Cell Culture – 51

3.2.5 Lentiviral Infection 52
3.2.6 Sequential Salt Extractions – 52
3.2.7 Growth Curves 53
3.2.8 Peptide Pull Down 53
3.2.9 Real-time polymerase chain reaction (RT-PCR) 53
3.2.10 Chromatin Immunoprecipitation (ChIP) 54
3.2.11 ChIP Primers 54
3.2.12 Immunoblot 55
3.2.13 Antibodies 55
3.3 Results 57
3.3.1 The Contribution of Individual Bromodomains to the Tumor Suppressor Function of PBRM1 57
3.3.2 The Effect of PBRM1 on the Affinity of PBAF to Bulk Chromatin 60
3.3.3 The Contribution of Individual Bromodomains to the Affinity of PBAF to Bulk Chromatin - 61
3.3.4 PBRM1 Binding to Acetylated Histone Peptides 63
3.3.5 The Role for Individual Bromodomains in PBRM1 Localization to a Discrete Genomic Site 64
3.4 Discussion 65
CHAPTER 4. SEQUENTIAL SALT EXTRACTIONS FOR THE ANALYSIS OF BULK CHROMATIN BINDING PROPERTIES OF CHROMATIN MODIFYING COMPLEXES 71
4.1 Introduction: 71
4.2 Protocol: 73
4.2.1 Preparation 73
4.2.2 Salt Extraction 73
4.2.3 Sequential Salt Extraction in the Presence of a "Reader" Inhibitor 75
4.2.4 Sequential Salt Extraction in the Presence of a "Writer" Inhibitor 75
4.2.5 Sequential Salt Extraction Following DNA Damage 75
4.2.6 Non-Sequential Salt Extraction 75

4.3 Representative Results 76
4.4 Discussion 82
CHAPTER 5. PBRM1 REGULATES STRESS RESPONSE IN EPITHELIAL CELLS 85
5.1 Introduction 85
5.2 Materials and Methods 87
5.2.1 Cell culture 87
5.2.2 Cell culture and treatments 88
5.2.3 Generation of cell lines 88
5.2.4 Lentiviral Infection 89
5.2.5 3D culture 89
5.2.6 Immunofluorescence staining 90
5.2.7 Confocal microscopy 90
5.2.8 TopFlash Reporter Assay 90
5.2.9 Annevin V Apoptosis detection in NMuMG cells 91
5.2.10 Immunoblotting 91
5.2.11 Antibodies 91
5.2.12 Migration assay 92
5.2.13 H_2-DCFDA staining for intracellular ROS using flow cytometry 92
5.2.14 Stress treatments and H_2-DCFDA staining using microplate reader 92
5.2.15 H_2O_2 detection assay 92
5.2.16 Viability assays using CellTiter-Glo® 93
5.2.17 LDH assays using LDH Cytotoxicity Assay Kit II (Abcam, ab65393) 93
5.2.18 H_2-DCFDA staining for MCF10A and MCF10A-T1K followed by flow cytometry 93
5.2.19 RNA-seq 93
5.2.20 ATAC-seq 94
5.2.21 qRT-PCR 94
5.2.22 TCGA analysis 95
5.3 Results 95

5.3.1 Knockdown of PBRM1 in normal epithelium promotes growth and a loss of epithelial cell maintenance 95
5.3.2 PBRM1 regulates genes involved in cell adhesion, signaling, stress response, and apoptosis. 96
5.3.3 PBRM1 is predicted to cooperate with transcription factors involved in response to stress. 102
5.3.4 Knockdown of PBRM1 results in elevated ROS under cellular stress conditions. 103
5.3.5 PBRM1 expression is cytoprotective under high stress conditions 106
5.3.6 PBRM1-regulated transcriptional effects under cellular stress conditions 108
5.3.7 PBRM1 has cell-type specific roles on viability: 111
5.3.8 PBRM1 displays stress response phenotype in renal cancer cells: 114
5.4 Discussion 116
CHAPTER 6. FUTURE DIRECTIONS 118
6.1 Introduction 118
6.2 PBRM1-regulated transcriptional effects are amplified under stress 119
6.3 PBRM1 regulates FOXO target genes in a stress dependent manner 125
6.4 PBRM1 regulates ROS levels in cancer 125
6.5 PBRM1 binds to H3K14/18Ac *in vitro* 126
6.6 Proposed mechanism of PBRM1 regulation of stress response genes 127
6.7 Future directions 130
6.8 Conclusions 131
APPENDIX A. SUPPLEMENTAL MATERIAL FOR CHAPTER 2 132
APPENDIX B. SUPPLEMENTAL MATERIAL CHAPTER 5 137
REFERENCES 144
PUBLICATIONS 158

LIST OF TABLES

Table 1.1: Summary of the results from three peptide screens with recombinant BDs[22,24,25]. 21

LIST OF FIGURES

Figure 1-1: BAF is mutated in 20% of cancers. Mutations in a particular subunit often occur in a cancer specific manner. 18
Figure 2-1 Characterization of PBRM1 in ccRCC cells 34
Figure 2-2 Presence of PBRM1 resulted in decreased proliferation rate of ccRCC cells 36
Figure 2-3 Summary of differentially expressed genes in Caki2 cells upon PBRM1 re-expression 37
Figure 2-4 Downregulation of genes involved in cell proliferation upon PBRM1 re-expression 40
Figure 2-5 Alteration of metabolism upon PBRM1 re-expression 42
Figure 2-6 Alteration of cell-cell adhesion upon PBRM1 re-expression 44
Figure 2-7 Comparative analysis of genes with differential expression in the presence of PBRM1 between ccRCC cells and ccRCC TCGA biospecimen 47
Figure 3-1 The BAF and PBAF complexes coexist in all cell types. 50
Figure 3-2 Missense mutations in PBRM1 identified from ccRCC patient samples indicated with black bars. Data obtained from the COSMIC database[55]. 56
Figure 3-3 Proliferation and gene expression is altered in PBRM1 BD mutant cell lines 58
Figure 3-4 Chromatin binding properties of BAF and PBAF complexes. 62
Figure 3-5 Chromatin binding properties are altered in PBRM1 BD mutants. 64
Figure 3-6 PBRM1 binding to acetylated histone peptides. 67
Figure 3-7 Quantitative chromatin immunoprecipitation (ChIP) in Caki2 cells 68
Figure 3-8 Proposed models for PBRM1 recognition of histone marks. 69
Figure 4-1 Non-sequential compared to sequential salt extractions in OVCA429 cells 78
Figure 4-2 Comparison of incubation times of PBAF and PRC1 elution profiles 79
Figure 4-3 Effectiveness of (+) JQ1 on inhibiting BRD4 binding 80
Figure 4-4 Alterations in binding when chromatin landscaped is modified 81
Figure 4-5 Changes in PBRM1 binding after DNA Damage 82
Figure 5-1 Knockdown of PBRM1 in normal epithelium promotes growth and a loss of epithelial cell maintenance. 98

Figure 5-2 PBRM1 regulates genes involved in cell adhesion, signaling, stress response, and apoptosis and is predicted to cooperate with transcription factors involved in response to stress. 100
Figure 5-3 Knockdown of PBRM1 results in elevated ROS under cellular stress conditions. .. 105
Figure 5-4 PBRM1 expression is cytoprotective under high stress conditions. 107
Figure 5-5 PBRM1-regulated transcriptional effects under cellular stress conditions 109
Figure 5-6 PBRM1 has cell-type specific roles on viability. 112
Figure 5-7 PBRM1 displays stress response phenotype in renal cancer cells. 115
Figure 6-1 Shared gene ontology and predicted transcription factor binding 121
Figure 6-2 PBRM1 transcriptional regulation is amplified under conditions of cellular stress. 123
Figure 6-3 Regulation of FOXO4 targets by PBRM1 126
Figure 6-4 Peptide pull down assay with nuclear lysate from human cell lines 128
Figure 6-5 ER Stress response 129

ABSTRACT

Author: Porter, Elizabeth, G. PhD
Institution: Purdue University
Degree Received: May 2019
Title: Elucidating the Role of Polybromo-1 in Targeting the PBAF Complex Under Stress.
Committee Chair: Emily Dykhuizen

DNA organization is an intricate and dynamic process. The approximately two meters of DNA in a single cell is wrapped around small proteins called histones. Histones can be compacted into dense coils or loosely distributed along DNA, allowing for cells to control gene expression. This combination of DNA and histones forms chromatin. This work has focused on understanding the role of Polybromo1 (PBRM1), which is a member of a chromatin remodeling complex. PBRM1 is mutated in 3% of all human cancers and is mutated in 40% of renal clear cell carcinomas (ccRCC), the most common type of kidney cancer. Through my work characterizing PBRM1 as a tumor suppressor, we have found PBRM1 acts as a stress sensor. PBRM1 is a member of the Polybromo1 BRG1 associating factors (PBAF) complex which is a subtype of the larger BAF family of chromatin remodelers. Although BAF is essential for cell viability, knockdown of PBRM1 shows minor phenotypic changes in many cell types under standard cell culturing conditions. However, when cells without PBRM1 experience external stress, the reactive oxygen species levels in the cells are elevated and remain high compared to cells with wild type PBRM1. Depending on the cellular environment of the cell, increase in ROS can be growth promoting or growth inhibiting. PBRM1 is a structurally unique protein, containing two bromo-adjacent homologs, a high mobility group and six tandem bromodomains. Due to the multiple reader domains, it is likely PBRM1 acts to target the complex. Taking advantage of a RCCC cell line not expressing PBRM1, we re-expressed full length PBRM1 containing an asparagine to alanine mutation in each bromodomain, disrupting the acetyl-lysine binding. We have found that the bromodomains are cooperative and are facilitating binding of PBAF to chromatin. We found defects in PBRM1's ability to suppress growth, bind to chromatin, and regulate gene expression when any of the bromodomains were mutated besides the third bromodomain. These results correlated with patient data. Using acetylated histone peptides, we have identified potential combinations of marks that PBRM1 prefers over single marks. Further work needs to be done to

characterize how these histone modifications are altered under stress and they contribute to the role of PBRM1 in stress response.

CHAPTER 1. INTRODUCTION

1.1 Introduction

The human genome is intricately organized and dynamically regulated. The Human Genome Project revealed that though the human genome is significantly larger than lower organisms like yeast and drosophila, this increase in size was not reflected by the number of genes it encoded. In fact, the ~20,000 know genes only account for approximately 5% of the genome[1]. The non-coding regions contain structural elements like centromeres and telomeres, that allow for kinetochore formation during mitosis or repetitive sequences that protect the encoded regions during replication. Other regions, such as enhancers, facilitate the transcription of distal regions. When cells are not going through mitosis, 3D organization of DNA is critical for regulating gene expression and establishing lineage specific transcriptional profiles. This is accomplished by chromatin, which is composed of proteins know as histones and DNA. Histones form octamers containing two copies of H2A, H2B, H3, and H4, wrapped twice by approximately 147 base pairs of DNA[2]. There are two major forms of chromatin: euchromatin and heterochromatin. Euchromatin contains actively transcribed and cell cycle-dependent genes[3]. Nucleosomes, in this region can be loosely distributed to allow for the transcriptional machinery access to the DNA or for cell cycle dependent genes, nucleosomes can be deposited or removed providing temporal regulation of gene expression. Heterochromatin, on the other hand, is densely packed regions of the genome[3]. In stem cells, genes expression patterns are not solidified, allowing for multiple progenitor lineages. As cells differentiate the pattern of gene expression becomes more established. Inactive genes are strongly repressed by closely packed nucleosomes, obstructing access of transcriptional machinery and transcription factors. Heterochromatin also keeps noncoding regions compacted, preventing damage[3]. Nucleosomes not only give DNA 3D structure but act as a platform for epigenetic modifications that denote types of chromatin and signal for reorganization.

Epigenetics is the change in gene expression without altering the underlying DNA sequence. Two epigenetic mechanisms, DNA methylation and modifications of histones, act as a code to dictate chromatin structure[4]. Histones have unstructured tails that protrude from the core of the nucleosome and can be post-translationally modified[2]. These modifications include but are not limited to acetylation, methylation, phosphorylation, and ubiquitination[3]. These post

translational modifications (PTMs) are deposited by writer proteins that include histone acetyl-transferases (HAT), histone methyltransferases (HMT), kinases, and ubiquitin ligases and removed by histone deacetylases (HDAC), demethylases (HDM), phosphatases, and deubiquitinases (DUB), respectively[3].

Histone PTMs denote different chromatin elements (i.e., promoters or enhancers) as well as active or repressed chromatin. Histone methylation defines both active and repressed chromatin. For example, di- and tri- methylation of histone 3 lysine 9 (H3K9me2/3) and tri-methylation of histone 3 lysine 27 (H3K27me3) are associated with heterochromatin[3]. On the other hand, modifications such as H3K4me3 and H3K36me3 are associated with active transcription and elongation[3]. Alternatively, histone acetylation is often found in active regions. Acetylation neutralizes positively charged lysine residues, weakening the interaction of the histone with negatively charged DNA. Additionally, these marks can recruit chromatin effector proteins. Besides establishing lineage specific expression, PTMs changes can regulate gene expression in response to stimuli such as changes in nutrient availability, oxidative stress and DNA damage, allowing cells to adapt to environmental changes.

Once these marks are deposited, they act as signals to recruit proteins that regulate chromatin structure. Most chromatin interacting proteins contain reader domains that recognize different PTMs or bind DNA. Examples of these domains include chromodomains and PHD domains, recognizing histone methylation, AT-hooks and ARID domains that interact with DNA, and bromodomains that bind acetylated lysines. These domains target proteins to distinct regions of the genome. For example, H3K27me3 recruits the Polycomb Repressive complex 1 (PRC1) to regions of the genome that need to be silenced[5]. Once recruited, PRC1 complexes oligomerize and spread across the region, compacting and repressing the region of chromatin. When chromatin needs to be activated, remodeling complexes like Brahma-related gene 1 (BRG1) associating factors (BAF) are recruited. These large multiple protein complexes bind to nucleosomes and use energy from ATP to slide, unwrap, or eject nucleosomes, opening up the DNA, allowing for transcription factors and transcriptional machinery, such as RNA-polymerase II, access. These epigenetic mechanisms are critical for proper cell homeostasis. These epigenetic regulators are frequently mutated and lead to diseases such as cancer.

1.2 BAF in Cancer

BAF is one of most frequently mutated complexes in human cancers. In 2013, two independent screens identified that members of the BAF chromatin remodeling complexes are mutated in 20% of human cancers[6,7]. The majority of mutations lead to the loss of function of the subunits, indicating that BAF is functioning as a tumor suppressor[8]. Intriguingly, members of these complexes are mutated in a cancer specific manner. For example, BAF 47 is mutated in almost all malignant rhabdoid tumors, BRG1 is mutated in 35% of non-small cell lung cancer, ARID1a is mutated in 50% of ovarian carcinomas and PBRM1 is mutated in 40% of renal clear cell carcinoma (ccRCC) (Figure)[9–11]. BAF remodelers are critical for maintaining proper gene expression, however it is unclear why the mutational rates of particular subunits are elevated in specific cancer types. This phenomenon may be due to cell type specific functions of BAF.

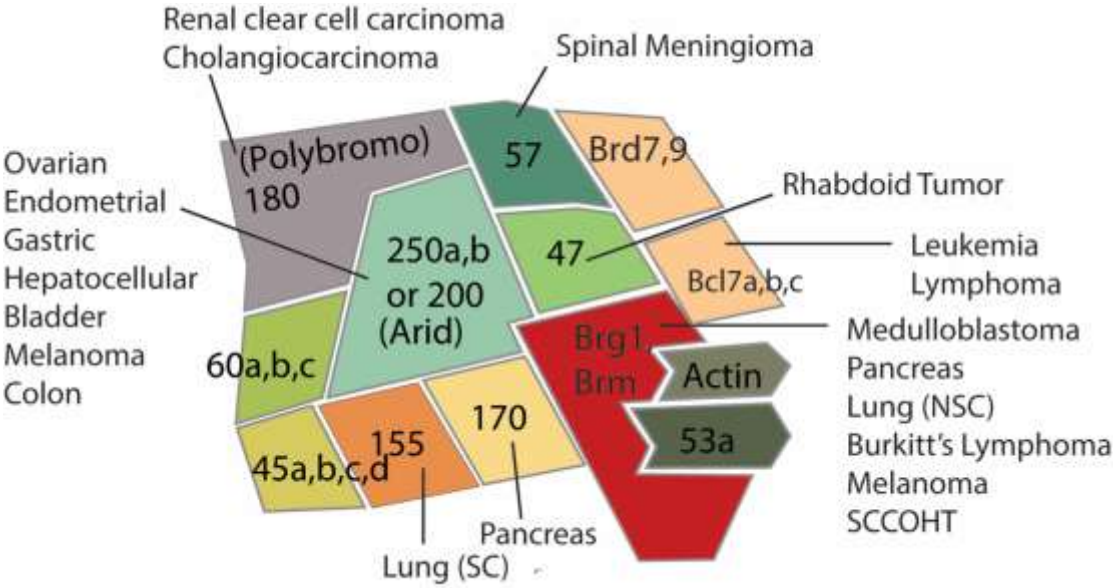

Figure 1-1: BAF is mutated in 20% of cancers. Mutations in a particular subunit often occur in a cancer specific manner.

1.3 SWI/SNF

The BAF chromatin remodelers are the human homologs of the yeast SWItch/Sucrose Non-Fermentable (SWI/SNF) complex which was first discovered for its role in regulating genes like *SUC2*, which encodes for an invertase, allowing for cleavage of sucrose into fructose and

glucose and genes involve in yeast mating type[12–14]. Genetic screens demonstrated that five proteins (*SWI1, SWI2/SNF2, SWI3, SNF5*, and *SNF6*) were needed for expression of these genes and depletion of these proteins in combination did not intensify the phenotype, indicating a cooperative nature between these proteins[13]. Purification of these SWI/SNF proteins revealed that they formed a 2 MDa complex[15], larger than the sum of all the know complex members. Biochemical analysis revealed eleven unique subunits. Promoters of repressed genes in SWI/SNF depleted yeast strains showed accumulation of nucleosomes and gene expression could be rescued by the depletion of histones H2A and H2B[12]. Analysis of the activity of this complex revealed SNF2 was an ATPase helicase that used the energy from ATP to disrupt the interaction of nucleosomes and DNA, allowing the nucleosome to be moved[16]. The mechanism of SWI/SNF remodeling of nucleosomes to promote gene expression revealed a new mechanism of gene regulation.

1.4 Composition of Human BAF

The identification of a human homolog of SNF2, BRG1, promoted the characterization of the human complex. Purification of BRG1 from human cells identified multiple complexes containing 9-13 proteins that were termed BRG1-associating factors (BAF)[15]. Size fractionation of BAF revealed two distinct sized complexes: BAF and PBAF[15,17]. Both complexes share four core members: BRG1, BAF 155, BAF 170, and BAF 47. Though BRG1 alone has the ability to remodel chromatin in the presence of ATP, work from the Kingston demonstrated this activity is enhanced by the presence of BAF 155, BAF 170, and BAF 47[18]. However, PBAF uniquely contains an additional 180 kDa protein referred to as BAF180 or Polybromo-1 (PBRM1). PBRM1 contains six tandem bromodomains (BD), which bind to acetylated lysines, two bromo-adjacent homologs (BAH), involved in protein-protein interaction and a high mobility group (HMG) that interacts with DNA[17]. Though there is no SWI/SNF equivalent, PBRM1 resembled another yeast chromatin remodeler, Remodeling the Structure of Chromatin (RSC). Three of the RSC subunits, RSC1, 2, and 4, together contain all of the domains identified in PBRM1[17]. It is hypothesized that over evolution, these yeast proteins fused together to form a single protein.

Besides the addition of PBRM1, BAF and PBAF have a few other compositional differences. For example, BAF can incorporate BRG1 or its isoform, BRM. BRG1 and BRM are 75% identical, however BRG1 is exclusively incorporated into PBAF. Additionally, PBAF also

exclusively contains BAF200 (ARID2), BRD7 and BAF 45a where BAF incorporates ARID1a/b, BRD9, BCL7 a, b, c, SS18, and BAF45b, c, d. Additionally, both complexes also contain BAF60a,b,c,, actin, BAF 53a,b and BAF 57. Though BAF and PBAF are the most well-defined complexes, it is predicted that there are over hundred variations of the BAF complex in each cell. Adding to the intricacies of these complexes, new BAF family members are still being discovered. The most recent is the G-BAF, which contains GLSTR1, BRG1, BRD9, BAF60, BAF53a, SS18, and BAF155[19]. The functional importance of this complex is still under investigation.

1.5 PBRM1 domains

The most intriguing aspect of PBRM1 is its copious number of binding domains. PBRM1 contains six tandem bromodomains (BDs), two BAH domains, and an HMG motif. Little is known about the BAH domains or the HMG motif. The BAHs are predicted to be involved in protein-protein interactions and have been reported to be involve in PCNA ubiquitination during post replicated repair[20]. The HMG domain is involved in DNA binding. Here we will focus on the BDs. Of the 46 known bromodomain containing proteins, 11 have double bromodomains, but only PBRM1 contains six[21,22]. Bromodomains are 110 amino acid domains comprised of four alpha helices (-A, -B, -C, and -Z) connected by the BC and the ZA loops[23]. The lengths of the loops are predicted to allow for substrate specificity[22]. A conserved asparagine in the binding pocket forms a hydrogen bond with the acetylated lysine, allowing for binding[23]. Bromodomains have inherently weak interactions with acetylated lysines (~500M K_d for BD2 of PBRM1with H3K14Ac)[24]. The 61 identified bromodomains are grouped into seven families[22]. All six PBRM1 BDs are found in the same family along with the BRG1 and BRM BDs. Structural comparison shows that BD1 and BD3 as well as BD2, BD5, and BD4 are similar[22]. BD6 is the most structurally different. Overall the binding pocket of BDs is well conserved, however the surface area of the binding pocket can vary in charge. Most of the PBRM1 BDs have a negatively charged surface to facilitate interaction with positively charged histones, however, BD3 has a positively charged surface area[22]. The bromodomains are predicted to target PBAF to distinctive regions on the genome, but it is unclear if PBRM1 binds to regions of elevated histone acetylation or if the BDs recognize a defined sequence of marks. Many studies have attempted to characterize if the individual bromodomains preferentially bind particular histone acetylation marks (Table 1). Comparing the results of these

studies shows little overlap and may indicate that recombinantly expressed individual domains are promiscuous.

Table 1.1: Summary of the results from three peptide screens with recombinant BDs[22,24,25].

	Chandrasekaren et al.	Charlop-Powers et al.	Filippakopoulos et al.
BD1	H3K4Ac	H3K36Ac	H2AK36Ac, H2BK85Ac, H3K56Ac, H3K64Ac, H4K44Ac, H4K77Ac,H4K79Ac, H4K91Ac
BD2	H3K9Ac	H2BK155Ac, H3K14Ac	H2A36Ac, H2B85Ac, H3K14Ac
BD3	H3K9Ac	H3K115Ac, H4K12Ac, H2BK15Ac, H2BK120Ac	H2A15Ac, H2A36Ac, H2B23Ac, H2B85Ac, H3K18Ac, H3K36Ac, H3K56Ac,H3K115Ac, H3K122Ac,H4K77Ac, H4K79Ac, H4K91Ac
BD4	H3K23Ac	H3K36Ac	Not in Screen
BD5	H3K14Ac	H3K36Ac	H2A36Ac, H2B85Ac,
BD6	No sites identified	H2BK24Ac, H2BK116Ac	H2A36Ac, H2B43Ac, H2B85Ac, H3K56Ac

To understand the role of the BDs, we studied them in the context of the full-length protein. Using a re-expression system in Caki2 cells, with a loss of PBRM1 expression mutation, we have seen that adding PBRM1 back into cells causes a decrease in growth[26]. Our work has demonstrated that the PBRM1 BDs are cooperative. We mutated the conserved asparagine of each BD. Mutation of any of the BDs, besides BD3, prevents PBRM1 from functioning properly in growth suppression, chromatin binding, and gene expression[27]. This indicates that the BDs are essential for PBRM1 function and that the bromodomains are acting cooperatively.

1.6 Distinct functions of BAF and PBAF

The function of PBRM1 is still being elucidated. BAF and PBAF are conserved in higher organisms and the distinct composition of PBAF compare to BAF indicates unique function of the two complexes. Early studies showed that PBAF and not BAF had the ability to transcriptionally activate RXR, VDR, and PPAR[28], indicating they regulated distinct sets of genes. Mouse knockout

studies demonstrated that both BAF and PBRM1 are critical in development but have independent functions. *BRG1-/-* embryos are lethal pre-implantation. *BRG1 +/-* embryos either exhibited birth defects such as exencephaly and died shortly after birth and pups that survive are prone to tumor formation (15%)[29]. Homozygous PBRM1 knockout mice are lethal at day 14.5 due to defects in heart and placental development, however *PBRM +/-* mice, in contrast, are phenotypically normal[30]. Additionally, conditional homozygous knockout adult mice are phenotypically normal besides an age-related defect in hematopoietic stem cell[31].

1.7 PBRM1 in DNA damage response

PBRM1 is also known to play a role in DNA damage response. PBRM1 is necessary for silencing of actively transcribed genes during rapid DNA repair. This silencing is dependent on the phosphorylation of PBRM1 by AMT and the ATPase activity of BRG1[32]. PBAF is also necessary for ubiquitination of PCNA to allow for replication fork loading to during post replicated repair following UV damage[20]. Finally, PBRM1 has been seen to localize at centromere and be important for kinetochore formation during mitosis[17]. Together, these results indicate that PBRM1 is important in genome integrity and stability. However, PBRM1-mutated cancers do not exhibit genome instability or a high mutational burden.

1.8 PBRM1 in renal clear cell carcinoma

PBRM1 is mutated in 3.5% of all human cancers and the majority of these mutations are in ccRCC. Kidney cancer is the 13th most frequent cancer worldwide with renal clear cell carcinoma being the most common form of kidney cancer with 62,000 new cases every year[33]. In 90% of ccRCC cases, chromosome p3 is deleted, which contains Von Hippel-Lindau (VHL), an E3 ubiquitin ligase, BAP1, a deubiquitinase, SETD2, a methyltransferase and PBRM1, a chromatin remodeler[34]. The loss of one copy of these tumor suppressors increases the chance for biallelic loss, which can occur through mutation or epigenetic silencing. VHL, PBRM1, SETD2, and BAP1 are lost in 80%, 40%, 10% and 15% of all ccRCC cases, respectively. Though combinations of these mutations are common, mutations in BAP1 and PBRM1 are mutually exclusive[33].

Though PBRM1 is important for DNA damage response and kinetochore formation, cancers with loss of PBRM1 have a low mutational burden and do not exhibit genomic instability. As mentioned above, PBRM1function in normal tissue is not well define and likewise it is unclear how loss of PBRM1 promotes tumorigenesis. Knockdown of PBRM1 in most cell lines, normal and cancer, shows minor changes in proliferation (REF). Several studies have attempted to determine how loss of the frequently mutated tumor suppressors causes tumorigenesis. Loss of VHL or PBRM1 alone is not sufficient to cause tumorigenesis. To investigate how loss of both PBRM1 and VHL contribute to the development of ccRCC, Nargund et al., created condition kidney knockout mice for -/-PBRM1, -/-VHL, and -/-PBRM1, -/-VHL[35]. Though depletion of PBRM1 in the kidney resulted in hydronephrosis, no tumors formed. Loss VHL alone led to polycystic kidney disease (PDK). However, it was not until, both VHL and PBRM1 were knockout that tumors formed in the kidneys. VHL is important for the ubiquitinating hypoxia inducible factors (HIF), marking them for degradation[36]. Normally, HIF transcriptional factors are expressed under hypoxic conditions and activate genes like vascular endothelial growth factor (VEGF) which promotes angiogenesis, providing an oxygen source to tissues with low oxygen levels as well as regulating the shift from aerobic to anaerobic metabolism. HIF-1 transcription factors are comprised of two proteins, HIF-1α and HIF-1β, that form a heterodimer. Though HIF-1β is constitutively expressed, HIF-1α has oxygen dependent domains (ODD) that make HIF-1α susceptible to ubiquitination by VHL when oxygen is present, preventing HIF-1 from being active under normoxia[37]. In ccRCC, the loss of VHL allows for HIF-1 activity, increasing angiogenesis and a shift in metabolism. Though it is still unclear why depletion of both PBRM1 and VHL are necessary for tumor formation, it is hypothesized that the increase of a hypoxic environment driven by the accumulation of HIF-1 is kept in check by PBRM1.

1.9 PBAF in immune therapy response

Recent studies have corelated patients with loss of PBRM1 mutations with an increased response to immunotherapy. Immunotherapy has been a tremendous breakthrough in cancer treatment. The immune system is designed to detect and kill tumor cells. Cancer cells have adapted to override this system by expression ligands, such as PD-L1. PD-L1 is the ligand for the PD-1 receptor on T-cell. Recognition of the PD-L1 by the PD-1 receptor prevents T-cell mediated cytotoxicity. Treatment with an antibody against PD-L1, blocks the recognition of the antibody

and allows for T-cell mediated cell death. Though this is a very effective treatment, only a small percentage of patients respond to this treatment.To identify why only a subset of patients respond to these treatment, CRISPR/Cas9 screens were performed and identified that loss of all three unique PBAF (PBRM1, BRD7, and ARID2) subunits caused sensitivity to PD-1 inhibition[38,39].

1.10 Conclusion

In this dissertation, we will discuss our findings of PBRM1 as a tumor suppressor, in targeting, and in stress response. We have developed an inducible PBRM1 re-expression system in the ccRCC cell line, Caki2. Re-expression of PBRM1 causes a 20-30% decrease in proliferation. Using this system, we have found that PBRM1 is important for regulating the expression of genes in cell adhesion, apoptosis, and hypoxia. We examined how the six tandem bromodomains work together to effect cell proliferation, gene expression, and chromatin interaction in the context of the full length of the protein. We found that activity of five of the six bromodomains are necessary for PBRM1 function, with BD2 and BD5 being the most important and BD3 having no identified function. Additionally, we validated that H3K14Ac is important for PBRM1 binding, however, it has the greatest affinity to the combination of H3K14/18Ac. We have also identified that PBRM1 protects cells from stress. Cells lacking PBRM1 have elevated reactive oxygen species (ROS) and are more sensitive to external stress. We hypothesize that PBRM1 is protecting cells from stress by upregulating stress response genes. We predict that under stress, H3K14Ac and H3K18Ac are deposited at the promoters of stress genes, recruiting PBRM1 and upregulation gene expression.

The role of PBRM1 in regulating stress is a potential mechanism for how it acts as a tumor suppressor. Under normal conditions, we hypothesize that PBRM1 prevents the accumulation of ROS and when the stress cannot be resolved PBRM1 activates apoptosis. However, without PBRM1 activity, ROS accumulates, activating growth pathways and increasing the chance for DNA damage and transformation. Understanding PBRM1's role in stress response will help us better understand how inactivation of PBRM1 leads to tumor formation and will help us identify more efficacious treatments for patients with PBRM1 mutant cancers.

CHAPTER 2. PBRM1 REGULATES THE EXPRESSION OF GENES INVOLVED IN METABOLISM AND CELL ADHESION IN RENAL CLEAR CELL CARCINOMA

The following chapter is reproduced and modified with permission from Chowdhury, B., Porter, E.G., Stewart, J.C., Ferreira, C.R., Schipma, M.J., and Dykhuizen, E.C. *PLoS One*. 2016 Apr; 11(4): e0153718. doi:10.1371/journal.pone.0153718. ©2016 Chowdhury et al.

2.1 Introduction

Kidney cancer is among the ten most common cancers in America, comprising approximately 62,000 new cancer cases and 14,000 deaths every year. Renal cell carcinoma (RCC) is the most common (~80%) and lethal type of kidney cancer in adults with clear cell RCC (ccRCC) as the most prevalent and aggressive subtype[33] (2). ccRCC is named for its characteristic histological appearance caused by high glycogen and lipid content resulting from a glycolytic metabolic shift to a "Warburg effect"-like state[34]. Approximately 80% of ccRCCs have inactivation of VHL (von Hippel-Lindau), an E3 ubiquitin ligase involved in the degradation of hypoxia-inducible factor (HIF) transcription factors, HIF1α and HIF2α[36]. Although inheritance of VHL mutations causes a predisposition for ccRCC, deletion of VHL is not sufficient to cause cancer, and the loss of VHL alone provides neither prognostic nor therapeutic prediction values. Thus, other factors are required to drive ccRCC progression. In order to better understand genetic events causing ccRCC, exome sequencing of patient tumors has uncovered several novel genes significantly mutated in ccRCC, all of which encode for proteins that regulate chromatin. These novel genes include Polybromo-1 (PBRM1), BAP1, SETD2, KDM5C, and KDM6A. Polybromo-1 is the second most commonly mutated gene in ccRCC, with mutation rates at ~40%[11,40–43] PBRM1 is a subunit of a subcomplex of the mammalian SWI/SNF (SWItch/Sucrose-NonFermentable) or BAF (BRG1 or BRM associated factors) chromatin remodeling complex termed PBAF (PBRM1-BAF). BAF complexes use energy from ATP to regulate transcription by altering chromatin structure and the placement of Polycomb across the genome. Subunits of the BAF complex are mutated in over 20% of human tumors[6,7]yet the mechanisms involved in tumor suppression are still unclear.

Several studies have attempted to elucidate the molecular function of PBRM1 in ccRCC using transcriptional data from patient samples. While the panel of genes differentially regulated in *PBRM1*-mutated tumors express a hypoxic signature, no clear definition of PBRM1-regulated genes has come from these analyses, most likely due to the high heterogeneity of ccRCC tumors[43–45]. To overcome these obstacles, we report the development of isogenic ccRCC cell lines that permit dissecting the transcriptional role of PBRM1 in tumor suppression. We performed a comprehensive RNA-Seq analysis using a ccRCC cell line engineered with and without PBRM1 re-expression in order to specifically identify PBRM1 regulated genes. From this RNA-Seq dataset of PBRM1-regulated genes we identified several quintessential pathways involved in ccRCC oncogenesis including metabolism and hypoxia. In addition, we identified many genes involved in cell adhesion that are uniquely regulated by PBRM1 and could be used to specifically characterize and treat PBRM1-mutated ccRCC tumors.

2.2 Materials and Methods

2.2.1 Cell culture

Caki-1 and Caki-2 cells (American Type Culture Collection, Manassas, VA) were cultured in McCoy's 5A (Corning Mediatech, Inc., Manassas, VA) supplemented with 10% fetal bovine serum (Omega Scientific,Inc, Tarzana, CA), 1% antibiotics (100 U/ml penicillin and 100 μg/ml streptomycin; Corning Mediatech, Inc., Manassas, VA), 1% nonessential amino acids (Corning Mediatech, Inc., Manassas, VA) and 1% L-glutamine (Corning Mediatech, Inc., Manassas, VA) at 37°C in a humidified atmosphere in a 5% CO2 incubator. A704 and A498 cells (American Type Culture Collection, Manassas, VA) were cultured in Eagles Minimum Essential Media supplemented with 10% fetal bovine serum (Omega Scientific,Inc, Tarzana, CA), 1% antibiotics (100 U/ml penicillin and 100 μg/ml streptomycin; Corning Mediatech, Inc., Manassas, VA), 1% nonessential aminoacids (Corning Mediatech, Inc., Manassas, VA) and 1% L-glutamine (Corning Mediatech, Inc., Manassas, VA). All cells were maintained at 37°C in a humidified atmosphere in a 5% CO_2 incubator.

2.2.2 Constructs

PBRM1 knockdowns were performed using an empty pLKO.1 vector or pLKO.1 vector containing shRNA to human PBRM1 (TRCN0000015994, ThermoFisher Scientific, Waltham,

MA). PBRM1 re-expression was performed by cloning full length PBRM1 from pBabepuroBAF180 (a gift from Ramon Parsons Addgene plasmid # 41078) into tet-inducible conditional lentiviral vector TetO-FUW (a gift from Rudolf Jaenisch Addgene plasmid # 20323), which was used with pLenti CMV rtTA3 Hygro (w785-1) (a gift from Eric Campeau Addgene plasmid # 26730) for tetracycline inducible expression.

2.2.3 Lentiviral Infection

HEK293T cells were transfected with lentiviral constructs along with lentiviral packaging vectors pMD2.G and psPAX2. After 48 h, supernatants were collected, and virus isolated using ultracentrifugation at 20,000 r.p.m. for 2 h. Viral pellets were re-suspended in PBS and used to infect ccRCC cell lines by spinfection. Cells were selected with puromycin and/or hygromycin for one week to maintain stable lines. For inducible vectors, doxycycline was added to the culture media at 2 µg/mL for at least 72 hours prior to experiments.

2.2.4 Sulforhodamine B assays

Sulforhodamine B assay was performed in 96-well plate format. Cells were fixed *in situ* by incubation with 50 µL of trichloroacetic acid at 4°C for 1 hour. After discarding the fixative solution, wells were rinsed thoroughly with tap water and air dried. Staining was performed by adding 50 µL of 0.4% Sulforhodamine B in 1% acetic acid solution to every well and the plate was incubated for 10 minutes at room temperature. Unbound Sulforhodamine was removed by washing the wells with 1% acetic acid. After air drying the plates, bound stain was solubilized with 10 mM Tris Base and the absorbance at a wavelength of 515 nm was read by Synergy 4 Hybrid Microplate Reader (BioTek, Winooski, VT).

2.2.5 RNA isolation

Total RNA was extracted using TRIzol reagent (Life Technologies Corporation, Grand Island, NY) and cleaned up using RNeasy Mini Kit (Qiagen Inc., Valencia, CA) according to the manufacturer's instructions.

2.2.6 Library Construction and Sequencing

Library construction (100 bp, paired-end) and sequencing were carried out by Beijing Genomics Institute (BGI). The total RNA samples were enriched for mRNA by targeting

polyadenylated (poly(A)) using oligo (dT) magnetic beads. Isolated mRNA was resuspended in fragmentation buffer and sonicated into short fragments of about 200 bp. mRNA was reverse transcribed into a single strand of causing random hexamer-primers. The second strand of cDNA was synthesized using DNA polymerase and the double stranded cDNA was purified with magnetic beads. End reparation and 3'-end Adenine addition were performed subsequently. Thereafter sequencing adaptors were ligated to the fragments and the fragments were enriched by PCR amplification. During the QC step, Agilent 2100 Bioanalyzer and ABI StepOnePlus Real-Time PCR System were used to qualify and quantify the sample libraries. Finally, the library products were sequenced on the Illumina HiSeq2000.

2.2.7 Transcriptome Analysis

The quality of DNA reads, in fastq format, was evaluated using FastQC. Adapters were trimmed and reads of poor quality and those aligning to rRNA sequences were removed. The remaining clean reads were aligned to the human reference genome (hg19) using STAR[46]. Read counts for 25,369 genes were calculated using htseq-count[47] in conjunction with a standard gene annotation file for hg19 obtained from UCSC (University of California Santa Cruz; http://genome.ucsc.edu). Differential expression was determined using DESeq2[48] using the counts from htseq-count as input (read counts pertaining to 25,369 genes in each of the samples). Built-in normalization algorithms of DESeq2 were used and an FDR-adjusted p-value of 0.05 used as the cutoff for determining differential gene expression. A pathway analysis was performed on gene lists using GeneCoDis[49–51] and Pre-ranked Gene Set Enrichment Analysis[52] to identify pathways enriched among genes that were upregulated and downregulated. Sequencing data for all the samples have been submitted at GEO (GSE76199). The data will be publicly available on acceptance of this manuscript for publication but currently reviewers can privately access the data by logging into their 'My NCBI' account and visiting http://www.ncbi.nlm.nih.gov/geo/query/acc.cgi?acc=GSE76199

2.2.8 Real-time polymerase chain reaction (RT-PCR)

Total RNA was converted into cDNA using iScript Reverse Transcription Kit (Bio-Rad Laboratories, Inc., Hercules, California). All of the primers are listed in **Table S1**. Real-time PCR was performed using a Bio-Rad CFX Connect Real-Time system and a Super Real Pre-Mix Kit.

The results were analyzed using the $2^{(-\Delta\Delta CT)}$ comparative method. Each sample was tested in triplicate.

2.2.9 Immunoblot Analysis

Cells were lysed in cold Radio-Immunoprecipitation assay (RIPA) buffer containing freshly added protease inhibitor. The lysed cells were incubated on ice for 30 min and thereafter centrifuged at 14000 × g for 10 min at 4°C, and the supernatants were collected. Total protein was denatured for 10 min at 95°C, separated on a 10–15% SDS-polyacrylamide gel, and transferred to a PVDF membrane (Immobilon FL, EMD Millipore, Billerica, MA).. The membrane was blocked with 5% bovine serum albumin (VWR, Batavia, IL) in PBS containing 0.1% Tween-20 (PBST) for 30 mins at room temperature and then incubated in primary antibodies overnight at 4°C. The primary antibodies used were directed against IGFBP3 (Santa Cruz Biotechnology Inc., Dallas, TX; sc-9028), Phospho-AKT (Ser473) (Cell Signaling Technology, Danvers, MA; 4060), Cleaved PARP (Asp214) (Cell Signaling Technology, Danvers, MA; 9541), AKT (Cell Signaling Technology, Danvers, MA; 9272), BRG1 (Abcam Plc, Cambridge, MA; ab110641), PBRM1 (Bethyl Laboratories, Montgomery, TX; A301-591A) and TBP (Abcam Plc, Cambridge,MA;ab818). The primary antibodies were detected by incubating the membranes in goat-anti-rabbit or goat-anti-mouse secondary antibodies (LI-COR Biotechnology, Lincoln, NE) conjugated to IRDye 800CW or IRDye 680 respectively for 1 h at room temperature, and the signals were visualized using Odyssey Clx imager (LI-COR Biotechnology, Lincoln, NE).

2.2.10 Cell cycle distribution assays

Cells were harvested in the logarithmic growth phase and counted by MOXI Z Mini Automated Cell Counter (ORFLO Technologies, Ketchum, ID). 5 X 10^6 cells were washed twice with ice cold PBS, resuspended in cold ethanol and incubated overnight at −20°C. The cells were centrifuged, and the supernatant was discarded. After the cells were washed twice with PBS, they were resuspended and stained with 50 μg/ml propidium iodide (PI), 100 μg/ml RNase A, and 0.2% Triton X-100. The samples were incubated in the dark at 4°C for 30 min and then analyzed via flow cytometry. Approximately 20,000 cells were examined per sample.

2.2.11 Apoptotic assay

The percentage of cells undergoing apoptosis was determined using Annexin V-FITC/PI Apoptosis Detection Kit (BD Biosciences, Franklin Lakes, NJ). Cells were collected in logarithmic growth phase, washed twice with cold PBS, and adjusted to a density of 1×10^6 cells/ml in binding buffer. The cell suspension (100 µl) was placed in a Falcon tube and was sequentially incubated in annexin V-FITC (5 µl) followed by PI (5 µl) at 20°C–25°C in the dark for 15 min. Then 400 µl binding buffer was added and the samples were analyzed by flow cytometry within one hour.

2.2.12 Exposure to Hypoxia

For hypoxia treatment, cells were plated 16 hours before placement in a modular incubator chamber (Billups-Rothenberg, Inc., Del Mar, CA) flushed with a gas mixture of 0.5% O_2, 5% CO_2 and 94.5% N_2 (Indiana Oxygen Company, Indianapolis, IN) at 37˚C for 6 hours.

2.2.13 Glucose Uptake Assay

Cells were plated (20,000 cells/well) in 96 well plates. After 16 hours, media from each well was aspirated and fresh media added (200µl/well). Fresh media was also added to wells not having cells and this served as control. After 6 hours of incubation, the media was collected and glucose content quantified using a glucose assay kit (Eton Bioscience, Inc., San Diego, CA) according to the manufacturer's instructions. Glucose uptake was derived by subtracting the glucose content of media in wells having cells from those of wells not bearing cells (control). Glucose uptake rate (uM/hr/Absorbance) was finally calculated by dividing glucose uptake with time of treatment (6 hours) and relative number of cells (A_{515nm} determined by the Sulforhodamine assay).

2.2.14 Imaging of actin cytoskeleton

Cells were plated on coverslips and grown until they achieved 70% confluency. The cells were washed twice with PBS and fixed in 3.7% methanol-free formaldehyde solution in PBS for 10 minutes at room temperature. The coverslips are rinsed thoroughly with PBS and permeabilized with 0.1% Triton X-100 in PBS for 5 minutes. The coverslips were blocked for 30 mins with PBS containing 1% BSA and then treated with 50 µL of Phalloidin conjugated to Texas Red (1:40; ThermoFisher Scientific, Waltham, MA) for 30 mins at Room Temperature. The coverslips were

thoroughly rinsed with PBS containing 0.1% Tween 20, mounted on glass slides with Prolong Gold antifade containing DAPI (ThermoFisher Scientific, Waltham, MA) and imaged by Evos FL fluorescence microscope (ThermoFisher Scientific, Waltham, MA) as well as LSM 710 confocal microscope (Carl Zeiss Microscopy, LLC, Thornwood, NY). A total of five fields were counted for each condition (approximately 100-150 cells/field) by three independent observers in a blinded test. Each observer recorded the number of total cells, as determined by DAPI staining, as well as the number of cells with high concentrations of cortical actin staining as determined by Phalloidin staining. Finally, the percentage of cells with cortical F-actin in the two groups was determined and Fisher's Exact Test was performed to evaluate the significance

2.2.15 *In vitro* Scratch Test

Caki2+Vector and Caki2+PBRM1 cells were grown to 90% confluence in a 6 well plate. Scratches were made using a 1000µl pipet tip and the cells were rinsed gently with media to remove non-adherent cells. Fresh media was added to the cells and ten designated points on the scratch were imaged at 0h. The cells were allowed to incubate for 24 h and the designated points were imaged once again. ImageJ software was used to measure the average width (µm) of the scratch at 0h and 24 h and the cell migration/average closure rate was computed from the difference of the scratch width at 0h and 24h.

2.2.16 Cholesteryl ester (CE) fingerprinting by mass spectrometry

Total lipid from the Caki2+Vector and Caki2+PBRM1 cells was extracted in accordance with the Bligh and Dyer protocol [53]. The chloroform phase containing lipids was dried under N_2 stream and dissolved in 100µL of $CHCl_3$/MeOH/H_2O (vol/vol/vol proportion of 300/665/35) containing 300mM ammonium acetate. The volume of 8 µL of lipid extract was flow injected using a G1377A micro-autosampler into an ESI source of a Agilent 6410 triple-quadrupole mass spectrometer operated in positive ion mode for each MRM [586.2000 →369.1016 (CE12:0), 612.2000 → 369.1016 (CE 14:1), 614.2000 → 369.1016 (CE14:0), 640.6000 → 369.1016 (CE16:1), 642.6000 → 369.1016 (CE16:0), 664.6000 → 369.1016 (CE18:3), 666.6000 → 369.1016 (CE 18:2), 668.6000 → 369.1016 (CE18:1), 670.6000 → 369.1016 (CE18:0), 688.6000 → 369.1016 (CE20:5), 690.6000 → 369.1016 (CE20:4), 692.6000 → 369.1016 (CE20:3), 694.6000 → 369.1016 (CE20:2), 696.6000 → 369.1016 (CE20:1), 698.6000 →

369.1016 (CE20:0), 716.6000 → 369.1016 (CE22:6), 718.6000 → 369.1016 (CE22:5), 720.6000 → 369.1016 (CE22:4), 722.6000 → 369.1016 (CE22:2) and 724.6000 → 369.1016 (CE22:1)]22-23. Instrument's dwell time was 20ms and collision energy 15. Data was collected for 1 min, in which 106 scans per CE species have been obtained. Data was processed for chronogram smoothing and subsequently the CE peak list was generated using Agilent Mass Hunter B.06.00 software. The proportion of CE species in every sample was obtained by dividing the total ion intensity (sum of 106 scans) for each CE species by the total ion intensity obtained for all CE species assayed[54]. A semi-quantitative comparison of the proportion of CE species in Caki2+PBRM1 and Caki2+Vector was performed and CE species displaying significant (Student's T-test p-value <0.05) differences between the two groups were plotted.

2.3 Results & Discussion

2.3.1 PBRM1 expression in RCCs

In order to identify ccRCC cell lines with PBRM1 loss, we obtained a panel of ccRCC cell lines from ATCC and tested them for PBRM1 mRNA and protein expression. As depicted in Fig 1.1A, all of the cell lines express mRNA for PBRM1 using primers that span the exon 22/23 junction[41]. This is in accordance with reports from human tumors that report loss of PBRM1 protein function through mutation, not transcriptional silencing[11]. Using immunoblot analysis (Fig 1.1B), we determined that the cell lines 786O, 769P, Caki1, and A498 express PBRM1 in accordance with reports of being genetically wild type, ACHN expresses PBRM1 and has a heterozygous nonsense mutation[55], and the cell lines A704 and Caki2 do not express PBRM1, as previously reported[44]. The loss-of-function gene mutations have been identified for A704[55] but to the best of our knowledge, the sequencing of the PBRM1 gene in Caki2 has not been previously reported. Using Sanger sequencing, we identified a previously uncharacterized 4 bp deletion in exon 17, accounting for the loss of protein expression in this cell line (Fig 1.1C).

2.3.2 Generation of Isogenic cell lines for controlled studies of PBRM1 function.

We created complementary cell lines using lentiviral knockdown of PBRM1 in A498 and Caki1 and the re-expression of PBRM1 in A704 and Caki2 using lentiviral re-expression of PBRM1 with a tet-inducible vector (Fig 1D). We confirmed reincorporation of PBRM1 into the BAF complex using immunoprecipitation followed by immunoblot analysis (Fig 1E). In addition,

we used glycerol gradient analysis to confirm that PBRM1 is fully reincorporated specifically into the PBAF complex and that overexpression doesn't result in PBRM1 monomer or alterations in PBAF complex stoichiometry (Fig S1). We did not observe any large-scale destabilization or re-organization of the BAF or PBAF complexes in Caki2 cells or in Caki1 cells upon PBRM1 knockdown, although we did observe a reproducible increase in ARID2 protein levels with decreased PBRM1, which may play a role in altering PBAF-mediated transcription in ccRCC with PBRM1 mutations.

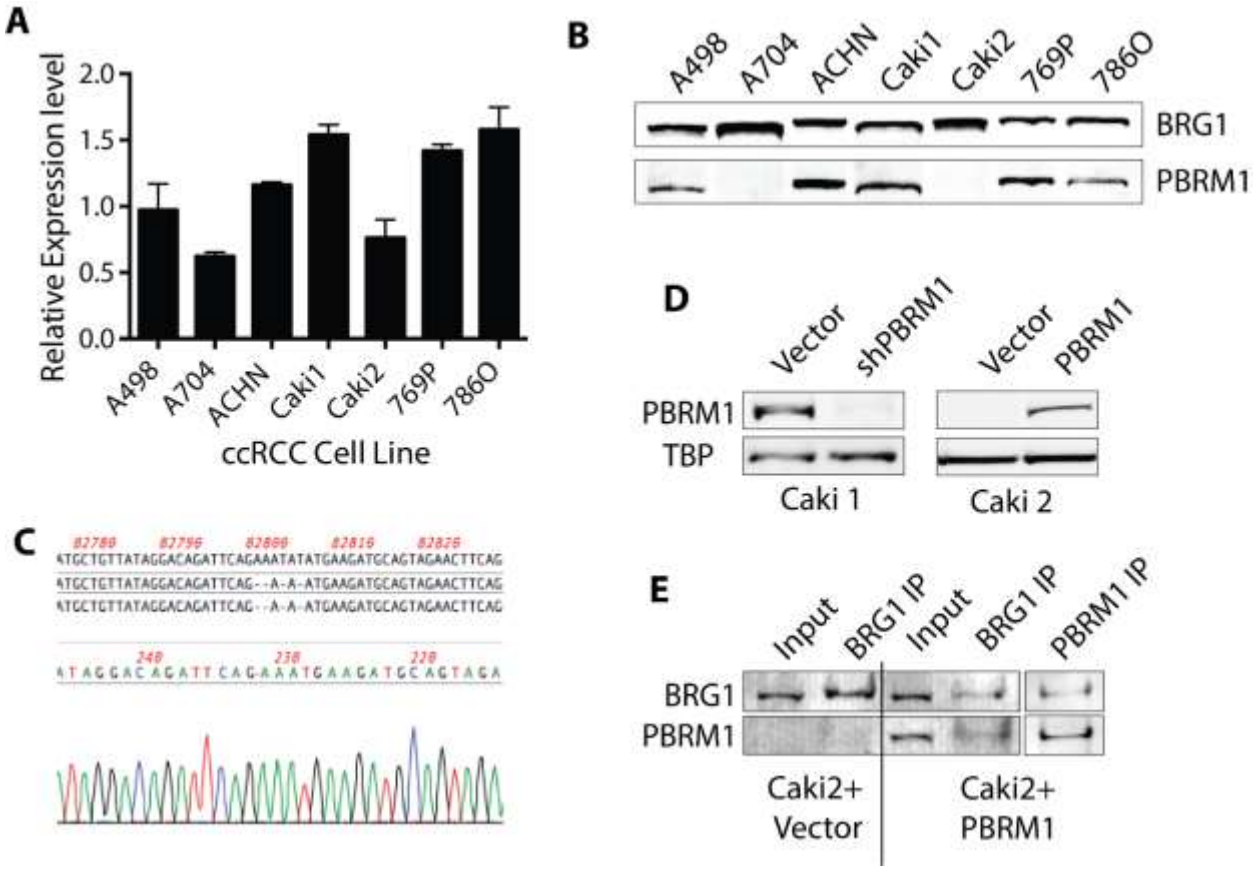

Figure 2-1 Characterization of PBRM1 in ccRCC cells

A) Relative transcript expression of PBRM1 in ccRCC cell lines. B) Protein levels of BRG1 and PBRM1 in ccRCC cell lines. C) Characterization of deletion in exon 17 of PBRM1 gene in Caki2 cells. D) Protein levels of PBRM1 in isogenic ccRCC cells (Caki1 with PBRM1 knockdown and Caki2 with PBRM1 re-expression). E) BRG1 and PBRM1 blotting in BRG1 or PBRM1 immunoprecipitates of Caki2+Vector and Caki2+PBRM1.

2.3.3 Effect of PBRM1 expression on cell proliferation

We performed proliferation analysis with PBRM1 knockdown in Caki1 cells and A498 cells and were surprised to find no significant effect on proliferation under standard cell culture conditions (Fig 2.2A and 2.2B). We hypothesized that due to the heterogeneity of mutations in ccRCC, PBRM1 may serve a redundant role in tumor suppression with other mutated genes in these ccRCC cell lines. Thus, we focused on cell lines with PBRM1 mutations with the assumption that loss of PBRM1 acts as a driver in these cancers. Although the effects of re-expressing PBRM1 in Caki2 and A704 were modest, we observed a definitive role of PBRM1 re-expression in reducing cellular proliferation under standard cell culture conditions (Fig 2.2C and 2.2D). Due to the low proliferative rate of the A704 cell line, we pursued the isogenic Caki2 cell lines for further investigation of the role of PBRM1 on gene transcription.

2.3.4 Differentially expressed genes upon PBRM1 re-expression in Caki-2

To identify key pathways influenced by PBRM1 activity, we performed an RNA-Seq analysis of Caki2 cells with and without PBRM1 re-expression (Caki2+Vector and Caki2+PBRM1). Hierarchical clustering with un-normalized counts as well as normalized regularized-logarithm transformed count data demonstrated similarities between the biological replicates illustrated by Euclidean distances (Fig SI2). DESeq2 analysis, comparing the transcript expression of Caki2+PBRM1 and Caki2+Vector cells revealed that 2,464 genes were differentially expressed (FDR-padj<0.05). Of these, 65 were upregulated and 6 were downregulated more than two-fold in Caki2+PBRM1 compared to Caki2+Vector cells. 97% of the differentially expressed genes (n=2,393) underwent mild to moderate (0 - 2 $\log_2$ fold) levels of differential expression upon PBRM1 re-expression. GO analysis established that upregulated genes enriched biological processes such as cell adhesion (GO:0007155), apoptotic process (GO:0043065), negative regulation of cell proliferation (GO:0008285), carbohydrate metabolic process (GO:0005975) and response to hypoxia (GO:0001666) among others (Fig 2.5B and Table S2) and downregulation of genes involved in mitotic cell cycle (GO:0000278), G1/S transition (GO:0000082) and metabolic processes (GO:0044267) (Fig 2.3C).

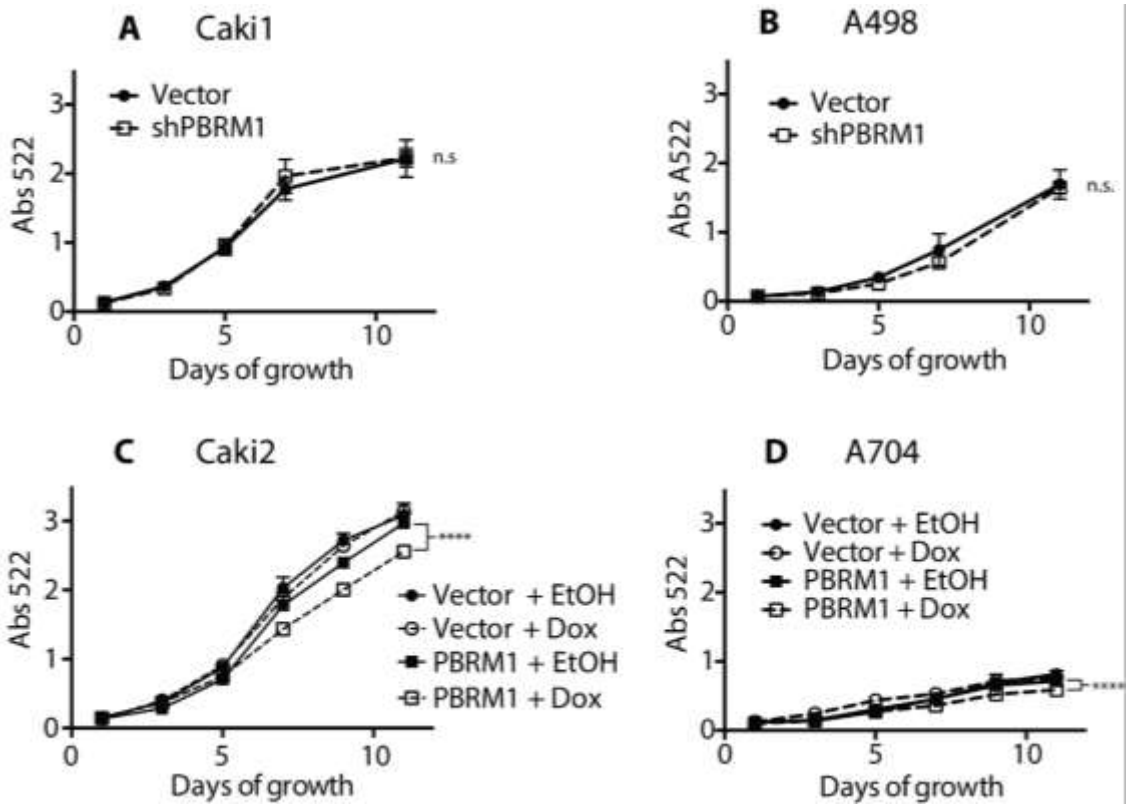

Figure 2-2 Presence of PBRM1 resulted in decreased proliferation rate of ccRCC cells

Cellular proliferation rate was monitored in A) Caki1 and B) A498 with either control knockdown or PBRM1 knockdown, as well as C) Caki2 and D) A704 with either control vectors or PBRM1 re-expression vectors. Both cell lines were treated with ethanol or doxycycline to control for cell line variation or doxycycline effects. n = 8 independent biological replicate experiments. $P < 0.0001$ (****) (two-way ANOVA test) between PBRM1 re-expression cell lines treated with ethanol (EtOH) or Doxycycline (Dox) at day 11. Error bars represent s.e.m.

Figure 2-3 Summary of differentially expressed genes in Caki2 cells upon PBRM1 re-expression

A) Hierarchical Cluster Dendrogram of Caki2+Vector and Caki2+PBRM1 samples sequenced. B) GO Biological Processes enriched by genes upregulated upon PBRM1 re-expression. C) GO Biological Processes enriched by genes downregulated upon PBRM1 re-expression.

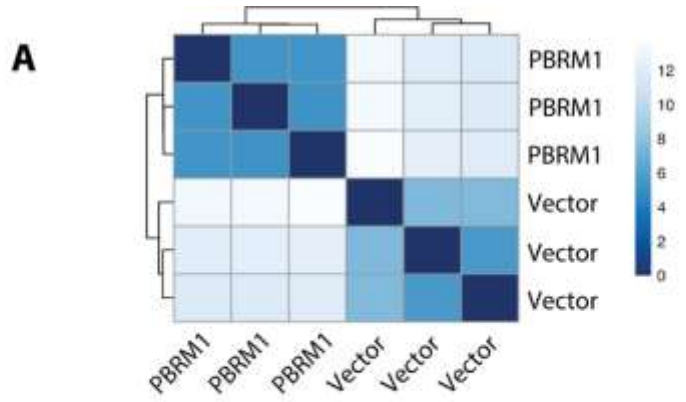
A
PBRM1
PBRM1
PBRM1
Vector
Vector
Vector
12
10
8
6
4
2
0
PBRM1
PBRM1
PBRM1
Vector
Vector
Vector

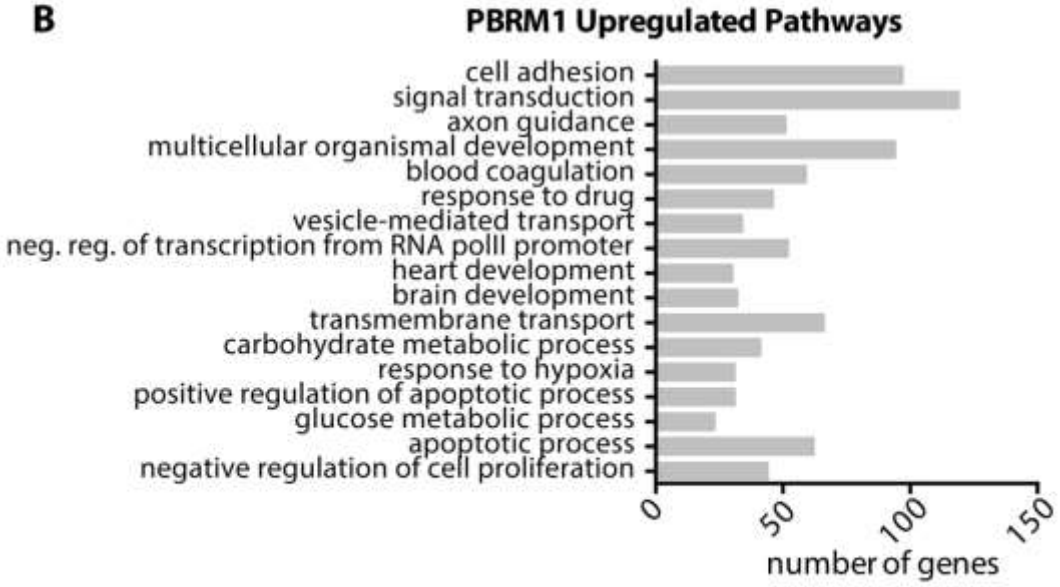
B
PBRM1 Upregulated Pathways
cell adhesion
signal transduction
axon guidance
multicellular organismal development
blood coagulation
response to drug
vesicle-mediated transport
neg. reg. of transcription from RNA polII promoter
heart development
brain development
transmembrane transport
carbohydrate metabolic process
response to hypoxia
positive regulation of apoptotic process
glucose metabolic process
apoptotic process
negative regulation of cell proliferation
0
50
100
150
number of genes

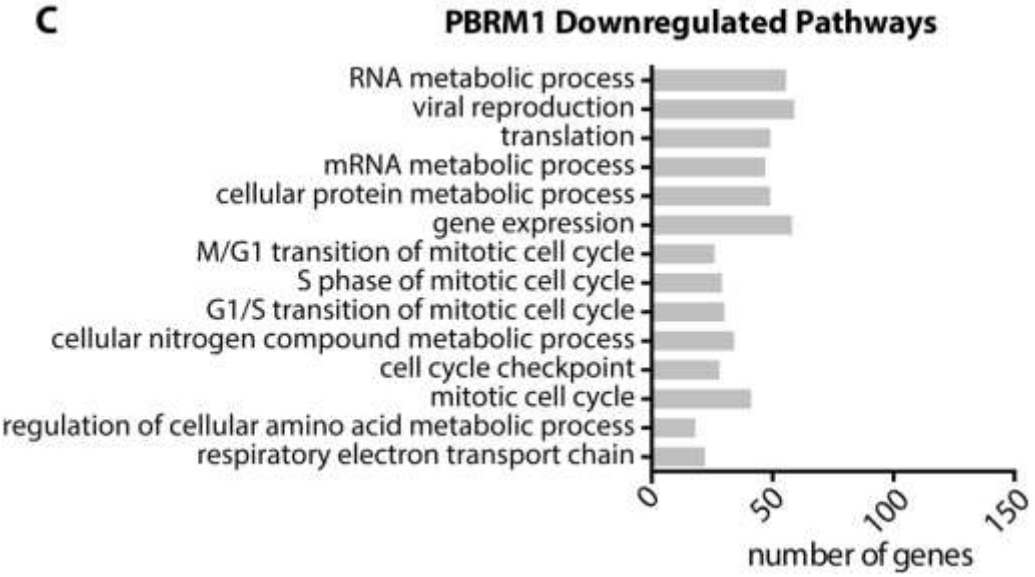
C
PBRM1 Downregulated Pathways
RNA metabolic process
viral reproduction
translation
mRNA metabolic process
cellular protein metabolic process
gene expression
M/G1 transition of mitotic cell cycle
S phase of mitotic cell cycle
G1/S transition of mitotic cell cycle
cellular nitrogen compound metabolic process
cell cycle checkpoint
mitotic cell cycle
regulation of cellular amino acid metabolic process
respiratory electron transport chain
0
50
100
150
number of genes

2.3.5 PBRM1 in cell cycle and apoptosis

In accordance with inhibition of proliferation observed upon PBRM1 re-expression (Fig 2.2C), RNA-seq analysis revealed downregulation of genes involved in cell cycle including 30 genes associated with G1/S transition and qRTPCR confirmed the downregulation of several representative genes (Fig 2.4A). Flow cytometric analysis demonstrated a role for PBRM1 in G1/G0 arrest with a significant reduction in S-phase cells upon PBRM1 re-expression in Caki2 cells (Fig 2.4B). This is similar to the cell cycle effects observed upon PBRM1 re-expression in PBRM1 mutant breast cancer[56]. To further define the G1/G0 arrest observed with PBRM1 re-expression we wished to determine whether increased apoptosis contributes to the G1/G0 cell cycle block.

From the transcriptional analysis, we observed upregulation of both pro-apoptotic and anti-apoptotic genes (data not shown) and validated some of them by qRTPCR (Fig S2). Low levels of apoptotic markers Annexin V and cleaved PARP[57], in both Caki2+Vector and Caki2+PBRM1 cells led us to conclude the G1/G0 cell cycle block observed for the Caki2+PBRM1 cell line did not result in increased apoptosis (S2 Fig).

2.3.6 PBRM1 in hypoxia

ccRCC is characterized by a metabolic shift mediated through altered hypoxic signaling. PBRM1-deficient tumors in particular display a hypoxic transcriptional signature, possibly implying that deletion of PBRM1 acts in concert with, or facilitates, pro-oncogenic hypoxic pathways[41,58]. In apparent contradiction to this, we observe hypoxia-response genes as significantly upregulated upon PBRM1 re-expression. This is in agreement with the observation that SWI/SNF subunits BRG1, BAF155, and BAF57 are required for the induction of HIF1α target genes in other cell types[59,60]. The diversity of HIF1α and HIF2α aberrations in ccRCC makes it challenging to evaluate their individual contribution to supporting ccRCC; however, Shen et al have documented the enhancement and inhibition of cell growth upon knocking down HIF1α and HIF2α respectively in the Caki2 cells as well as in mouse xenografts supporting the hypothesis that HIF1α itself acts as a tumor suppressor and is often deleted in renal cancer cell lines, while HIF2α is the primary oncogenic driver[61–63]. Therefore, it follows that PBRM1 may act as a tumor suppressor by facilitating the expression of HIF1α but not HIF2α target genes.

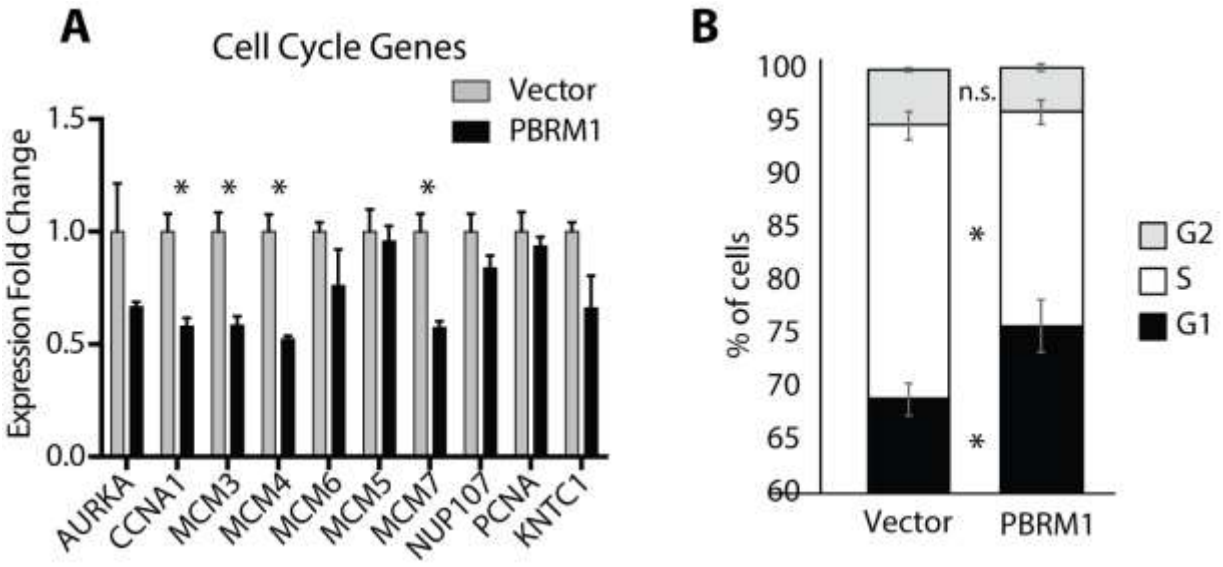

Figure 2-4 Downregulation of genes involved in cell proliferation upon PBRM1 re-expression

A) Validating relative expression of genes regulating cell cycle (identified in RNA_seq data) in Caki2+Vectorand Caki2+PBRM1 cells by qRTPCR. A designation of * = P < 0.05 (paired Student *t*-test). n = 3 independent biological replicate experiments. Error bars represent s.e.m. B) Percentage of cells in different stages of cell cycle (G1, S and G2) determined by flow cytometric analysis. A designation of * = P < 0.05 (paired Student *t*-test). n = 3 independent biological replicate experiments. Error bars represent s.e.m.

Consequently, we explored the changes in gene expression of IGBP 1, PHD3 and HIF1α, which are upregulated in Caki2+PBRM1. IGFBP1 is a member of the IGFBP family, which are HIF target genes that play important roles in regulating glucose availability by binding to insulin-like growth factors. Under normoxia, IGFBP1 was upregulated upon PBRM1 re-expression (Fig2.5A), and hypoxia induced dramatic increase in the levels of more than 4-fold for IGFBP1 (and also other members of the IGFBP family like IGFBP3 and IGFB4) in Caki2+PBRM1. In contrast, hypoxic exposure did not bring about any change in levels of IGFBP1 or the other members of the IGFBP family in Caki2+Vector cells. HIF1α and PHD3 are canonical HIF targets, and exposure to hypoxia resulted in increase of steady state levels of HIF1α and PHD3 in Caki2+PBRM1 but not in Caki2+Vector. On the other hand, hypoxia induced an increase in VEGF expression (a classic oncogenic HIF target gene, widely used in studying hypoxia response and not implicated in our RNA-seq data) in both Caki2+PBRM1 and Caki2+Vector cells, driving home the point that PBRM1 may regulate the expression of a subset of HIF target genes, possibly distinguishing between HIF1α and HIF2α targets[62].

2.3.1 PBRM1 in glycolysis and cholesterol homeostasis

One of the defining features of ccRCC is the increase in glycolysis and activation of the PI3K signaling pathway[11]. Many of the PBRM1 upregulated genes, including the hypoxia-response genes, have been shown to decrease PI3K signaling through the inhibition of insulin receptor signaling and glycolysis[11]. These genes code for glycolytic enzymes, solute carriers, and proteins involved in cholesterol homeostasis. We identified genes upregulated by PBRM1 that inhibit glycolysis, as well as several genes downregulated by PBRM1 involved in facilitating glycolysis and confirmed the expression several of them using qRTPCR (Fig 2.5B). In accordance with this result we observed a significant decrease in glucose uptake (p=1.2e-5) upon PBRM1 re-expression (Fig 2.5C) as well as a decrease in PI3K signaling using immunoblot analysis of AKT phosphorylation (Fig 2.5D).

The histological appearance of lipid accumulation in ccRCC is well established and leads to the name “clear cell” renal carcinoma[64,65]. Among all lipid classes, Cholesteryl-esters illustrate the most dramatic alterations in their profile in ccRCC[64,66]. Though the precise molecular mechanism is unknown, the increased accumulation in cholesteryl oleate (CE18:1) and decreased accumulation in cholesterol linoleate (CE18:2) has been characterized in ccRCC[64,66].

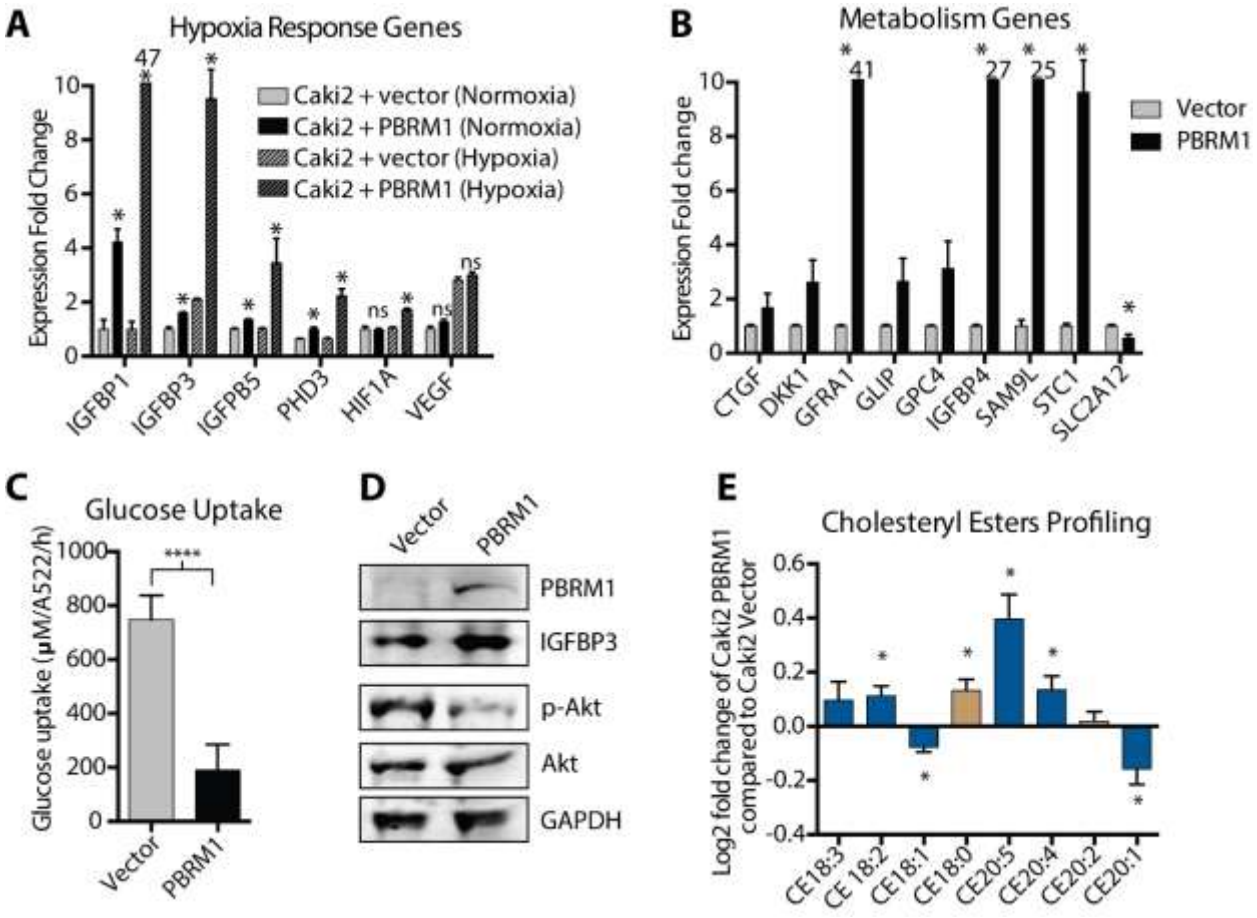

Figure 2-5 Alteration of metabolism upon PBRM1 re-expression

A) Relative expression of genes regulating hypoxic response in Caki2+Vectorand Caki2+PBRM1 cells subjected to normoxic and hypoxic (0.5% O_2) conditions. A designation of * indicates $p < 0.05$ (Student *t*-test). n = 3 independent biological replicate experiments. Error bars represent s.e.m. B) Validating relative expression of genes regulating primary metabolic processes (identified in RNA_seq data) in Caki2+Vectorand Caki2+PBRM1 cells by qRTPCR. C) Determination of glucose uptake in Caki2+Vectorand Caki2+PBRM1 cells. A designation of **** indicates $p < 0.0001$ (paired Student *t*-test). n = 5 independent biological replicate experiments. Error bars represent s.e.m. D) Immunoblot of IGFBP3, phosphorylated AKT and unphosphorylated AKT in Caki2+Vectorand Caki2+PBRM1 cells. (E) Semi-quantitative estimation of alteration of cholesteryl esters in Caki2+PBRM1 compared to Caki2-Ø. Bars depicted in blue reverse the differences observed during the progression from normal kidney epithelium to ccRCC and bars depicted in tan compound those differences. A designation of * = $P < 0.05$ (paired Student *t*-test). n = 3 independent biological replicate experiments. Error bars represent s.e.m.

Upon PBRM1 re-expression in Caki2 cells, we observed a decrease in CE18:1 and an increase in CE18:2 which was in agreement to previous studies (Fig 2.5E)[64,66]. Additionally we observed the increased representation of CE16:0, CE20:5, CE20:4 and decreased representation of CE20:1 in comparing the lipid profile of Caki2+PBRM1 with that of Caki2+Vector, which was consistent with the comparison of normal kidney tissue and renal cell carcinoma obtained from nephrectomies from six patients reported earlier [66]. The increased representation of CE20:3 and CE22:4 upon PBRM1 re-expression in Caki2 cells was not consistent with the profile of normal kidney tissue in the earlier study[66]. We are reporting the novel observation of the increased representation of CE16:0, CE18:1, CE24:0, CE22:0 and CE22:4 upon PBRM1 re-expression, which have not been quantified in any study to the best of our knowledge (S3 Fig).

2.3.2 PBRM1 in cell adhesion

Cell adhesion is essential in adherent cells serving as molecular scaffolds linking the cellular cytoskeleton to the extracellular environment[67]. Normal and non-metastasizing cells are observed to form close focal contacts while metastasizing cells maintain limited areas of close contact, suggesting that aberrations in cell adhesion may be responsible for certain aspects of malignant cell behavior[68]. The relationship between cell adhesion and actin cytoskeleton is intertwined as the dynamic equilibrium of actin polymerization and disassembly dictate the type and function of the resultant adhesions complexes[69]. qRTPCR of representative genes involved in cell adhesion confirmed the upregulation upon PBRM1 re-expression as determined by RNA-seq (Fig 2.6A). Immunofluorescence of F-actin demonstrated a significant increase in the percentage of cells with cortical actin cytoskeleton in Caki2+PBRM1 with respect to Caki2+Vector (Fig 2.6B and S3 Fig). The "cortical actin cytoskeleton" phenotype, a hallmark of epithelial cells[70,71] is believed to promote cell-cell contact and act as an important player in cellular morphogenesis[72–74]. In cancers of epithelial cell origin, the cortical actin cytoskeleton is disrupted and subsequently reorganized to facilitate cell migration and invasion[75–78]. Re-expression of PBRM1 also caused a significant inhibition of cell migration in an in vitro scratch test[79](Fig 2.6C), further validating PBRM1 in the regulation of cell adhesion and the maintenance of a more epithelial cell state.

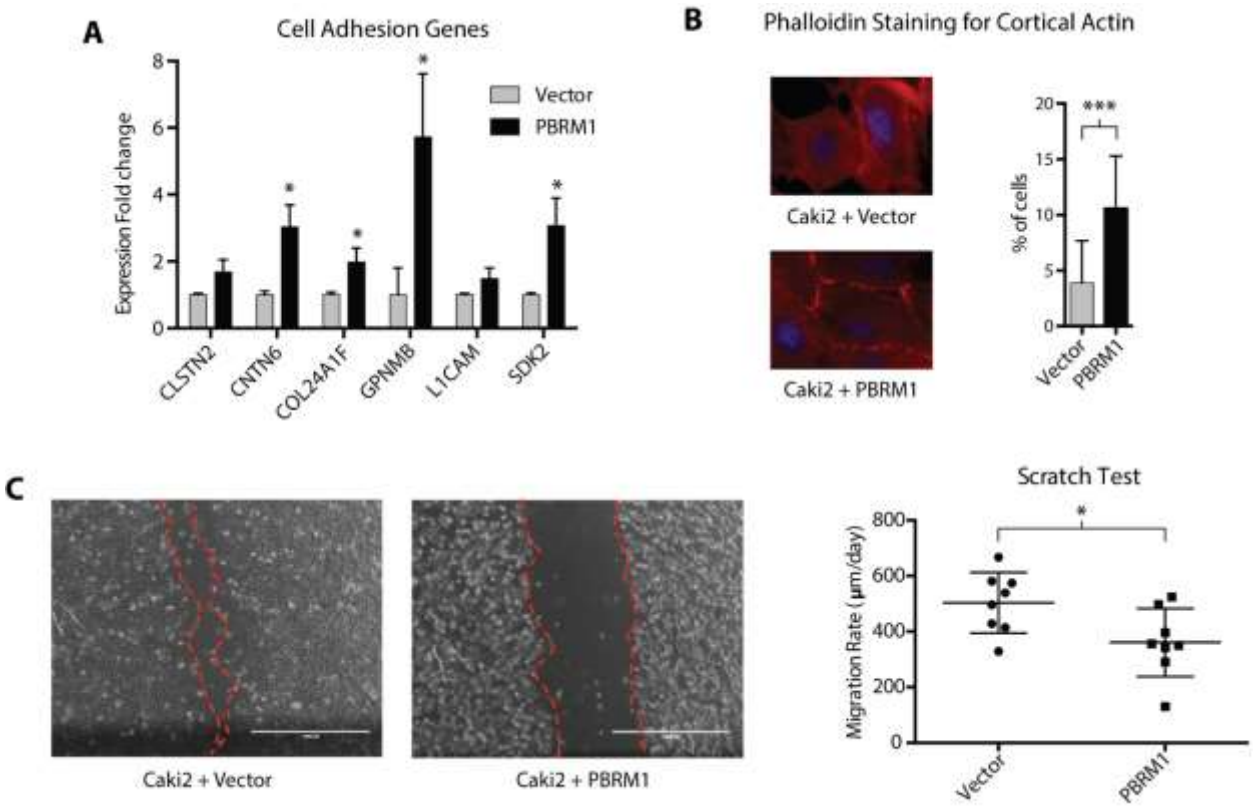

Figure 2-6 Alteration of cell-cell adhesion upon PBRM1 re-expression

A) Validating relative expression of genes regulating cell-cell adhesion (identified in RNA_seq data) in Caki2+Vectorand Caki2+PBRM1 cells by qRTPCR. A designation of * indicates $p < 0.05$ (Student *t*-test). n = 3 independent biological replicate experiments. Error bars represent s.e.m. B) Phalloidin staining of F actin (red channel) and DAPI staining of nucleus (blue channel) in Caki2+Vectorand Caki2+PBRM1 cells. A designation of *** indicates $p < 0.001$ (Fisher's exact *t*-test). n = 5 independent biological replicate experiments. Error bars represent s.e.m. C) *In vitro* scratch assay illustrating cell migration 24 hours after scratch wound inflection. A designation of * indicates $p < 0.05$ (Student *t*-test). n = 8 independent biological replicate experiments. Error bars represent s.e.m.

2.3.3 Differentially expressed genes in PBRM1 mutant tumors derived from patient samples

In order to further investigate the set of PBRM1 induced differentially expressed genes that may be clinically relevant, we compared the transcription profile of 499 ccRCC specimens deposited at TCGA. 354/499 specimens are reported to have no mutation in PBRM1 gene while the remaining 145 have mutations in the PBRM1 gene (Fig 2.7A and S5 Fig). A comparison between the transcription profile in (i) ccRCC patients with and without mutated PBRM1 and (ii) Caki2 cells with and without PBRM1 were originally envisioned to identify clinically relevant transcriptional targets of PBRM1. A major caveat, however, is that ccRCC is a heterogeneous cancer characterized by a metabolic shift[80] but not absolutely defined by a particular mutation or set of mutations. Therefore, ccRCC patients without mutated PBRM1 may have alterations in different genes that affect the same pathways, making the mutational status of PBRM1 irrelevant. Therefore, pathways uniquely regulated by PBRM1 in patient samples don't include classical metabolic pathways known to be universally deregulated in ccRCC (Fig 2.7A, S5 Fig). Of the genes co-regulated in patient samples and Caki2 cells, 286 were upregulated and only 42 were downregulated (FDR adjusted $p < 0.05$). The upregulated genes were involved in biological processes like cell adhesion (GO:0007155; GO:0007157; GO:0022409) and actin cytoskeleton organization (GO:0030036) indicating a unique role for PBRM1 in the expression of these genes that is not redundant with other tumor suppressor genes commonly mutated in ccRCC (Fig 2.7B). The changes in expression in ccRCC patients of representative genes involved in cell adhesion that were also altered upon PBRM1 re-expression in Caki2 cells were validated by qRTPCR (Fig 2.7C).

2.4 Conclusion

ccRCC is a metabolic cancer characterized by a shift to aerobic glycolysis facilitated by alterations in hypoxia transcriptional pathways. Fundamental pathways driving ccRCC (and therapeutics targeting these pathways) have been elucidated as a result of deciphering the mechanism of VHL, the most commonly mutated gene in ccRCC. Still, the loss of VHL and increase in HIF transcriptional activity is not sufficient to cause or drive cancer, indicating that additional factors are required for promoting oncogenesis, including the mutation of epigenetic regulators such as PBRM1. Using a ccRCC with a loss-of-function PBRM1 mutation, we found that re-expression of PBRM1 reverses some of the metabolic effects characteristic of ccRCC,

PBRM1 is a subunit of the SWI/SNF chromatin remodeling complex, which has been found to be involved in developmental transitions and the maintenance of cell-type specific transcriptional programs. It acts in conjunction with transcription factors and can be recruited in response to signaling; for PBRM1 this recruitment is likely tied to patterns of histone acetylation that define certain gene targets. PBRM1 upregulated genes include targets of retinoic acid receptor[81,82] and FOXO4[83,84] binding, in addition to HIF1α binding, all of which have been implicated in antagonizing ccRCC progression. To mechanistically understand the relevance of the downstream transcriptional targets we identified in ccRCC, the next step will be to define PBRM1 binding across the genome and determine cooperating transcription factors. This will further our understanding of ccRCC progression and uncover new therapeutic targets of PBRM1-mutated ccRCC.

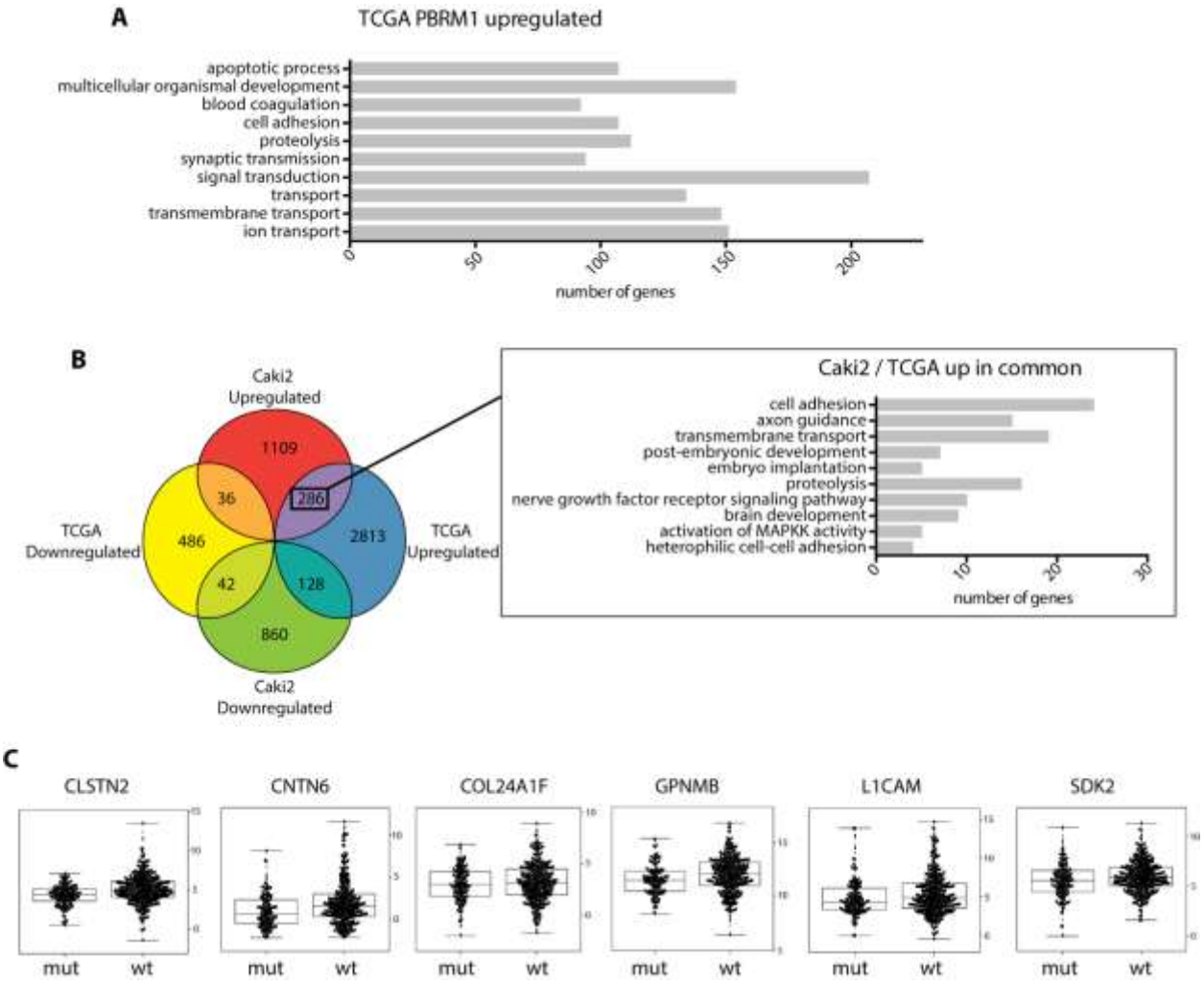

Figure 2-7 Comparative analysis of genes with differential expression in the presence of PBRM1 between ccRCC cells and ccRCC TCGA biospecimen

A) GO Biological Processes enriched by genes upregulated in TCGA ccRCC biospecimen with no PBRM1 mutation compared to ccRCC biospecimen with PBRM1 mutations. B) Venn diagram illustrating the number of differentially expressed genes overlapping between the 2 datasets (Genes with differential expression in 1. Caki2+PBRM1 with respect to Caki2+Vector and 2. ccRCC biospecimen with no PBRM1 mutation with respect to biospecimen with PBRM1 mutations). Inset illustrates GO Biological Processes enriched by upregulated genes in both (1) PBRM1 re-expressed Caki2 cells and (2) TCGA ccRCC biospecimen with no PBRM1 mutation. C) Box Plot showing the relative expression (log_2 RSEM) of genes involved in cell adhesion in TCGA biospecimen including increased glucose uptake, shifts in cholesterol esters, and increased insulin/PI3K signaling. In addition, we have found a unique role for PBRM1 in regulating cell adhesion genes as confirmed by co-occurrence in ccRCC tumors with PBRM1 mutation. Further work will be needed to determine whether this gene signature truly represents increased metastatic potential in PBRM1-mutant ccRCC, and ultimately, if this gene signature can be used to design or predict effective therapeutics.

CHAPTER 3. POLYBROMO-1 CONTRIBUTE TO CHROMATIN ASSOCIATION AND TUMOR SUPPRESSION IN CLEAR CELL RENAL CARCINOMA

The following chapter is reproduced and modified with permission from Porter, E.G., and Dykhuizen, E.C. *The Journal of Biological Chemistry*. 2017 Feb; 292(7): 2601-2610. doi 10.1074/jbc.M116.746875.

3.1 Introduction

Chromatin structure in eukaryotic cells is intricately tied to proper gene expression. The structure of chromatin is regulated by multiple factors, most prominently the post-transcriptional modification (PTM) of histones. Histone methylation, phosphorylation, and acetylation control DNA structure by altering nucleosome interaction with DNA and by recruiting effector proteins to specific regions of the genome. Effector proteins are targeted to these regions through chromatin recognition domains that can bind to these modifications[85,86]. One such chromatin recognition domain is the bromodomain (BD), a highly conserved 110 amino acid domain comprised of 4 α-helices that form a hydrophobic pocket that preferentially binds acetyl-lysines on histone tails[23,87]. One example of a BD containing protein is Polybromo-1 (PBRM1), which contains six consecutive BDs, two bromo-adjacent homolog (BAH) domains involved in protein-protein interactions[88], and a high-mobility group (HMG), which are typically DNA-interacting domains[17,89]. PBRM1 is a subunit of the Polybromo-1-associated BRG1- or hBRM-associated factors (P- BAF) complex, which is a member of mammalian SWI/SNF family of chromatin remodeling complexes along with the highly related BRG1-or hBRM-associated factors (BAF) complex (Fig3.1). These complexes use energy from ATP to insert, remove, or slide nucleosomes, effectively controlling DNA accessibility[90,91]. PBAF shares many of the same subunits as the BAF complex, and of the subunits exclusive for PBAF (PBRM1, ARID2, BAF45A, and BRD7), all except PBRM1 have closely related homologs in the BAF complex[92]. PBRM1, with a uniquely high number of chromatin interacting domains, is the defining subunit of the PBAF complex and is likely involved in unique function of PBAF not observed for BAF.

Recent studies have identified PBRM1 mutations in 40% of renal clear cell carcinomas (ccRCC), the most common form of kidney cancer, making PBRM1 the second most frequently mutated gene after Von Hippel-Lindau (VHL)[11,41,43,93]. Studies have indicated that PBRM1 acts as a tumor suppressor in ccRCC, though the mechanism is unclear[26,41]. Due to the presence of the multiple BDs, it is likely that PBRM1, via the BDs, targets PBAF to sites of histone acetylation at genes that need to be expressed for the regulation of proper cell growth. Exome sequencing of patient tumors indicates that PBRM1 mutations most often lead to the complete loss of PBRM1 expression; however, missense mutations are observed in approximately 15% of cases, leading to the expression of mutant forms of PBRM1[11]. By mapping the location of these mutations, we noticed a high incident of missense mutations in BD2 and BD4, though mutations have been identified in all the BDs except BD3 (Figure 3.2)[55]. While mutations are observed throughout the domains, many have been predicted to affect acetyl-lysine binding or domain stability[94]. Missense mutations that occur outside the domains include sites of post-translational modification such as phosphorylation or acetylation[95], as well as putative LLXXL nuclear hormone receptor binding sites that might contribute to PBRM1 function through other mechanisms.

Our lab recently characterized the effects of re-expressing wild type PBRM1 in Caki2 cells, a ccRCC cell line with loss of PBRM1 expression[26]. We observed that re-addition of PBRM1 significantly decreased the proliferative rate of these cells and upregulated genes involved in cell adhesion, apoptosis, and negative cell proliferation. Using the phenotype we characterized in Caki2 cells, we sought to define how each BD contributes to PBRM1 function in ccRCC. By creating PBRM1 mutants with a single inactive BD, we determined that the ability of PBRM1 to regulate growth and gene expression is completely reliant on BD2-mediated binding to chromatin, which appears to be facilitated through association with histone 3 lysine 14 acetylation (H3K14Ac). Additionally, we observed that mutation of BD1, BD4, BD5, and BD6 moderately affected PBRM1 chromatin association and tumor suppressor function, and that mutation of BD3 has no effect on PBRM1 function, perfectly agreeing with the mutational spectrum from patient tumors.

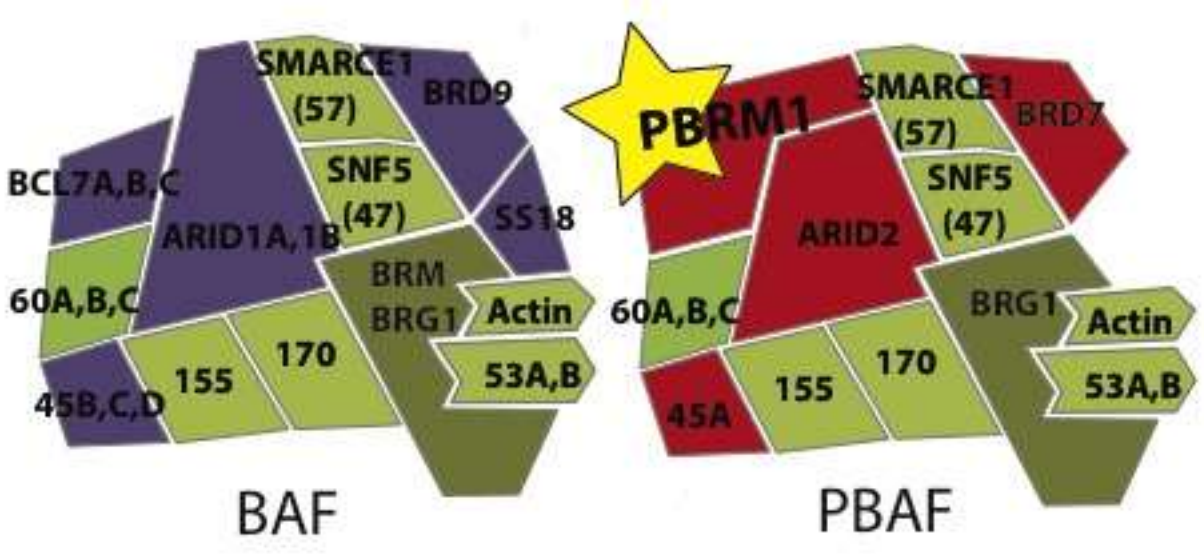

Figure 3-1 The BAF and PBAF complexes coexist in all cell types.

Though BAF and PBAF share many subunits (green), BAF exclusively contains ARID1A/B, BAF45B/C/D, BRD9, SS18, and BLC7A/B/C (purple), while PBAF exclusively contains PBRM1, ARID2, BAF45A, and BRD7 (red). PBRM1 is the most distinguishing feature of PBAF with no homolog in BAF.

3.2 Materials and Methods

3.2.1 Recombinant Protein Expression

Recombinant PBRM1 (His-tagged BD2 construct) was a gift from Nicola Burgess-Brown (Addgene plasmid # 39103). Mutagenesis of BD2N263A was accomplished with the Phusion Site-Directed Mutagenesis kit (Thermo Scientific, Rockford, IL). Wild type and mutated BD2 were expressed in BL21(DE3) competent E. coli cells (New England Biolabs Inc, Ipaswih, MA) and expression was induced by IPTG (1mM). Protein purification was performed by lysing cells resuspended in Binding Buffer (20mM Tris HCl, 150 mM NaCl, 20 mM Imidazole) with a probe sonicator and debris was pelleted by centrifugation. Supernatant was incubated with His60 Ni Superflow Resin. Resin was washed with Binding Buffer and protein was eluted in Elution Buffer (20mM Tris HCl, 150 mM NaCl, 500 mM Imidazole.)

3.2.2 Thermal Shift Assay

Purified protein (5 μg) was incubated with varying concentrations of H3K14Ac peptide (Anaspec, Fremount, CA) in 10 mM Hepes pH 7.0, 140 mM NaCl, along with 7.5X SYPRO Orange (Sigma Aldrich, St. Louis, MO) as described in Vivoli et al., 2014[96]. Differential scanning fluorimetry was performed with Applied Biosystem StepOneTM Real-Time PR System and Tm values were calculated using GraphPad Prism 6 graphing software.

3.2.3 Cell Culture

Caki 1 and Caki 2 cells (American Type Culture Collection Manassas, VA) were grown in McCoy's 5A media (Corning Mediatech, Inc., Manassas, VA) supplemented with 10% fetal bovine serum (Omega Scientific Inc. Tarzana, CA), 1% antibiotics (100 U/mL penicillin and 100 μg/mL streptomycin; Corning Mediatech, Inc., Manassas, VA), 1% nonessential amino acids (Corning Mediatech, Inc., Manassas, VA) and 1% L-glutamine (Corning Mediatech, Inc., Manassas, VA) at 37°C in a humidified atmosphere in a 5% CO_2 incubator. Serum starvation was accomplished by growing Caki1 (American Type Culture Collection Manassas, VA) in McCoy's 5A media (Corning Mediatech, Inc., Manassas, VA) supplemented with 0.2% fetal bovine serum (Omega Scientific Inc. Tarzana, CA), 1% antibiotics (100 U/mL penicillin and 100 μg/mL streptomycin; Corning Mediatech, Inc., Manassas, VA), 1% nonessential amino acids (Corning Mediatech, Inc., Manassas, VA) and 1% L-glutamine (Corning Mediatech, Inc., Manassas, VA) at 37°C in a humidified atmosphere in a 5% CO_2 incubator for 16h.

HEK-293T and HeLa cells (American Type Culture Collection Manassas, VA) were grown in DMEM media (Corning Mediatech, Inc., Manassas, VA) supplemented with 10% fetal bovine serum (Omega Scientific Inc. Tarzana, CA), 1% antibiotics (100 U/mL penicillin and 100 μg/mL streptomycin; Corning Mediatech, Inc., Manassas, VA), 1% Sodium Pyruvate (Corning Mediatech, Inc., Manassas, VA) and 1% L-glutamine (Corning Mediatech, Inc., Manassas, VA) at 37 °C in a humidified atmosphere in a 5% CO_2 incubator.

3.2.4 Constructs for Mammalian Cell Culture –

PBRM1 knockdown was performed by transfection with empty pLKO.1 vector or shPBRM1 pLKO.1 (TRCN0000015994, ThermoFisher Scientific, Waltham, MA). PBRM1

mutagenesis was accomplished with In-Fusion®HD cloning kit (Clontech Laboratories, Inc. Mountain View, CA). Mutagenesis was performed on each BD using pBabepuroBAF180 (a gift from Ramon Parsons Addgene plasmid # 41078). After confirming proper mutation using sanger sequencing, full length PBRM1 containing a single point mutation was cloned from pBabepuroBAF180 into tet-inducible conditional lentiviral vector TetO-FUW (a gift from Rudolf Jaenisch Addgene plasmid # 20323) which was used with pLenti CMV rtTA3 Hygro (w785-1) (a gift from Eric Campeau Addgene plasmid # 26730) for tetracycline inducible expression.

3.2.5 Lentiviral Infection

HEK293T cells were transfected with lentivirus constructs along with packaging vectors pMD2.G and psPAX2. After 48 h, the supernatant was collected and concentrated by ultracentrifugation (17,300 rpm for 2 h) and resuspended in 200 µL PBS. Cells were infected with concentrated virus using spinfection (1500 rpm in swing bucket centrifuge for 1 h). Fresh media was added 16 h after infection and cells were allowed to recover for 24 h before selection. Cells were selected for 2 weeks with puromycin (0.6µg/mL) (Sigma Aldrich, St. Louis, MO) and hygromycin (200 µg/ml) (Corning Mediatech, Inc., Manassas, VA). Cells were cultured with 2 µg/mL doxycycline (EMD chemicals, San Diego, CA) for 72 h prior to experiments to induce protein expression.

3.2.6 Sequential Salt Extractions –

Cells ($1x10^7$ cells) were harvested and washed with PBS for each cell line. Cells were resuspended in 1 mL of Buffer A (0.3 M sucrose, 60 mM KCl, 60 mM Tris pH 8.0, 2 mM EDTA, 0.5% NP-40, + protease inhibitors) and rotated at 4 °C for 10 min. Samples were spun down at 6500 xg for 5 min. The pellet was resuspended in 200 µL of mRIPA (50 mM Tris pH 8.0, 1% NP-40, 0.25% sodium deoxycholate, + protease inhibitors) by pipetting up and down 15 times and incubated on ice for 2 min. Then the sample was centrifuged for 3 min at 6500 xg. The supernatant was saved in a separate tube and labeled as the 0 mM fraction. The pellet was sequentially resuspended in 200 µL of mRIPA with increasing NaCl concentrations (100 mM, 200 mM, 300 mM, 400 mM, and 500 mM). The process for 0 mM was repeated for each salt concentration. Bolts LDS sample buffer (Invitrogen) with 10% Beta-Mercaptoethanol (Amresco, Solon, OH) was added to each sample and 30 µL each fraction was loaded onto a 4-12% gradient gel (Invitrogen)

for immunoblot analysis of the BAF subunits of interest. Image J was employed to quantitate the protein bands.

3.2.7 Growth Curves

Cells ($3x10^5$) were plated onto a 60 mm plate with 3 mL of media containing doxycycline (2 µg/mL). Cells were grown for 72 hours before the cells were trypsinized and counted with the Moxi cell counter (Orflo, Ketchum, ID). Cells ($3x10^5$) were replated. This was repeated three times for each cell line and results were averaged.

3.2.8 Peptide Pull Down

Streptavidin Agrose Ultra Performance resine (15µl) (Solulink, San Diego, CA) was washed three times with Binding Buffer (0.5 mM DTT, 150 mM NaCl, 50 mM Tris). The resin was resuspended in 300 µL of binding buffer with 2 µg of biotin labeled peptide (Anaspec, Fremount, CA) and samples were rotated at 4 °C for 1 h.. The following peptides were used: H3 (21-44), H3K9Ac (1-21), H3K14Ac(1-21), H3K18Ac(1-21), H3K23Ac(15-23), H3K27Ac(21-44), H3K9/14Ac (1-21), H3K 14,18,23,27 (1-30). Cells ($1.5x10^6$ were harvested and lysed in 500 ul of Buffer A (25 mM Hepes pH 7.6, 25 mM KCl, 5 mM $MgCl_2$, 0.05mM EDTA, 0.1% NP-40, and 10% glycerol) and centrifuged. The nuclei were then resupended in 250 µL of IP buffer (25 mM Tris pH 8, 300 mM NaCl, 1 % NP-40, 1 mM EDTA + protease inhibitors) and rotated at 4 ºC for 10 min. The samples were then spun down at 15,000 rpm for 5 min. The 250 µL of lysate was added to the peptide and resin solution and rotated overnight. The samples were washed for 10 min three times in binding buffer. The resin was resuspened in SDS loading buffer and boiled for 5 min. Nuclear lysate input, along with the samples were processed for immunoblot analysis.

3.2.9 Real-time polymerase chain reaction (RT-PCR)

Total RNA was converted into cDNA using iScript Reverse Transcription Kit (Bio-Rad Laboratories, Inc., Hercules, California). Primers used were published in[26]. Real-time PCR was performed using a Bio-Rad CFX Connect Real-Time system and a FastStart Universal SYBR Green Master (Roche, Indianapolis, IN). The results were analyzed using the $2(-\Delta\Delta CT)$ comparative method. Each sample was tested in quadruplicate.

3.2.10 Chromatin Immunoprecipitation (ChIP)

Cells were harvested and counted. Cells ($6x10^6$) were resuspended in 10 mL of PBS with 1% formaldehyde (Thermo Scientific, Rockford, IL) and allowed to crosslink for 8 min. Crosslinking was quenched by the addition of glycine to a final concentration of 125 mM and incubated for 5 min. Cells were washed three time with PBS and resuspended in 10 mL of Rinse Buffer 1 (50 mM Hepes pH 8, 1 mM EDTA, 0.5 mM EGTA and 100 mM NaCl) and incubated on ice for 5 min and then pelleted by centrifugation at 600xg for 3 mins. Cells were resuspended in 5 mL of Rinse Buffer 2 (50 mM Hepes pH 8, 140 mM NaCl, 1mM EDTA, 10% Glycerol, 0.5% NP-40, and 0.25% Triton X 100) and incubated on ice for 5 mins. Cells were then pelleted by centrifugation (600xg) at 4 ºC. The cells were then resupended in 1 mL ChIP Immunoprecipitation buffer (50 mM Hepes pH 7.5, 300mM NaCl, 1mM EDTA, 1% Trition X100, 0.1% DOC, 0.1% SDS + protease inhibitors.) Samples were sonicated with a Branson Sonifier 250 probe sonicator for 7 mins in 30 sec burst followed by 30 sec on ice at a duty cycle of 35% and an output of 3. After sonication, debris was pelleted by centrifugation at 20,000xg for 10 mins at 4 ºC. Supernatant was collected and 450 µg was precleared with 15 µl of Dynabeads Protein G (Thermo Scientific, Rockford, IL). Lysate (200 µg) was incubated with 2 µg of antibody for 3 hr followed by an hour incubation with 15 µl of washed Dynabeads. Following incubation, beads were washed two times for 5 min with ChIP IP buffer, followed by washes with DOC Buffer (10 mM Tris pH 8, 250 mM LiCl, 0.5% NP-40, 0.5% DOC) and 1x TE buffer. Beads were rotated at room temperature for 20 min in 150 µl Elution Buffer (1% SDS, 100 mM $NaHCO_3$) for 20 min. The elution step was repeated a second time. Following elution, NaCl was added to a final concentration of 200 mM and samples were uncrosslinked at 65 ºC overnight. EDTA (10 mM) and Tris (40 mM) were added to each sample along with 60 µg of RNase (Amresco LLC, Solon, OH) and 40 µg of Proteinase K (New England Biolabs Inc, Ipaswih, MA). Samples were incubated at 37 ºC for 30 min followed by 55 ºC for 2.5 hr. DNA was isolated using phenol chloroform extraction followed by DNA precipitation. The DNA pellets were resupsended in 20 µl of 1x TE and RT-PCR was performed as described above.

3.2.11 ChIP Primers

CNTN6 locus chr3:1,134,629-1,445,278 length: 310,649 bp

1: Chr3:1,134830-1134940 +201 from TSS

F: GCTGTGTCTGCTGCAATGAG, R: CAGTGACTTCTCCCCCAACC

2: Chr3:1,135824-1135958 +1195 from TSS

F: TTGCTTGTTTTGAGCAATTTTCAT, R: AGGAGGGAAAAAGAGTCTGCT

3: Chr3:1,138124-1138273 +3495 from TSS

F: TCTTTCTTTTCTTCAGGATCACCA, R: GTGGCAAACAAGAGAACAAGT

4: Chr3:1,138324-113956 +3695 from TSS

F: GCCTCTTTGTACTTCAGTTTCCC, R: GAGTGCTTCTTAATTGCCAGG,

3.2.12 Immunoblot

Protein samples from cell lysates, SSE, IPs, and peptide pull downs were denatured for 10 min at 100 °C, separated on a 4-12% SDS-polyacrylamide gel (Invitrogen), and transferred to a nitrocellulose membrane (Millipore). The membrane was blocked with 5% bovine serum albumin (VWR, Batavia, IL) in PBS containing 0.1% Tween-20 (PBST) for 30 min at room temperature and then incubated in primary antibodies overnight at 4 °C. The primary antibodies were detected by incubating the membranes in goat-anti-rabbit or goat-anti-mouse secondary antibodies (LI-COR Biotechnology, Lincoln, NE) conjugated to IRDye 800CW or IRDye 680 respectively for 1 h at room temperature, and the signals were visualized using Odyssey Clx imager (LI-COR Biotechnology, Lincoln, NE).

3.2.13 Antibodies

ARID1A: Santa Cruz sc-32761 (immunoblot)

ARID2: Santa Cruz sc-81050 (immunoblot)

PBRM1: Bethyl A301-591A (immunoblot)

Bethyl A301-590A (immunoprecipitation, ChIP)

SS18: Santa Cruz sc-28698 (immunoblot)

IgG Rabbit: Santa Cruz sc-2027 (ChIP)

H3K14Ac: Millipore 07-353 (ChIP)

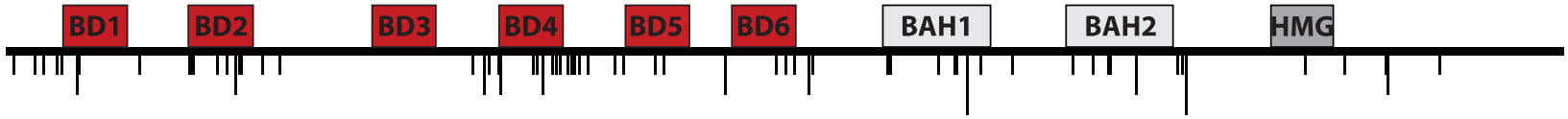

Figure 3-2 Missense mutations in PBRM1 identified from ccRCC patient samples indicated with black bars. Data obtained from the COSMIC database[55].

3.3 Results

3.3.1 The Contribution of Individual Bromodomains to the Tumor Suppressor Function of PBRM1

As a subunit of the PBAF chromatin remodeling complex, PBRM1 presumably acts as a tumor suppressor by controlling chromatin structure at specific regions of the genome. PBRM1 contains six tandem BDs, which are predicted to bind acetylated lysines in order to target chromatin remodeling activity to regions of histone acetylation[23]. Due to the frequency of missense mutations found in the BDs (Fig 3.2), we predict that even a mutation within a single BD can alter the functional properties of PBRM1. To examine how each individual BD contributes to the tumor suppressive function of PBRM1, we utilized our Caki2 PBRM1 doxycycline-inducible system[26] and systematically mutated each BD to disrupt acetyl-lysine binding. The highly conserved asparagine located at the end of the αB helix forms a hydrogen bond with the acetylated lysine, anchoring it in the binding pocket[23,24,87]. BD1 is unusual in that it has a tyrosine at this position instead of an asparagine; however, it has been shown to perform the same role[24]. To confirm this role in vitro we performed a thermal shift assay[96] with recombinant BD2 and H3K14Ac peptide, a confirmed ligand for this BD[24]. A reproducible dose-dependent shift in the melting temperature (Tm) of the BD was observed upon incubation with H3K14Ac peptide (Fig 3.3A). In contrast, the Tm of the asparagine mutant (BD2N263A) did not increase upon incubation with the H3K14Ac peptide (Fig 3.3A). It is also important to note that the Tm of the mutant was not significantly shifted compared to wild type, implying that this conserved asparagine is critical for acetyl-lysine binding but not domain stability, which was noted previously for BDs from BRD4[97]. To study the role of each BD, we created eight cell lines mutating this highly conserved residue in the six BDs of PBRM1: Caki2+Vector, Caki2+PBRM1WT, Caki2+PBRM1mBD1 (Y127A), Caki2+PBRM1mBD2 (N263A), Caki2+PBRM1mBD3 (N463A), Caki2+PBRM1mBD4 (N601A), Caki2+PBRM1mBD5 (N739A), and Caki2+PBRM1mBD6 (N855A). PBRM1 expression was even across the seven lines after treatment with doxycycline (Fig 3.3B). In addition, we confirmed that all the mutants were incorporated into the complex with equivalent efficiency by immunoprecipitation of the PBRM1 followed by immunoblotting for BRG1, the ATPase subunit of the PBAF complex (Fig 3.3B).

Figure 3-3 Proliferation and gene expression is altered in PBRM1 BD mutant cell lines

A) Thermal shift stability assays indicate that mutation of conserved asparagine 263 to alanine in recombinant BD2 abrogates binding to an H3K14Ac peptide. B) Immunoblot analysis of protein expression level of PBRM1 and BRG1 in the BD mutant cell lines from lysates (top) and PBRM1 immunoprecipitations (bottom). C) Proliferation rate of BD mutant cell lines normalized to Caki2+Vector cells. n = 3 independent biological replicates D) Transcriptional analysis by qRTPCR of PBRM1 dependent genes (IGFBP4 and CNTN6) in BD mutant cell lines normalized to Caki2+Vector cells. n = 6 independent biological replicates. A designation of * = $p < 0.05$, ** = $p < 0.01$, *** = $p < 0.001$, **** = $p < 0.0001$ (paired Student t-test). Error bars represent standard deviation.

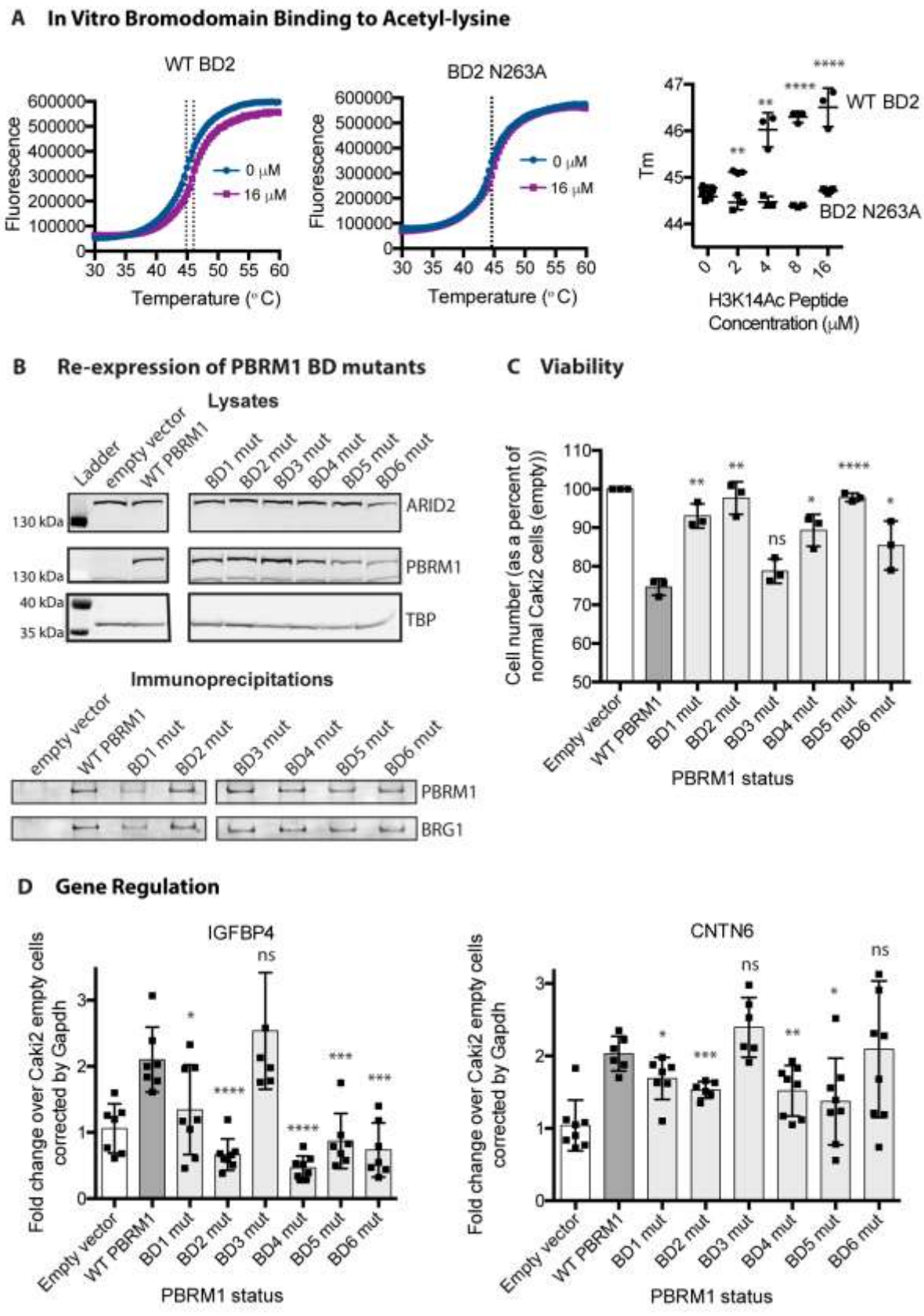
A In Vitro Bromodomain Binding to Acetyl-lysine
WT BD2
BD2 N263A
Fluorescence
Temperature (°C)
0 μM
16 μM
Tm
WT BD2
BD2 N263A
H3K14Ac Peptide Concentration (μM)
B Re-expression of PBRM1 BD mutants
Lysates
Ladder
empty vector
WT PBRM1
BD1 mut
BD2 mut
BD3 mut
BD4 mut
BD5 mut
BD6 mut
ARID2
PBRM1
TBP
130 kDa
40 kDa
35 kDa
Immunoprecipitations
BRG1
C Viability
Cell number (as a percent of normal Caki2 cells (empty))
Empty vector
PBRM1 status
D Gene Regulation
IGFBP4
CNTN6
Fold change over Caki2 empty cells corrected by Gapdh
ns

Previously, we observed that re-expression of wild-type PBRM1 led to a significant decrease in growth of the Caki2 cells[26]. To determine if individual BDs contribute to the tumor suppressive phenotype of PBRM1, we performed growth curves for Caki2+Vector and Caki2+PBRM1WT, along with the six mutants. Surprisingly, cell proliferation compared to Caki2+PBRM1WT significantly increased when we mutated a single amino acid in five of the six BDs (Fig 3.3C). Mutation of BD1, BD2, BD4, and BD5 almost completely obliterated the tumor suppressive phenotype, whereas BD6 had moderate effects on the growth rate. Mutation of BD3 had no effect on the growth of cells, and this mutant was indistinguishable from Caki2+PBRM1WT. This dramatic effect on growth signifies the importance of individual BDs in the functionality of PBRM1, while also implicating that the BDs are working in a cooperative manner to suppress tumor growth.

From our previous study we determined that PBRM1 controls genes involved in pathways that influence cell growth and mobility[26]. If PBRM1 controls growth by regulating gene expression, we would expect that the BD mutations that disrupted growth suppression would be crucial in gene expression. To examine how the BD mutants influence gene expression, we chose CNTN6 and IGFBP4, two genes upregulated upon PBRM1 re-expression in Caki2 cells, which are involved in cell adhesion and metabolism respectively[26]. Mutation of BD2 and BD4 greatly impaired the ability of PBRM1 to upregulate gene expression, and mutation of BD1 and BD5 moderately impaired gene upregulation, and mutation of BD3 had no effect (Fig 3.3D). BD6 mutation significantly inhibited IGFBP4 upregulation but had no effect on CNTN6. Again, this data suggests a cooperative role for multiple BDs at all PBRM1 sites of action; however, results for BD6 suggest that this domain may only be required at a subset of PBRM1 gene targets.

3.3.2 The Effect of PBRM1 on the Affinity of PBAF to Bulk Chromatin

While we have shown that the individual BDs are important for tumor suppression and gene expression, it is unclear what global binding properties are dependent on the BDs. We first examined if PBAF has distinguishable chromatin binding characteristics compared to BAF. Although BAF and PBAF share many of the same subunits, PBRM1 contributes six additional chromatin interacting domains to the complex, leading us to the hypothesis that it binds more tightly to chromatin. Using a sequential salt extraction (SSE), we quantitated the relative binding strength of the BAF and PBAF complexes to chromatin in Caki1 cells, a ccRCC cell line

expressing wild type PBRM1. After isolating nuclei, we eluted nuclear proteins from the insoluble chromatin fraction using increasing concentrations of salt. The resulting fractions were run on a gel for immunoblot analysis of ARID1A, a BAF specific subunit, and PBRM1, the PBAF-specific subunit. The majority of PBRM1 eluted at 300-400 mM NaCl whereas the peak of elution for ARID1A was at 200-300 mM NaCl, indicating PBAF inherently binds tighter to chromatin than BAF (Fig 3.4A). This was not unique to ccRCC, as the same effect was observed in HeLa cells (Fig 3.4B). We next examined if this increase in affinity of PBAF over BAF was dependent on PBRM1. We repeated this experiment with Caki2+Vector and Caki2+PBRM1 and blotted for ARID2 (Fig 3.1) to identify PBAF in the absence of PBRM1. In Caki2+Vector, ARID2 elution peaked at 200-300 mM NaCl fraction, appearing very similar to the ARID1A (BAF) elution pattern. Upon re-expression of PBRM1, ARID2 elution shifts to a higher salt concentration, indicating that in the absence of PBRM1 PBAF still associates with chromatin, but its affinity now appears more similar to BAF, as indicated by ARID1A staining. (Fig 3.4C). To validate that this is a general role for PBRM1 in the PBAF complex, and not unique to Caki2 cells, we knocked down PBRM1 in Caki1 and observed a shift in the ARID2 elution to a lower salt concentration, similar to what was observed in Caki2 cells (Fig 3.4D). To rule out the possibility that these observations are a result of differential growth rates due to loss or gain of PBRM1, we performed SSE on serum starved Caki1 cells and confirmed that the changes in chromatin affinity were inherent functions of PBRM1 and not reflective of alterations in cell cycle (Fig 3.4E) In total, these results indicate that PBRM1 is responsible for the previously unobserved increased strength of chromatin binding detected for PBAF compared to BAF.

3.3.3 The Contribution of Individual Bromodomains to the Affinity of PBAF to Bulk Chromatin -

After defining the chromatin binding properties of PBRM1 within the PBAF complex, we wanted to use this readout to determine if the BD mutations that disrupt PBRM1 function also disrupt the global association of PBAF with chromatin. We performed SSE on our six BD mutant lines and compared them to the SSE profile for wild type PBRM1 (Fig 3.5A). Since we saw the largest differential in elution at 200 mM between ARID1A and PBRM1 in Caki1 (Fig 3.4A) or between ARID2 with and without PBRM1 re-expression in Caki2 (Fig 3.4C), we compared the amount of PBRM1 eluted from chromatin at this salt concentration across all seven cell lines. In

cells containing wildtype PBRM1, approximately 18% of the complex elutes in the 200mM fraction.

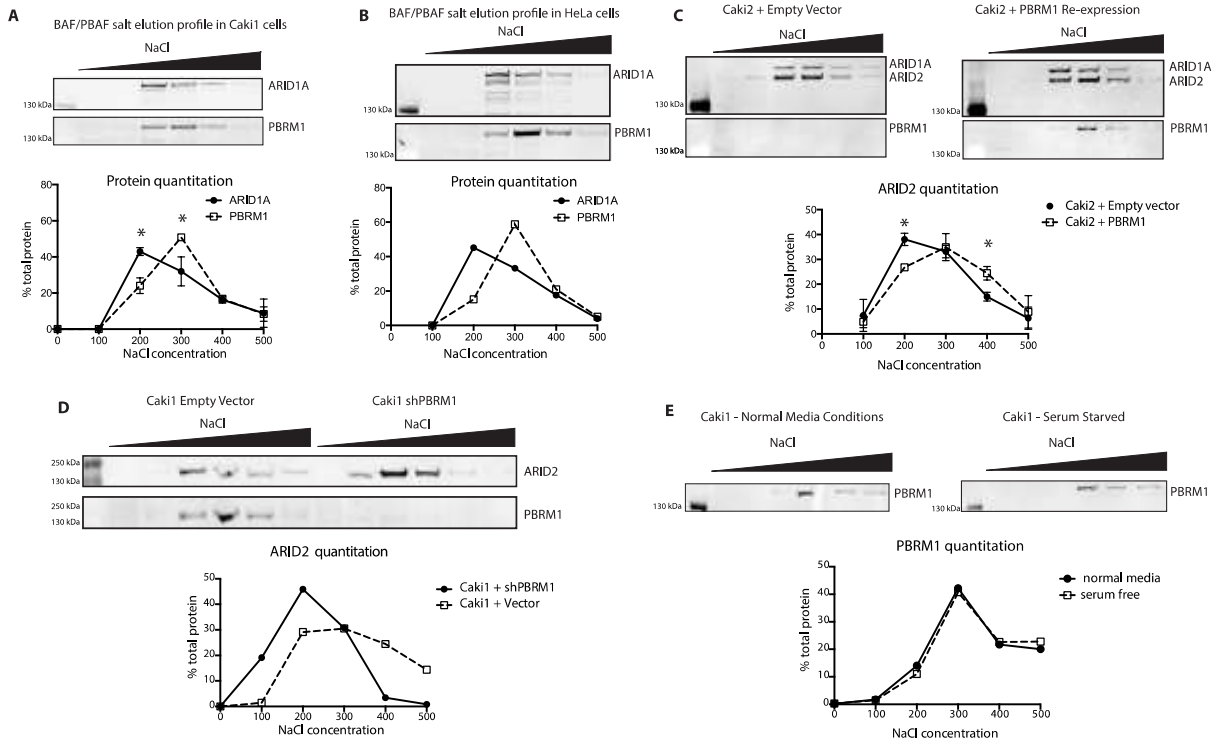

Figure 3-4 Chromatin binding properties of BAF and PBAF complexes.

A) Analysis of binding affinity to chromatin of the BAF (ARID1A) and PBAF (PBRM1) in Caki1 cells by sequential salt extraction (SSE). n = 2 independent biological replicates. B) SSE analysis of BAF and PBAF affinity in Hela cells. C) Analysis of PBAF affinity to chromatin in Caki2+Vector and Caki2+PBRM1WT cells indicated by the elution of ARID2. n = 4 independent biological replicates D) Analysis of PBAF affinity to chromatin Caki1+Vector and Caki1+shPBRM indicated by the elution of ARID2. E) Comparison of PBAF elution in Caki1 cells grown under normal conditions or serum starved conditions for 16h. A designation of * = p <0.05 (paired Student *t*-test). Error bars represent standard deviation.

However, mutation of a single asparagine in BD2 leads to approximately 33% of the PBAF complex eluting in 200mM salt, similar to that observed upon deletion of PBRM1 (Fig 3.5B). While these changes may appear small, they are very consistent between experiments and can be quantified for statistical analysis. Further validating this approach, a similar phenotype was recently observed in live cells for the BD2 mutant using fluorescence recovery after photobleaching (FRAP) using GFP-tagged PBRM1[98]. Mutation of BD1, BD4, and BD5 also significantly increased the amount of PBRM1 eluted at 200 mM, while mutation of BD6 slightly

increased the amount of PBRM1 eluted, although it was not statistically significant. In contrast, the mutation of BD3 caused no alteration in PBRM1 elution from chromatin, consistent with the cell proliferation, transcriptional profile and patient mutation data observed for the BD3 mutant.

3.3.4 PBRM1 Binding to Acetylated Histone Peptides

Several studies have attempted to determine the specific targets of individual PBRM1 BDs using recombinantly expressed single BDs with acetylated peptides but have shown very little agreement, except that BD2 binds H3K14Ac[22,24,25,99]. We decided to pursue a more holistic approach to define the affinity of the full PBRM1-containing complex to acetylated histone peptides. We incubated nuclear lysate from HeLa cells with biotin labeled acetylated histone peptides bound to streptavidin beads. We found that only H3K14Ac peptides are able to specifically enrich PBRM1 from lysates (Fig 3.6A), in agreement with in vitro studies defining a specific association between BD2 and H3K14Ac[22,24,25,99]. We confirmed this interaction in our PBRM1 re-expression system and determined that wild type PBRM1 preferentially binds H3K14Ac over unmodified H3 peptides, indicating PBRM1 binding to histones is at least partly mediated through H3K14 acetylation (Fig 3.6B). Using SS18, a BAF specific subunit (see Fig 3.1), we determined that binding of H3K14Ac is PBAF specific as SS18 showed no preference for the H3K14Ac peptide over the H3 peptide (Fig 3.6B), even though BAF also contains BDs with in vitro binding to H3K14Ac peptides[22]. Because BD2 has been shown to bind H3K14Ac in vitro and because mutation of BD2 most dramatically impedes PBRM1 function, we investigated the affinity of PBAF complexes from lysates for this acetylation mark. To determine if this association is mediated through BD2, we also incubated Caki2+PBRM1 mBD2 nuclear lysates with the peptides and found that mutation of BD2 leads to an approximately 50% loss in PBRM1 enrichment by the H3K14Ac peptide (Fig 3.6C). The loss of binding is not complete, likely due to promiscuous weak binding of the other PBRM1 BDs to acetylated peptides, including H3K14Ac peptides [22]. We tested this possibility by measuring the enrichment from lysates of PBRM1 to H3K14Ac peptides with additional acetylation marks. We did not observe a significant increase in enrichment upon incubation with H3 peptides containing acetylation at K9 and K14 but did see a dramatic increase in enrichment using H3 peptides with acetylation at K14, K18, K23, and K27. Further, mutation in any of the BDs, except BD3, reduces the affinity of PBRM1 to histone peptides containing multiple acetylated lysines. Together, this suggests that PBAF is targeted to

H3K14Ac via specific association with BD2 and that the association of BD1, BD4, BD5 and potentially BD6 to additional acetylation marks is required for maximal affinity of the PBAF complex to chromatin at sites of gene regulation.

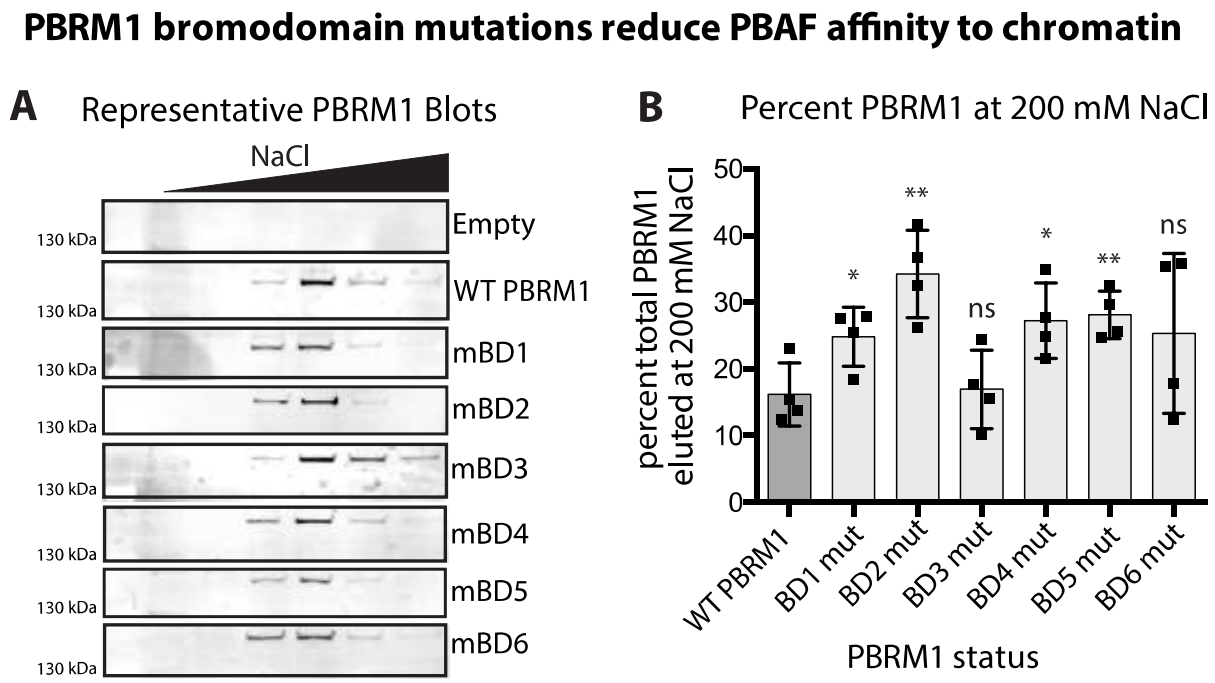

Figure 3-5 Chromatin binding properties are altered in PBRM1 BD mutants.

A) Representative immunoblot analysis of SSE assays designed to assess relative chromatin binding affinity of BD mutant PBRM1 re-expressed in Caki2 cells B) Analysis of binding affinity to chromatin by SSE of PBRM1 in the BD mutants indicated by the percentage of PBRM1 eluted at 200 mM NaCl. n = 4 independent biological replicates. A designation of * = $p < 0.05$, ** = $p < 0.01$ (paired Student *t*-test). Error bars represent standard deviation.

3.3.5 The Role for Individual Bromodomains in PBRM1 Localization to a Discrete Genomic Site

To extend these results to PBRM1 targeting at a discrete genomic locus in vivo, we performed a ChIP-Seq for PBRM1 in Caki2 cells (unpublished data). We did not observe PBRM1 enrichment at IGFBP4, indicating that IGFBP4 may be an indirect transcriptional target of PBRM1; however, we did identify a site of PBRM1 enrichment 3 kb downstream of the transcription start site (TSS) of CNTN6. We further confirmed both H3K14Ac and PBRM1 enrichment at CNTN6 (Fig 3.6A) using ChIP-qPCR and identified maximal enrichment of both H3K14Ac and PBRM1 binding at 200 bp downstream of the TSS. This is in agreement with published ChIP-Seq data

indicating that H3K14Ac is highest in the 1 kb region directly following the TSS[100]. Using this primer set, we performed PBRM1 ChIP-qPCR experiments with the BD mutations to define how mutations in the BDs affect PBRM1 enrichment in vivo. We found good agreement with the SSE and peptide pulldown assays indicating a strong role for BD2 and BD5 in PBRM1 binding, some role for BD1, 4, and 6, and no role for BD3 (Fig 3.6B).

3.4 Discussion

PBRM1 is a tumor suppressor frequently mutated in ccRCC[11,41,43,93]. Mutations in BAF subunits such as ARID1A lead to total loss of protein expression[10,101]; in contrast, PBRM1 is expressed with missense mutations in about 15% of ccRCC patients with PBRM1 mutations[11]. By mapping these missense mutations, we observed that point mutations in PBRM1 cluster in the BDs, suggesting that individual BDs may be critical for PBRM1 to act as a tumor suppressor. In this study, we have demonstrated that four of the six BDs of PBRM1 work in conjunction and are all individually necessary for full PBRM1 activity. By examining how individual domains contribute to the function of PBRM1, we have found that growth suppression, gene expression, chromatin binding, and acetylation recognition was completely obstructed by the loss of BD2 function, indicating that this BD is the most critical for PBRM1 function. This correlates with data from yeast, in which the second BD of PBRM1 homolog RSC4 binds H3K14ac and is the most essential for viability in yeast[102].

In addition to BD2, patient mutations have been observed in BD1, BD4, BD5 and BD6. In accordance with this, mutation of BD1, BD4, and BD5 in our cell-based system consistently decreased the PBRM1 activity for all of the phenotypes we explored, and BD6 decreased the effectiveness of PBRM1 in some settings. Mutation of the sixth BD moderately impaired growth suppression, but there was no significant change in affinity of the complex. Additionally, loss of BD6 significantly affected the transcription level of IGFBP4, a metabolism gene, but not CNTN6, a gene important in cell adhesion. Intriguingly, the structure of BD6 is the most structurally unique of the six PBRM1 BDs, as it contains an extra helix and has an unusually short ZA loop[22,103]. The length of the ZA loop is implicated to influence BD specificity, and this suggests that BD6 may recognize a unique substrate compared to the other PBRM1 BDs. The only histone peptides recognized by BD6 include acetylation marks on H2A and H2B core residues, although these interactions are weak[22], raising the possibility that BD6 may be involved in a function separate

from acetyl-lysine binding. Finally, mutation of BD3 seemed to have no effect on any of the phenotypes we explored, which was also consistent with patient data, in which no mutations were observed in this domain. Though the hydrophobic pockets of the BDs are conserved, the electrostatic potential of the surface of BD3 has a positively charged surface that may prevent interaction with histone tails[22]. Therefore, BD3 may bind to non-histone proteins that are not relevant for PBRM1 function in ccRCC. Alternatively, since only the individual domains have been crystallized and the structure of the whole protein is unknown, it is possible that BD3 is buried in PBRM1 and not involved in acetyl-lysine binding at all.

From the data in this study, it is clear that BD2 is pivotal for PBRM1 function, BD1, BD4, and BD5 all contribute significantly to PBRM1 function, and, BD6 and BD3 showed either inconsistent or no effect on PBRM1 activity. Previous studies that attempted to differentiate acetylation marks associated to with the individual domains [22,24,25] resulted in broad and conflicting results. Certain BDs appear to be promiscuous, binding to almost any acetylated peptide; in particular, BD1, BD3 and BD4 bound a wide array of peptides from all the histones[22]. In contrast, the same study only identified three peptides that interacted with BD2, one of which being H3K14ac, an interaction that has been well characterized[22,24,99]. It is important to note that BDs typically bind weakly to acetylation targets (10-100 μM) and are usually found in proteins or complexes with multiple chromatin binding domains, such as additional BDs, chromodomains, PHD fingers, high mobility group, and AT-rich interactive domains[22]. This suggests that for proper BD function, they work in conjunction with additional binding domains to obtain optimal affinity and specificity for chromatin targets. With our system, we have demonstrated that PBRM1 association with H3K14ac is dependent on BD2. From this data, we propose that BD2 initiates binding of the complex and anchors the complex to chromatin, allowing BD1, BD4, BD5, and possibly BD6 to bind to nearby acetyl-lysine residues (Figure 3.6).

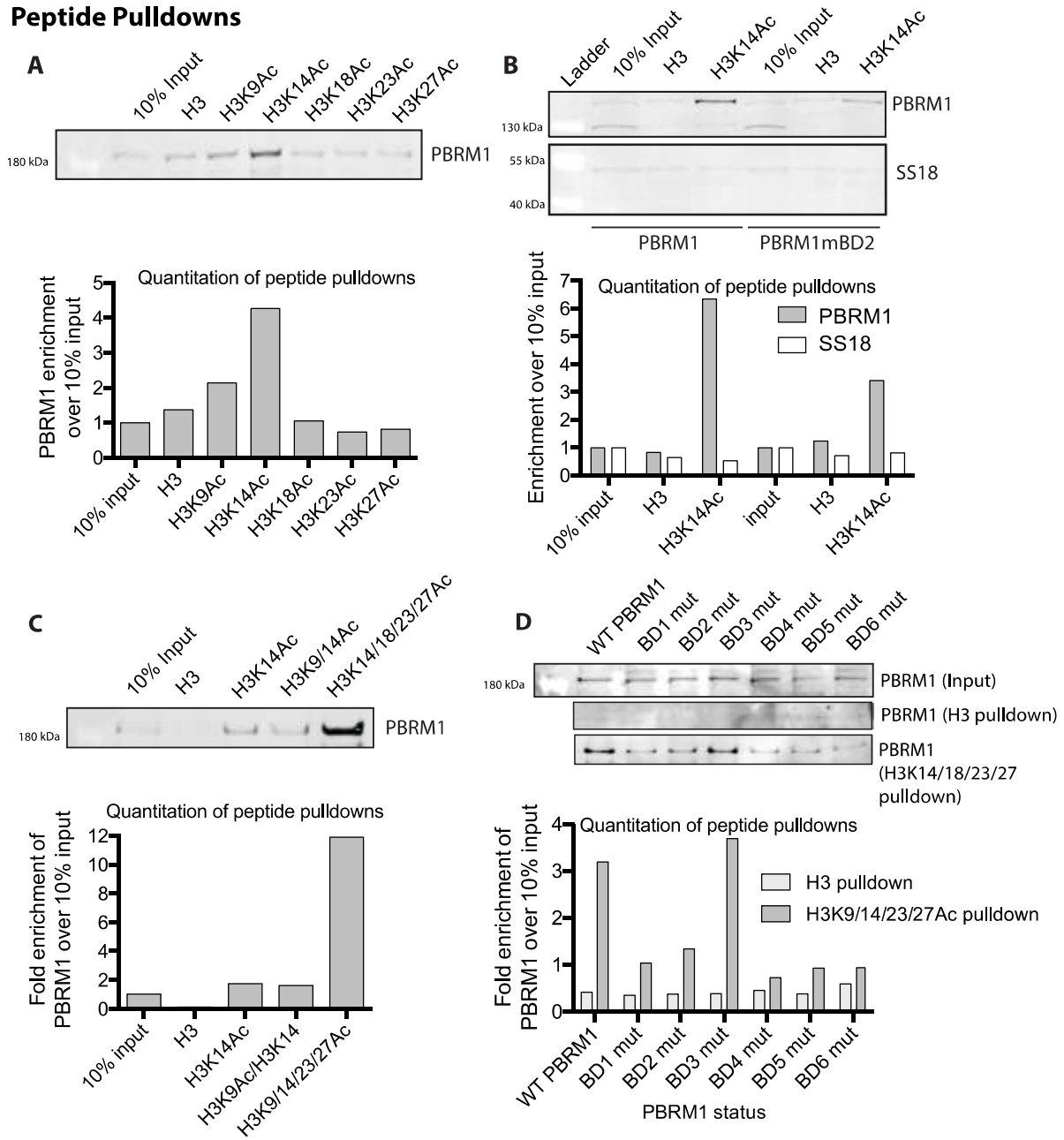

Figure 3-6 PBRM1 binding to acetylated histone peptides.

A) Immunoblot analysis of PBRM1 after peptide pull downs with H3 or singly acetylated peptide from HeLa nuclear cell lysate. B) Immunoblot analysis after peptide pull downs with H3 or H3K14Ac peptide from Caki2+PBRM1WT and Caki2+PBRM1mBD2 nuclear lysate. Enrichment of BAF (SS18) and PBAF (PBRM1) were determined by immunoblot analysis. C) Immunoblot analysis of PBRM1 after peptide pull downs with differentially acetylated peptides from HeLa nuclear cell lysate. D) Immunoblot analysis of PBRM1 after peptide pull downs with H3 or multiply acetylated H3 peptide from the nuclear lysates of Caki2 with re-expression of wild type and BD mutant PBRM1.

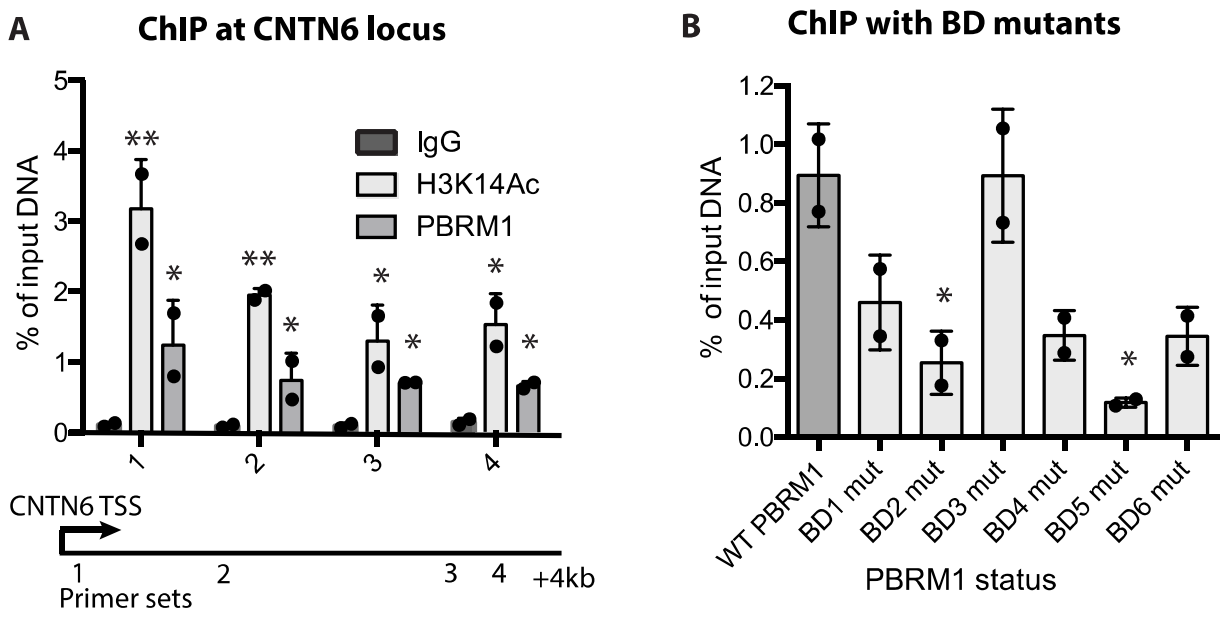

Figure 3-7 Quantitative chromatin immunoprecipitation (ChIP) in Caki2 cells

A) ChIP of PBRM1 and H3K14Ac enrichment at four sites across the CNTN6 locus in Caki2 cells. A designation of * = $p < 0.05$, ** = $p < 0.01$ (paired Student *t*-test) compared to IgG. Error bars represent standard deviation. B) PBRM1 ChIP at the CNTN6 locus (primer site 1) from Caki2 cells expressing wild type or BD mutant PBRM1. A designation of * = $p < 0.05$, (paired Student *t*-test) compared to WT PBRM1. Error bars represent standard deviation.

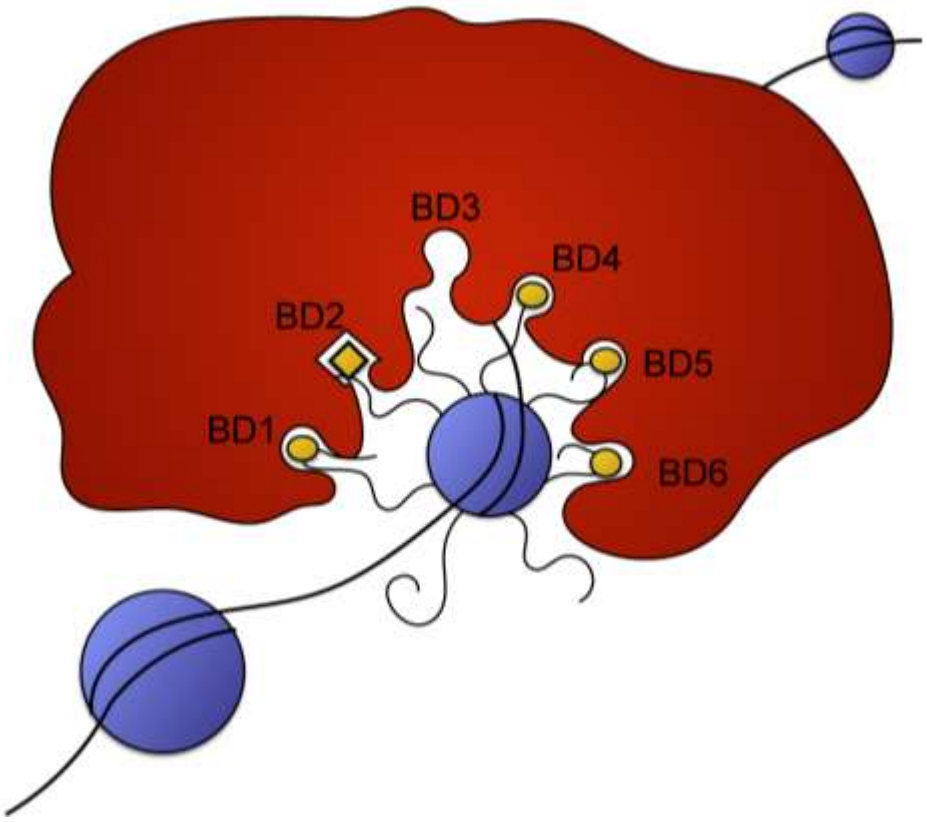

Figure 3-8 Proposed models for PBRM1 recognition of histone marks.

BD2 binds specifically to H3K14ac and the remaining bromodomains recognize a pattern of acetylation marks based on spatial orientation.

While many chromatin-modifying complexes display an array of chromatin binding domains, these domains are often expressed on separate proteins. PBRM1 with its six tandem BDs within a single protein makes it a very appealing model for dissecting the mechanism of these highly multivalent systems. We have found that four of these six domains are essential for proper function of the protein, which implies that these domains are acting cooperatively. We have determined that BD2 is the most important BD and that it interacts with H3K14Ac; however, the acetylation targets of the remaining domains are still unknown. Two possibilities are that, first, BD2 binds to H3K14Ac and the remaining BDs bind to any acetylation site in the near vicinity and stabilize the interaction of the complex with chromatin. The second possibility is that there is a defined set of acetylation sites that are dictated by the spatial arrangement of acetyl-lysines as opposed to peptide sequence. Recent ChIP-MS studies identifies PBRM1 associated with sites of H3K27Ac[104] even though peptide studies never indicated any particular specificity for this mark

by any of the recombinant BDs[22,24,99]. Currently this information is correlative and does not conclusively determine if H3K27Ac is required for PBRM1 targeting, or if it correlates with other acetylation marks required for PBRM1 targeting. The next step will be to further elucidate the combination of acetylation marks that define PBRM1 targets in vitro and in vivo, which will allow for further understanding of upstream pathways that regulate PBRM1 function in ccRCC.

CHAPTER 4. SEQUENTIAL SALT EXTRACTIONS FOR THE ANALYSIS OF BULK CHROMATIN BINDING PROPERTIES OF CHROMATIN MODIFYING COMPLEXES

The following chapter was reproduced and modified with permission from Porter, E.G., Connelly, K.E., and Dykhuizen, E.C., *J. Vis. Exp*. 2017 Oct; (128), e55369, doi:10.3791/55369 (2017).

4.1 Introduction:

DNA regulation in eukaryotic cells is an intricate and sophisticated system that is tightly controlled by an assortment of proteins that coordinate responses to intracellular and extracellular stimuli. DNA is wrapped around histone octamers to form nucleosomes, which can be loosely distributed along DNA or compacted into tight coils[105]. This structural arrangement of DNA and histones is known as chromatin, which is regulated by a network of proteins that read, write, and erase post translational modifications (PTM) on histones[3]. Some histone PTMs, such as acetylation, change the charge of the amino acid they are deposited on, altering interactions between histones and DNA[3]. Histone PTMs also serve to recruit transcriptional regulators, chromatin remodelers, DNA damage repair machinery, and DNA replication machinery to specific regions of the genome[85].

Most methods for studying chromatin interactions either probe small scale interactions or involve large genome-wide analyses. In vitro binding studies often utilize individual recombinant domains with histone peptides or DNA in assays such as electrophoresis mobility shift assays (EMSA), isothermal titration calorimetry, fluorescence polarization, and peptide pulldowns. Because these assays typically focus on an individual protein domain, they facilitate the understanding of a small piece of the puzzle, but do not allow us to understand the cooperative nature of multidomain proteins let alone their role in multi-protein complexes. Another layer of intricacy is added by the heterogeneous composition of most mammalian chromatin-modifying complexes. This protein heterogeneity, in combination with the dynamic nature of the chromatin landscape, makes it challenging to recapitulate the in vivo binding interactions of chromatin proteins to chromatin in vitro.

In vivo methods have made significant advances; however, they are often expensive, time consuming, and technically challenging. Chromatin immunoprecipitation followed by sequencing (ChIP-seq) is very useful for determining the localization of proteins and histone modifications across the genome, however it requires substantial optimization[106]. Proteins are often crosslinked to chromatin to preserve interactions; however, this can produce artificial interactions and may cause epitope masking[107]. Furthermore, the immunoprecipitations (IP) require highly specific antibodies, and extensive optimization of DNA shearing and IP conditions by ChIP-qPCR using a known binding site, which is often not available a priori. After optimization of ChIP conditions, processing of the samples is costly and requires several weeks to months to sequence and analyze. Though this method is invaluable for identifying the localization of chromatin bound proteins across the genome, the cost and time commitment make it prohibitive to use this method to generate hypotheses about how small changes may affect global binding properties.

In this paper, we describe how a sequential salt extraction (SSE) assay can be used to examine global binding profiles of chromatin-bound proteins and distinguish how changes in a protein, complex, or global PTM profile can alter interactions. Though salt extractions are a commonly and broadly used technique, we demonstrate how this sequential method is highly reproducible and versatile. SSE allows us to characterize how a single subunit of a complex or even a single domain contributes to the complex's overall affinity for bulk chromatin. SSE can also be used to determine if the binding of a protein is influenced by changes in chromatin landscape, providing interesting hypotheses for histone mark targeting that can be confirmed using ChIP-seq and other genome wide studies.

We originally adapted this method from Wu et al., to examine of the function of Polybromo1 (PBRM1) in the binding of the PBAF chromatin remodeler[27,108]. Using this technique, we determined the role of PBRM1 for chromatin binding within the PBAF chromatin remodeling complex and then determined the relative contribution of the six individual bromodomains to this function[27].

Here we describe how to optimize this method to explore chromatin binding in different cell types, to assess the relative binding affinity of similar chromatin modifying complexes, to examine the displacement of a protein from chromatin by a chemical inhibitor, and to determine the effects of chromatin binding after alterations to the chromatin landscape.

4.2 Protocol:

4.2.1 Preparation

1. Prepare 100 mL of hypotonic solution Buffer A: 0.3 M sucrose, 60 mM KCl, 60 mM Tris pH 8.0, 2 mM EDTA, and 0.5% NP-40. Store at 4 ºC. **Note:** Some cell lines, such as 293T, require less stringent lysing conditions. If cells lyse easily use Modified Buffer A: 25 mM Hepes pH 7.6, 25 mM KCl, 5 mM $MgCl_2$, 0.05 mM EDTA, 0.1% NP-40, and 10% glycerol.

2. Prepare a 250 mL stock solution of 2x mRIPA solution: 100 mM Tris pH 8.0, 2% NP-40, and 0.5% sodium deoxycholate.

3. Prepare a 100 mL stock solution of 5 M NaCl.

4. Using the 2x mRIPA and 5M NaCl solutions, prepare 50 mL of 1x mRIPA solution for each of the six salt concentrations: 0 mM, 100 mM, 200 mM, 300 mM, 400 mM, and 500 mM NaCl. Prior to starting experiment, all solutions should be cooled on ice.

5. 5. Grow cell lines under desired conditions.

6. When determining the effects of knocking down a protein, SSE for the knockdown line must be compared to wildtype cells. These SSE must be performed side by side.

4.2.2 Salt Extraction

1. Harvest 8 million cells of each condition and wash twice with 5 mL of ice cold PBS. **Note:** It is critical to have equal number of cells to have equivalent protein concentrations. The exact number of cells may need to be optimized for individual cell lines. It is important not to have too many, as the increase in protein concentrations will prevent observation of the elution curve. However, with too few of cells there may not be enough protein to detect the curve and the chromatin pellet is harder to isolate and can be lost between fractions.

2. Re-suspend cells in 1 ml of Buffer A + protease inhibitors, transfer into 1.5 mL micro centrifuge tubes, and rotate top over bottom at 4 ºC for 10 min.

3. Isolate the nuclei by centrifugation at 6000 rcf for 5 min at 4 ºC**. Note:** After this step the nuclear envelope should still be intact, if not, use Modified Buffer A for future experiments.

4. Add 200 µL of mRIPA 0 mM NaCl + protease inhibitors to each nuclei pellet before resuspending pellet. Homogenize each sample by pipetting 15 times with a 1 mL pipette. The pellet should resuspend easily, however, the nuclei will lyse as it is pipetted and the sample will become thick and sticky and difficult to pipette. In order to draw up the pellet into your tip, tap the end of your pipette tip against the bottom of the centrifuge tube. The pellet will not fully dissolve once the DNA is released from the nuclei, but pipetting will break it up.

5. When all the samples have been homogenized, incubate all the samples on ice for 3 min. **Note:** The incubation time may need to be optimized depending on the protein of interest.

6. Isolate chromatin pellet by centrifuging the samples for 3 mins at 6500 rcf at 4 ºC.

7. Transfer supernatant to a clean 1.5 mL centrifuge tube. This will be your 0 mM fraction. This 0 mM mRIPA solution acts as a wash step to lysis the nuclei and remove any loose proteins not associated with chromatin.

8. Add 200 µL of mRIPA 100 mM NaCl + protease inhibitors to each chromatin pellet before resupspending pellet. Break up the chromatin pellet by pipetting the pellet up and down 15 times. **Note:** It is critical to be consistent with the number of times the pellet in pipetted.

9. Incubate on ice for 3 mins. This incubation step allows all samples to reach an equilibrium state, which is particularly important when there are multiple samples.

10. Centrifuge at 6500 rcf for 3 min at 4 ºC and transfer supernatant to a clean 1.5 ml tube.

11. Repeat 2.6-2.10 for the remaining salt concentrations. Note: After 500 mM NaCl mRIPA the pellet should be clear and gloopy and will not stay at the bottom of the tube. The pellet can be pulled out and placed in the lid of the centrifuge tube and then the supernatant isolated.

12. Add 70 µl of 4x protein loading dye to each fraction and load 30 µl of each fraction on to an SDS acrylamide gel for western blot analysis. **Note:** It is essential to load the gel as consistently as possible.

13. Following standard transfer on to a membrane, use primary antibodies of proteins of interest.

14. In order to quantitate the protein eluted in from the chromatin, incubate blot in infrared fluorescence IRDye secondary antibodies and image blot with an Odyssey imager. While other methods of development can be used, we recommend the Li-Cor system, as it is more quantitative in nature.

15. Use ImageJ to calculate the percentage of protein eluted at each salt concentration. By graphing the percentage of protein against the salt concentration, you will be able to see the elution pattern of your protein of interest and see differences of elution between two proteins, or the effects of treatments.

4.2.3 Sequential Salt Extraction in the Presence of a "Reader" Inhibitor

1. Harvest two sets of cells (4 million) and isolate the nuclei as in a standard SSE.
2. Re-suspend both sets in 200 µL of mRIPA 0 mM NaCl and incubate for 3 min. This will allow for the removal of any free protein in the nuclei.
3. Add 200 µL mRIPA 0 mM NaCl to each pellet. Add the inhibitor (2 µL of 1 mM (+)JQ1) to one sample and DMSO to the control set.
4. Agitate the pellet by pipetting 15 times and incubate on ice for 5 min.
5. Centrifuge at 6500 x g for 3 min at 4 ºC and transfer supernatant to a clean 1.5 mL tube.
6. Repeat 3.3 - 4 for all the salt concentrations and perform a standard western blot.

4.2.4 Sequential Salt Extraction in the Presence of a "Writer" Inhibitor

1. Treat cells with the inhibitor (10 µM SAHA) or DMSO for 3 h.
2. Harvest 4 million cells for each treatment.
3. Perform a standard SSE for the samples with the inhibitor added to all the buffers.

4.2.5 Sequential Salt Extraction Following DNA Damage

1. Treat cells with 1 µM doxorubicin for 1 h.
2. Change the media on the cells and allow them to recover for 3 h.
3. Harvest 8 million cells and perform the basic SSE.

4.2.6 Non-Sequential Salt Extraction

1. Harvest 12 million cells and wash with PBS.
2. Divide cells so that there are 2 million cells per micro centrifuge tube.
3. Re-suspend in 500 µL of Buffer A and incubate for 10 min.
4. Isolate the nuclei by centrifugation at 6000 x g.
5. Re-suspend pellets in a 200 µL of each of the mRIPA buffers + NaCl.

6. Homogenize each sample by pipetting 15 times with a 1 mL pipette tip

.

7. Incubate on ice for 3 min.

8. Isolate the chromatin by centrifugation at 6500 x g and transfer the supernatant to clean tubes. Add 70 μL of loading dye and run 30 μL on a SDS-page gel for western blot analysis

4.3 Representative Results

In this paper, we demonstrate the advantages and applications of the commonly used sequential salt extraction (SSE) method that we have adapted from the literature[108]. In Figure 4.1, we compare the reproducibility of SSE to extracting proteins non-sequentially by detecting the elution patterns of ARID1a and PBRM1. We consistently observe that ARID1a, a BAF subunit, elutes primarily at 200 mM NaCl and PBRM1, an exclusive PBAF subunit, elutes primarily at 300 mM NaCl. Figure 1a shows three independent replicates of SSE with 8 million OVCA429 cells. Figure 1b depicts a non-sequential salt extraction where nuclei isolated from 2 million cells were re-suspended in a single salt buffer. Though both methods conclude that ARID1a elutes at 200 mM and PBRM1 elutes at 300 mM, the SSE produces a well-defined binding profile and allows for a clear distinction of the binding of these two complexes. Furthermore, in the non-sequential method, the amount of protein eluted in the 400 mM and 500 mM NaCl buffers is lower than the 300 mM and is inconsistent between the three replicates. Though this issue may be resolved with further optimization of incubation time and centrifugation speed, this illustrates the reproducibility advantage of SSE.

Through our optimization, we found that other chromatin complexes may require more time to be eluted. In Figure 4.2, we demonstrate that the transcriptional activator, PBAF, elutes from chromatin consistently between SSEs with 3 min and 10 min incubation times. In contrast, elution of the transcriptional repressor, Polycomb Repressive Complex 1 (PRC1), indicated by BMI-1, requires a longer incubation time to be released from chromatin[109]. This phenomenon could be due to PRC1 being localized in more compact and inaccessible regions of the genome or could be due to differential binding kinetics for the two complexes.

After optimization for a particular protein, SSEs can be used to study how the strength of protein binding changes in different conditions. SSE can be used to examine the effectiveness of an inhibitor of protein-protein interactions. To demonstrate this concept, we utilized (+) JQ1, which is a BRD4 bromodomain inhibitor, to examine how it altered BRD4 binding (Fig 4.3A)[110].

We isolated nuclei from 4 million OVCA429 cells. To remove any unbound BRD4, an initial 0 mM wash was performed on both samples. Then a standard SSE was performed with DMSO or 1 μM (+) JQ1 added to each fraction. Samples were incubated for 5 min. We observe that BRD4 elutes earlier in the presence of the inhibitor compared to DMSO. To show that (+) JQ1 is specific for BRD4, we blotted for ARID1a and saw no change in elution (Fig 4.3B).

Next, we examined how protein binding can be altered when the landscape of the chromatin is modified. BRD4 contains two bromodomains that recognize acetylated lysine residues on histone tails[22]. To increase the level of histone acetylation, we treated OVCA429 cells with 10 μM of the histone deacetylase inhibitor suberanilohydroxamic acid (SAHA) for 3 h. SAHA (10 μM) was added to all the buffers during the SSE. By increasing the global histone acetylation levels, we observed an increase in BRD4 binding (Fig 4.4A). When blotting for ARID1a, we observe tighter binding of ARID1a as well, which is not surprising because subunits of the BAF complex, such as BRG1, BRM, and BRD9, all contain bromodomains[22,103](Fig 4.4B).

Lastly, to exhibit how SSE can be used to look at how protein binding changes when cells experience genomic alterations, we induced double stranded DNA breaks with the topoisomerase II inhibitor, doxorubicin[111]. We treated HEK293T cells with 1 μM of doxorubicin for an hour and allowed cells to recover for three hours. After performing the SSE, we blotted for PBRM1, which is involved in DNA damage repair[32]. We observed two peaks for PBRM1 binding: one at 300 mM and one at 500 mM NaCl (Fig 4.5). This suggests that some of the PBRM1 population is binding normally, but a subset of PBRM1 is more tightly bound to chromatin following DNA damage. This is just one example of how to use SSE to examine how chromatin interactions are altered in response to different external stimuli.

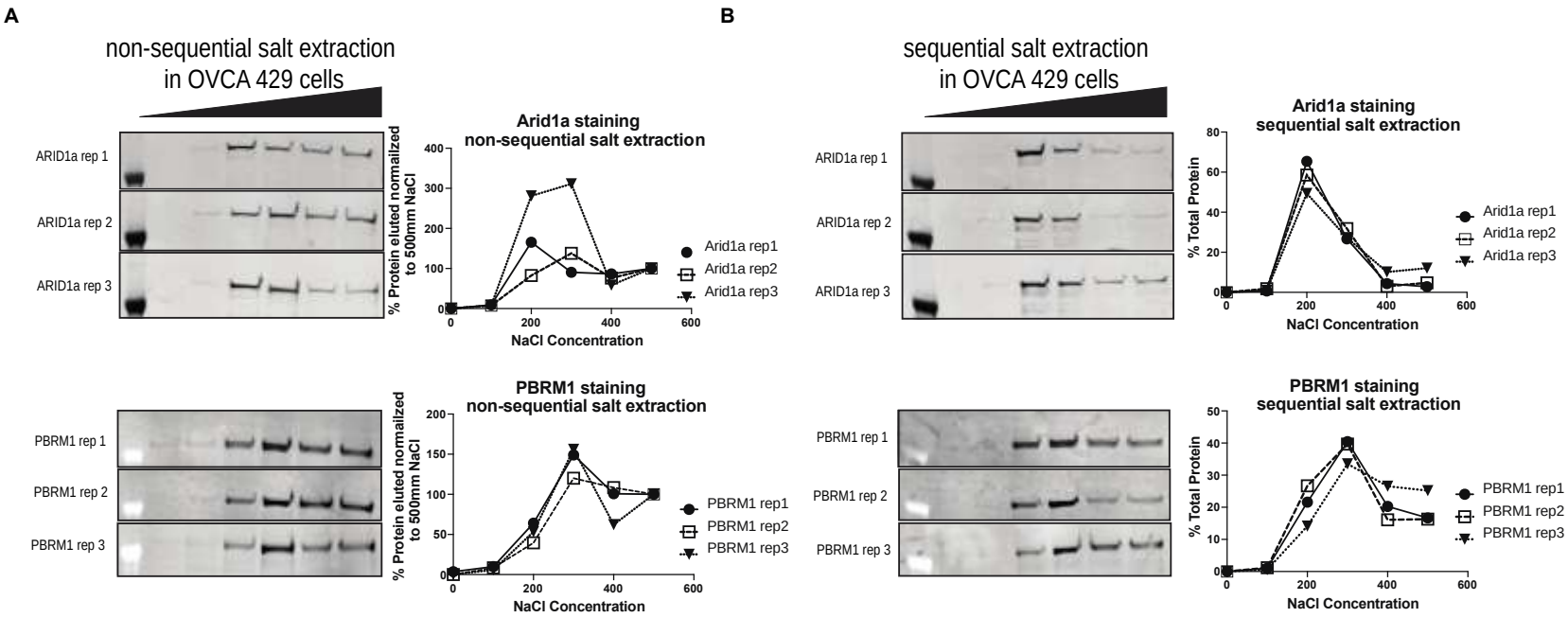

Figure 4-1 Non-sequential compared to sequential salt extractions in OVCA429 cells

A) Immunoblots and quantification of three independent replicates of ARID1a and PBRM1 elution profiles by the sequential salt extraction method. B) Immunoblots and quantification of three independent replicates of ARID1a and PBRM1 elution profiles in the non-sequential salt extraction method.

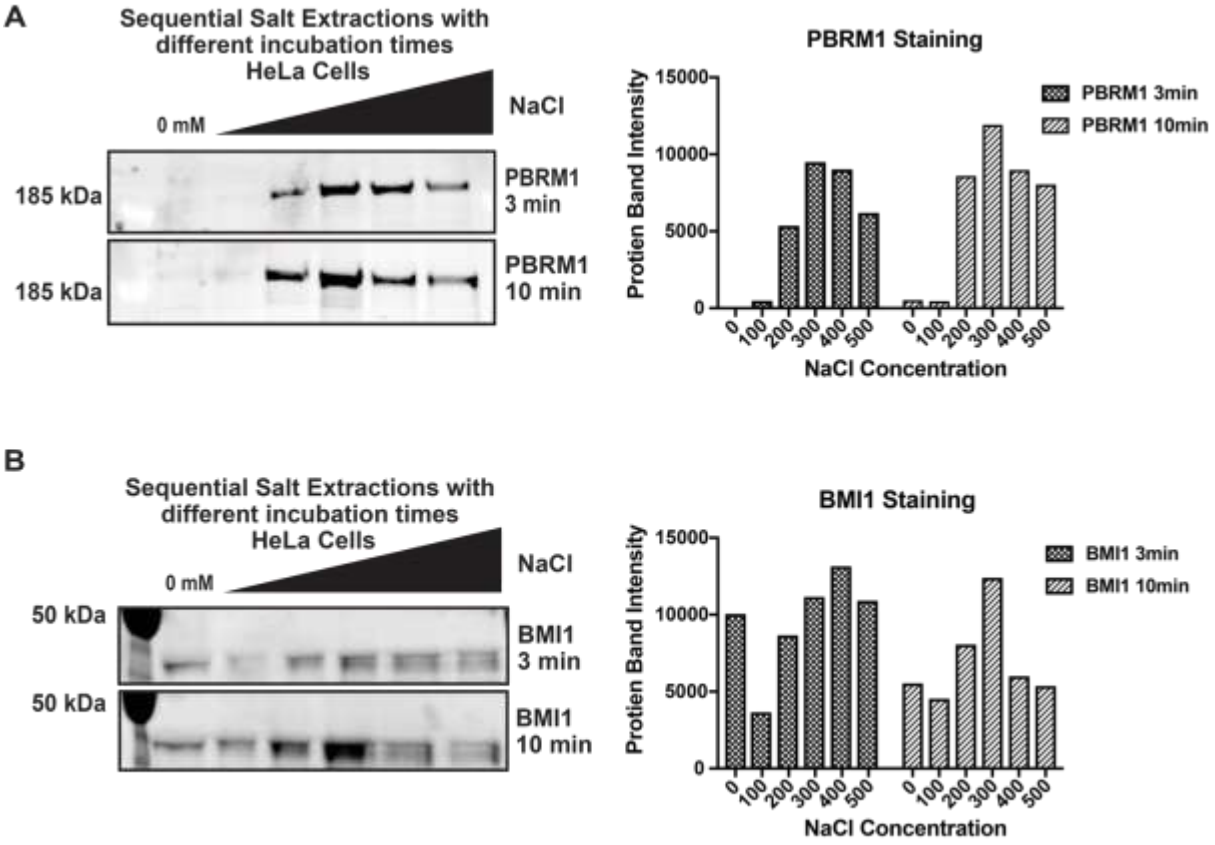

Figure 4-2 Comparison of incubation times of PBAF and PRC1 elution profiles

A) Comparison of PBAF (PBRM1) elution profiles with 3 and 10-minute incubation times. B) Comparison of PRC1 (BMI-1) elution profiles with 3 and 10-minute incubation times. the sequential method more reproducible, it clearly displays the different peaks of elution of BAF and PBAF. In replicate one, the multiple bands in the ARID1a blots is due to degradation of the protein. This can occur when the sample is not kept at 4 ºC at all steps of the experiment.

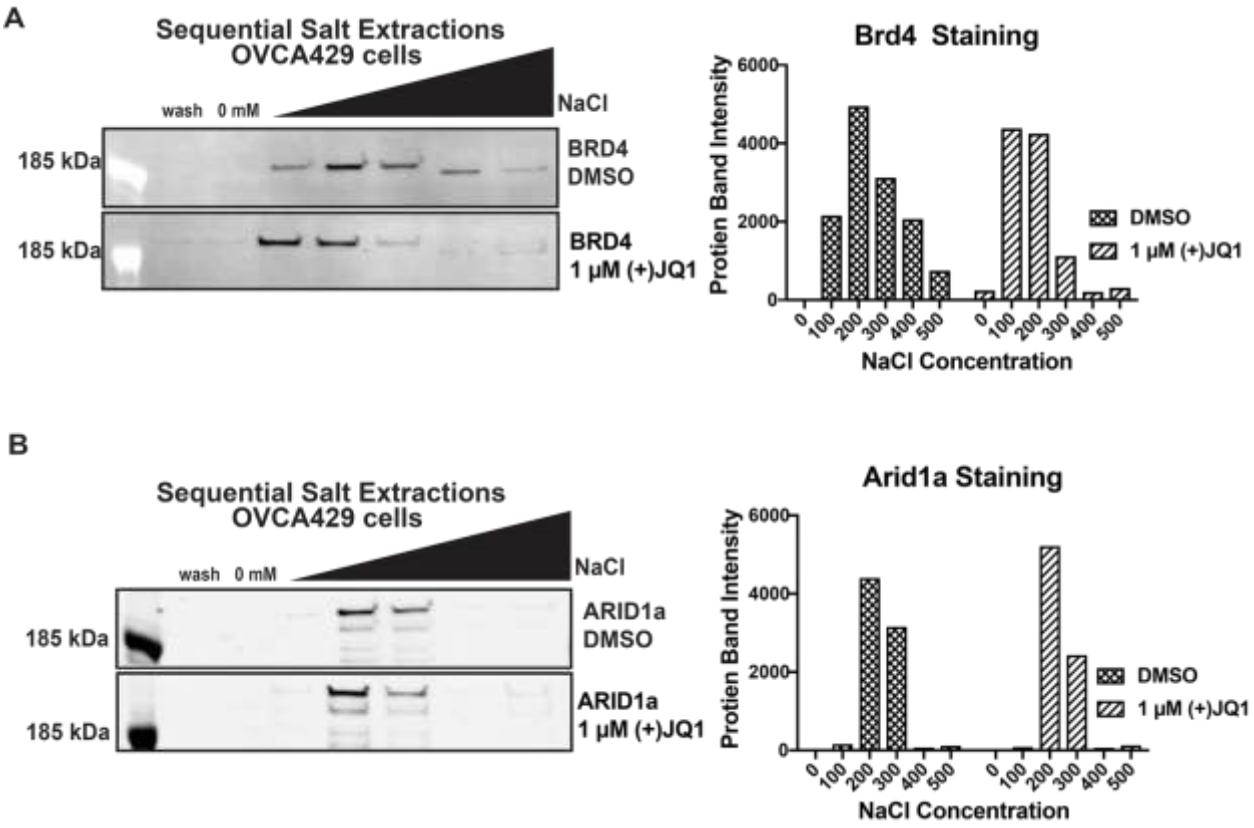

Figure 4-3 Effectiveness of (+) JQ1 on inhibiting BRD4 binding

A) Elution pattern of BRD4 in the presence of 1 μM (+) JQ1 compared to DMSO control in OVCA429 cells. B) Elution profile of ARID1a in the presence of 1 μM (+) JQ1 compared to DMSO control in OVCA429 cells. Band intensity is indicated for 0 mM- 500 mM fraction with DMSO or (+) JQ1.

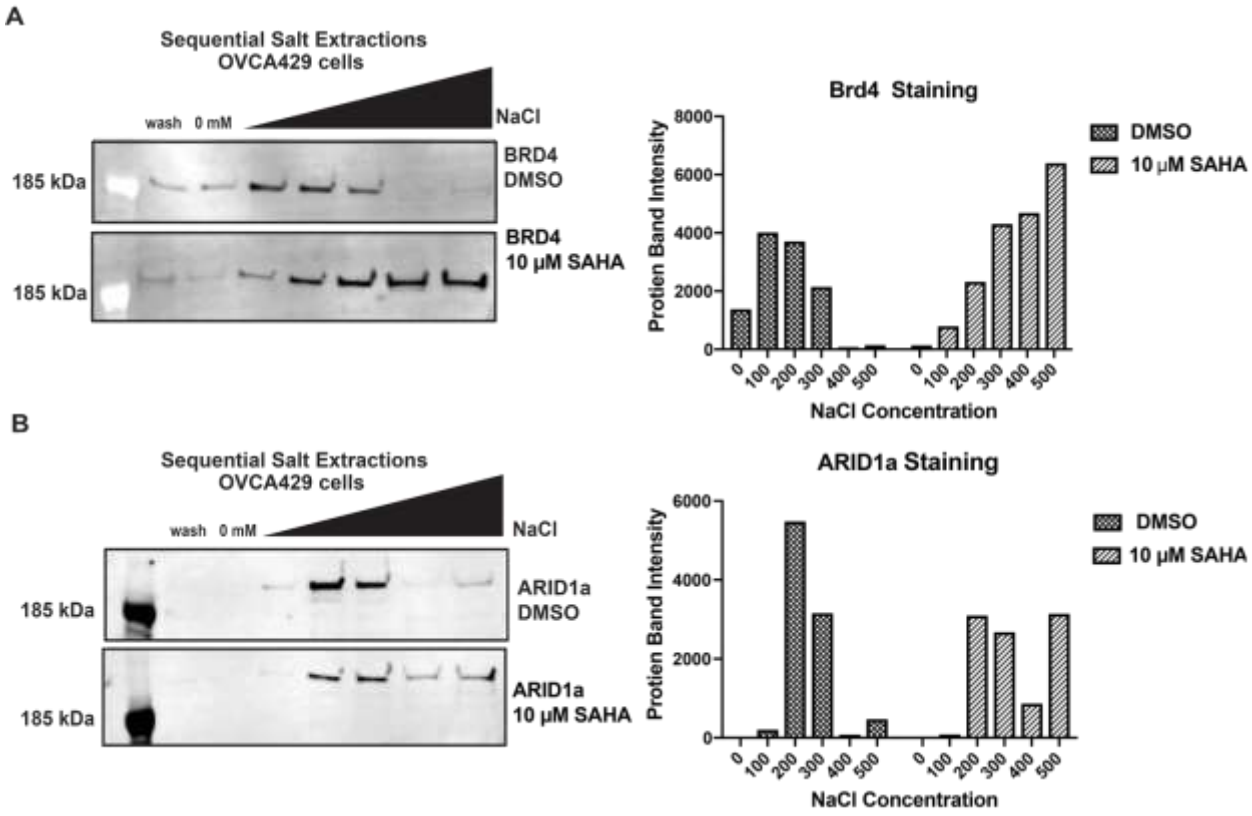

Figure 4-4 Alterations in binding when chromatin landscaped is modified

A) Comparison of BRD4 elution from OVCA429 cells treated with 10 µM SAHA for 3 hours compared to DMSO treatment. B) Elution profiles of ARID1a from OVCA429 cells treated with10 µM SAHA compared to DMSO. Band intensity is indicated for 0 mM - 500 mM fraction with DMSO or SAHA.

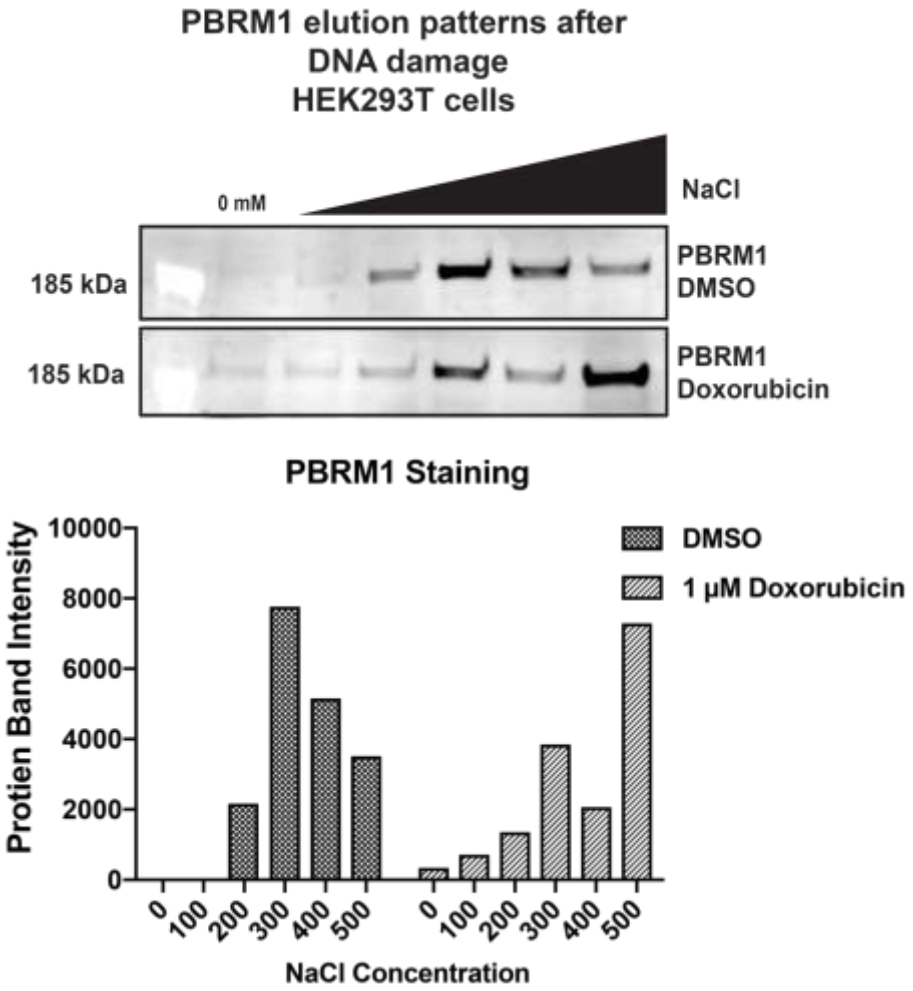

Figure 4-5 Changes in PBRM1 binding after DNA Damage

SSE results for PBRM1 binding from HEK293T cells treated with 1 µM Doxorubicin.

4.4 Discussion

Characterization of protein and chromatin interactions through salt extractions is a common method that has been employed for decades[112,113]; however, it has not been systematically optimized before to reveal its full utility. We demonstrate how this sequential method provides a rapid and inexpensive way to distinguish changes in chromatin binding when the protein or the environment is altered. SSE is highly adaptable and optimizable, and importantly, it is technically simple and requires no specialized equipment. The key aspects that need to be optimized prior to starting are: starting cell number, hypotonic buffer conditions, and incubation time.

The most important aspect of cell number is that it is consistent between all the samples. When looking at BAF complexes, using 8 million cells gives a good profile of how these complexes are binding; however, the number of cells (or the amount of buffer) may need to be adjusted depending on the abundance of the protein of interest. It is important to note that using fewer cells is challenging because at 400 mM and 500 mM NaCl it is hard to visualize the chromatin pellet. It is vital to make sure the pellet is not transferred with the supernatant after 400 mM NaCl.

In order to accurately evaluate nuclear proteins, the nuclei need to stay intact until they are lysed with 0 mM NaCl mRipa solution. Many commonly used hypotonic solutions are too harsh for cell lines such as HEK293T and HeLa cells. For these cell lines, it is recommended to use the modified Buffer A.

Finally, the incubation time may vary depending on the experiment. For BAF subunits the elution pattern does not change between a 3 min and 10 min incubation; however, the elution of the PRC1 complex drastically changes depending on how long the samples are incubated. Additionally, when evaluating the effect of an inhibitor on the binding of its target, the incubation time may need to be optimized depending on inhibitor kinetics.

When performing the experiment, it is important to be as consistent as possible with treatment of the samples. For each fraction, the salt buffer should be added to every sample prior to homogenization so that each sample is equally exposed. The point of pipetting is to break up the chromatin and help release the bound proteins. It is important to make sure the pellet passes through the pipette tip. Especially when using a larger number of cells, the chromatin pellet is challenging to pass through the pipette tip the first few times. We have found that a 1 mL tip works the best for this, as with minor tapping of the tip against the bottom of the micro centrifuge tube, we are able to draw up the pellet into the tip. After passing the chromatin pellet through the tip fifteen times, the pellet should smoothly move through the tip, though it will not dissolve. After incubating the samples on ice and isolating the chromatin by centrifugation, removing the supernatant with a 200 μL pipette tip allows for maximal removal without disrupting the chromatin pellet.

Though SSE requires technical consistency, it is simple, straightforward, and can be performed with common laboratory resources. It is important to note that the true power of this method is when it is coupled with other phenotypical examinations. For example, using this

technique, we compared the binding profiles of PBRM1 when each of its six bromodomains were mutated, we determined that all but one of the bromodomains were involved in the binding of PBRM1 to varying degrees[27]. Intriguingly, we found that the bromodomains that were the most important for binding were also essential for PBRM1 regulation of gene expression and control cell proliferation[27]. We also validated the changes in binding of these mutants to a discrete genomic locus by quantitative ChIP-qPCR[27].

We have shown only a few examples of how this technique can be used to study protein-chromatin interactions; however, in our lab, we have found that SSE is a versatile tool for investigating a wide array of questions regarding chromatin reader proteins. In combination with other analyses, this technique facilitates our ability elucidate the functionality of the components comprising these elaborate protein complexes. By understanding the importance of individual domains, we can identify whether they are potential therapeutic targets for the development of an inhibitor that blocks chromatin association.

We have demonstrated how SSE can be expanded to evaluate the effectiveness of a small molecule inhibitor on protein binding to chromatin. Additionally, by inhibiting epigenetic writers and erasers, SSE can determine the relationship between PTM levels and reader proteins. We have also shown the SSE can be used to determine changes in binding in response to external stimuli such as DNA damage. Though this is a simple technique, when applied in the proper conditions, it can greatly advance our knowledge of chromatin and its regulatory proteins.

CHAPTER 5. PBRM1 REGULATES STRESS RESPONSE IN EPITHELIAL CELLS

The following chapter has been provisionally accepted for pubication in *iScience,* published by Cell Press.

Porter, E.G., * Dhiman, A., * Chowdhury, B., Carter, B.C., Lin, H., Stewart, J.C., Kazemian, M., Wendt, M.K., and Dykhuizen, E.C., *iScience*. 2019 (*in revision*)

*These authors contributed equally to this work

5.1 Introduction

PBRM1, a gene which encodes a subunit of the PBAF chromatin remodeling complex, is mutated in over 3% of all cancers with the highest mutation rate occurring in clear cell renal cell carcinoma (ccRCC), where it is mutated in 40-50% of patients[11,41,43]. The PBAF chromatin remodeling complex is a minor subcomplex of the human SWI/SNF, or BAF, chromatin remodeling family, subunits of which (SMARCA4 (BRG1), ARID1A, and SMARCB1 (SNF5 or BAF47)) are also frequently mutated in cancers[6,7]. Along with PBRM1, the PBAF subcomplex exclusively contains ARID2, BRD7, BAF45A, as well as several subunits shared with the more abundant BAF complex [17,114,115]. PBRM1 is comprised of several domains associated with binding to chromatin including six tandem bromodomains (BDs), two bromo-adjacent homology (BAH) domains and a high mobility group (HMG), implicating PBRM1 as a chromatin targeting subunit of PBAF. For the most part, the chromatin signatures bound by PBRM1 have not yet been determined, although histone 3 lysine 14 acetylation (H3K14Ac) has been defined as a primary target for the second bromodomain (BD2) in vitro [24], and validated as the acetylation mark most critical for association of the full PBAF complex to histone peptides[27]. PBRM1 has homology to RSC1, RSC2 and RSC4 subunits of the yeast RSC chromatin remodeling complex, which also interacts with H3K14Ac, particularly during DNA damage[116,117]. However, unlike subunits of RSC, PBRM1 does not seem to be necessary for viability in the majority of mammalian cell types, and in fact, while PBRM1 is essential for embryonic heart development in mice[30,118], adult mice with knockout of PBRM1 are phenotypically normal except for an age-related hematopoietic stem cell (HSC) defect[31].

The most well-defined cellular role for PBRM1 is in DNA-damage repair[32,119], which is in line with observation of H3K14Ac at sites of DNA damage[120]; however, the low mutational burden and relative genome stability of PBRM1-mutant tumors makes it unclear how this role in DNA-damage repair relates to the tumor suppressive phenotypes of PBRM1[45]. As such, most of the focus has been on deciphering how transcriptional functions for PBRM1 relate to a role in tumor suppression. Transcriptional profiling of human ccRCC indicate that PBRM1 mutant tumors have a hypoxic transcriptional signature[45], which is in agreement with recent reports that mutation of PBRM1 amplifies the hypoxia inducible factor (HIF) transcriptional program signature induced upon von Hippel-Lindau (VHL) deletion in cell culture[121] and in a mouse renal cancer model [35]. Recent work with kidney specific (KSP and PAX8) Cre mouse models indicate that VHL knockout or PBRM1 knockout alone is not sufficient for cancer formation but that both are required for kidney tumor formation in mice[35,122,123].

While these recent mouse studies have solidified a role for PBRM1 as a bona fide tumor suppressor in renal cancer, the molecular mechanism by which PBRM1 acts as a tumor suppressor is still unclear. For example, PBRM1 exhibits tumor suppressive phenotypes in a subset of cancer cell lines[26,56,124], but PBRM1 knockdown in many cell lines produces no phenotype[26,121] or even decreases cellular viability[31]. In the renal cancer setting, this context-specific function is mediated, in part, through HIF1a expression, which is required for PBRM1's tumor suppressor phenotype in renal cell lines[62,125]; however, the context-dependent function observed in other cell types is still undefined. Here we used epithelial cell lines to define how the function of PBRM1 in non-transformed cells may relate to its function as a tumor suppressor. Through genome-wide transcriptional analysis, we have defined a general role for PBRM1 in regulating the expression of genes involved in stress response, particularly endoplasmic reticulum stress and apoptosis. To support this general function, we have found that loss of PBRM1 results in accumulation of reactive oxygen species (ROS) and a failure to induce apoptosis under a variety of high stress conditions. Based on our findings, we propose that PBRM1 acts to regulate stress response genes that restrain cellular proliferation under low stress conditions but protect cells under high stress conditions.

5.2 Materials and Methods

5.2.1 Cell culture

HK-2 were cultured in RPMI (Corning Mediatech) supplemented with 10% fetal bovine serum (J R Scientific), 1% antibiotics (100 units/ml penicillin and 100 g/ml streptomycin; Corning Mediatech), and 1% L-glutamine (Corning Mediatech) at 37 °C in a humidified atmosphere in a 5% CO2 incubator.

MEF cells were cultured in DMEM (Corning Mediatech) supplemented with 10% fetal bovine serum (J R Scientific), 1% antibiotics (100 units/ml penicillin and 100g/ml streptomycin; Corning Mediatech), 1% nonessential amino acids (Corning Mediatech), 1% L-glutamine (Corning Mediatech) and 0.1% β-mercaptoethanol (Gibco, Thermo Scientific) at 37 °C in a humidified atmosphere in a 5% CO2 incubator.

MCF10A cells were cultured in 1:1 DMEM (Corning Mediatech) and F12 (Corning Mediatech) supplemented with 29 mM Hepes (Amresco, LLC), 10 mM Sodium Bicarbonate (Macron), 5% Horse serum (Sigma), 10 µg/mL Insulin (Sigma), 10 ng/mL Epidermal Growth Factor (EGF) (Gold Biotechnology), 0.5 µg/mL hydrocortisone (Sigma), 100 ng/mL cholera toxin (Sigma), and 1% antibiotics (100 units/ml penicillin and 100 g/ml streptomycin; Corning Mediatech) at 37 °C in a humidified atmosphere in a 5% CO_2 incubator.

MCF10A T1K were cultured in DMEM (Corning Mediatech) supplemented with 10% fetal bovine serum (J R Scientific) 1% L-glutamine (Corning Mediatech), 1% antibiotics (100 units/ml penicillin and 100 g/ml streptomycin; Corning Mediatech), and 1% Sodium Pyruvate (Corning Mediatech) at 37 °C in a humidified atmosphere in a 5% CO_2 incubator.

NMuMG cells were grown in DMEM (Corning Mediatech) supplemented with 10% fetal bovine serum (J R Scientific), 10 µg/mL Insulin (Sigma), 1% L-glutamine (Corning Mediatech), 1% antibiotics (100 units/ml penicillin and 100 g/ml streptomycin; Corning Mediatech), and 1% Sodium Pyruvate (Corning Mediatech) at 37 °C in a humidified atmosphere in a 5% CO_2 incubator.

MDCK cells were cultured in DMEM (Corning Mediatech) supplemented with 10% fetal bovine serum (J R Scientific), 1% L-glutamine (Corning Mediatech), 1% antibiotics (100 units/ml penicillin and 100 g/ml streptomycin; Corning Mediatech), 1% nonessential amino acids (Corning Mediatech), 10 mM Hepes (HyClone) and 1% Sodium Pyruvate (Corning Mediatech), at 37 °C in a humidified atmosphere in a 5% CO_2 incubator.

Caki2 cells were grown in McCoy's 5A medium (Corning Mediatech) supplemented with 10% fetal bovine serum (J R Scientific), 1% antibiotics (100 units/ml penicillin and 100 g/ml streptomycin; Corning Mediatech), 1% nonessential amino acids (Corning Mediatech), and 1% L-glutamine (Corning Mediatech) at 37 °C in a humidified atmosphere in a 5% CO2 incubator. Caki2 Fuw and Caki2 Fuw+PBRM1 cells were cultured in the presence of doxycycline (1 µg/ml final concentration).

All the media were supplemented with 1:10,000 dilution of Plasmocin™ (InvivoGen).

5.2.2 Cell culture and treatments

Cells were seeded 24-72 h before treatment such that they were 50-80 % confluent at the time of experiment. For hydrogen peroxide treatment, indicated concentrations of freshly prepared hydrogen peroxide were added to the treatment groups for the indicated time periods in their regular media. For glucose starvation studies, the regular media was replaced with glucose free DMEM media (Corning Mediatech) or reduced glucose media for the indicated time periods. Following the completion of treatment, cells were washed once with PBS, harvested by trypsinization and either processed immediately or flash frozen and stored at -80 ^{o}C for future use.

5.2.3 Generation of cell lines

Knockdown was performed using shRNA-mediated knockdown with lentiviral construct pLKO.1. The shRNA constructs contain the following mature antisense sequences:
Human PBRM1: (TRCN0000015994) TTTGTAGATCAAAGACTCCGG
Mouse PBRM1: (TRCN0000081820) TTCTAGGTTGTATGCCTGTCG
Mouse Brd7 Clone ID: (TRCN0000030015) ATAATCATGGAGTAGCCAGGC
Mouse Brg1: (TRCN0000071386) TTCTCAATAATGTGTCGGGCG
Mouse Arid1a: (TRCN0000071395, Origene TG517733) ATTGTAGGTCATGTCATTTCG
Canine PBRM1-1: ACATCATCATACTCTTCCA
Canine PBRM1-2: ACCAACAGCCATACAACCA
c-Jun (TRCN0000042695): GCTTAAGCAGAAAGTCATGAAC
NRF2 (TRCN0000054658):GCCAAAGCTAGTATAGCAATAA
Caki2 FUW vector and Caki2 FUW PBRM1 as describes in Chowdhury et al. 2016.

Short guide RNA for mouse PBRM1 (sgPBRM1) was designed using the MIT CRISPR tool (http://crispr.mit.edu/) and the control sgRNA (sgControl) was taken from Alpsoy and Dykhuizen et al. 2018[19].

Mouse sgControl: GTAGCGAACGTGTCCGGCGT

Mouse sgPBRM1: TTCATCCTTATAGTCTCGGA

The sgRNA were ordered as single strand oligos, annealed and cloned into vector PX459 (pSpCas9(BB)-2A-Puro (PX459) V2.0 was a gift from Feng Zhang, Addgene plasmid # 62988). The constructs were introduced into NMuMG cells by transient transfection using Lipofectamine 3000 (Invitrogen). After 48 h of transfection, selection using puromycin (0.6 µg/ml) was done for 48 h. The efficiency of knockout constructs was confirmed by immunoblotting.

5.2.4 Lentiviral Infection

HEK293T cells were transfected with knockdown and knockout lentivirus constructs along with packaging vectors pMD2.G and psPAX2. After 48 h, the supernatant was collected and concentrated by ultracentrifugation (17,300 rpm for 2 h) and resuspended in 200 µl of PBS. Cells were infected with concentrated virus using spinfection (1500 rpm in swing bucket centrifuge for 1 h). Fresh medium was added 16 h after infection, and cells were allowed to recover for 24 h before selection. Cells were selected for 2 weeks with puromycin (0.6 µg/ml) (Sigma-Aldrich) and hygromycin (200 µg/ml) where applicable (Corning Mediatech). Caki2 cells were cultured with 2 µg/ml doxycycline (EMD Chemicals) for 72 h prior to experiments to induce protein expression which was confirmed by immunoblotting. The efficiency of all knockdown constructs was confirmed by immunoblotting.

5.2.5 3D culture

Cells were embedded between 2 layers of Cultrex® Basement Membrane Extract (BME) (R&D Systems) on 8-well Chamber Slide. Wells were pre-coated with BME (200 µl/well) to allow polymerization at 37°C for 15 minutes. Cells were then seeded at 20,000 cells/well density. After attachment (30 minutes at 37°C), cells were covered with a second layer of BME/culture medium (1:19, 5%) to polymerize overnight at 37°C. Cells were incubated for 10 days, and the medium was replenished every 3 days. At the end of incubation, cells were fixed and subjected to immunofluorescence analysis.

5.2.6 Immunofluorescence staining

Cells were washed twice with ice-cold PBS, added 2-3 volumes of ice-cold PBS-EDTA and shaken on ice for 15-30 minutes. BME was detached from the bottom of culture surface by gently scraping the bottom with a pipette tip. The solution was transferred to a conical tube and gently shaken on ice for 15-30 minutes. When BME was dissolved completely, the solution was centrifuged at 120g for 1-2 minutes. The supernatant was carefully aspirated, and cells were gently resuspended in the remaining supernatant. Pipetted approximated 15 µl of the cell suspension onto a glass bottom dish, allowed cells to settle and adhere to the glass. Cells were fixed using formalin for 20 minutes at room temperature (RT). Next, cells were permeabilized with 0.5% Triton X-100 in PBS for 5 minutes at RT and washed 3 times with 100 mM glycine in PBS at RT. Fixed cells were blocked for 1.5 hours with 10% goat serum. Cells were incubated overnight at 4°C with primary antibodies. The primary antibodies used were as follows: rat anti–α_6-integrin (Millipore; 1:100 in 0.2% Triton X-100, 0.1% BSA, 0.05% Tween 20 in PBS) and rabbit anti–Zo-1 (Invitrogen, 1:100 in 0.2% Triton X-100, 0.1% BSA, 0.05% Tween 20 in PBS). Cells were incubated with secondary antibody for 1 hour, followed by 3 washes at RT. Secondary antibodies were as follows: FITC goat anti-rat and Biotin-SP-conjugated AffiniPure goat anti-rabbit (Jackson ImmunoResearch). Cells were incubated with Texas Red Avidin D (Vector) for 1hour. Cell nuclei were counterstained with DAPI for 10 minutes and washed 3 times with PBS. Cells were incubated in PBS and imaged by confocal microscopy.

5.2.7 Confocal microscopy

Confocal laser scanning microscopy experiments were conducted using the Zeiss LSM 880 Upright Confocal.

5.2.8 TopFlash Reporter Assay

NMuMG cells were transfected with 10:1 ratio of M50 Super 8x TopFlash (Addgene 12456) to pcDNA3.1.CMV-renilla-Neo. The cells were transfected using Lipofectamine with 3:1 ratio of total DNA to lipofectamine reagent. After 24 h, the cells were trypsinized and 20,000 cells/well were plated in 96-well white tissue culture treated plates. After an additional 24 h of growth, the firefly and renilla luciferase levels were measured using the Dual Glo® assay system (Promega).

5.2.9 Annevin V Apoptosis detection in NMuMG cells

NMuMG cells were seeded at a density of ~ 1.5 X 10^6 cells/60mm dish and cultured for 24 h. The cells were then given treatments of 200 µM H_2O_2 in media for 0-4 h, followed by cell harvesting using Accutase (Innovative cell technologies) and apoptosis detection using the FITC Annexin V apoptosis detection kit (BD Pharmingen, Cat. # 556547) as per the manufacturer's instructions. The cells were immediately analyzed by flow cytometry using the Guava EasyCyte Benchtop Flow Cytometer (Millipore Sigma). The results were analyzed using FlowJo software.

5.2.10 Immunoblotting

Cells were given treatments as described before for the indicated time periods, followed by cell harvesting by trypsinization. Whole cell extracts were prepared by dissolving the cell pellets in RIPA buffer (50 mM Tris (pH 8.0), 150 mM NaCl, 0.1% SDS, 0.5% Na Deoxycholate, 1% NP-40) supplemented with freshly added PMSF, aprotinin, leupeptin and pepstatin, and incubation for 30 min at 4 ºC. The lysates were centrifuged at 13000 x g for 30 min at 4 °C and the supernatants were preserved. Protein concentration estimations for the supernatants were done using BCA protein assay kit (Pierce Biotechnology) with BSA as standard and whole cell extracts were run on a 4-12 % bis-tris gradient protein gel, transferred to PVDF membrane and probed with primary antibodies in 5% BSA at 4 °C for 16 h.

5.2.11 Antibodies

Cleaved PARP (Asp214) (7C9) (Mouse specific) Cell Signaling #9548

Cleaved PARP (Asp214) (Human Specific) Cell Signaling #9541

PBRM1 (Bethyl Laboratories-PBRM1 Antibody, #A301-591A)

β-actin (Santa Cruz Biotechnology, #sc-47778)

BRG1 (G-7) Santa Cruz sc-17796

BRD7 Bethyl A302-304A

Vimentin BD Biosciences 550513

E-Cadherin BD Biosciences 610182

GAPDH (6C5) (Santa Cruz sc-32233)

LaminB (A-11) sc-377000

Phospho-Akt (Ser473) (D9E) XP® (Cell Signaling #4060)

5.2.12 Migration assay

NMuMG cells were seeded at a density of ~ 1.5 X 10^6 cells/well in a 6-well plate and cultured for 24 h, after which scratches were made in each well. The migration of cells was followed at regular intervals as indicated.

5.2.13 H_2-DCFDA staining for intracellular ROS using flow cytometry

NMuMG cells were seeded at a density of ~ 2 x 10^6 cells/60mm dish and Caki2 cells were seeded at a density of ~ 3 X 10^6 cells/60mm dish. The cells were cultured for 48 h, harvested by trypsinization, washed once with PBS and stained for intracellular ROS by incubation with freshly prepared 10 µM H2-DCFDA (Invitrogen, Cat. # D399) in PBS for 30 min at 37 °C in dark. Following the incubation, the cells were centrifuged at 250 x g for 5 min, resuspended in PBS and immediately analyzed by flow cytometry. The results were analyzed using FlowJo software.

5.2.14 Stress treatments and H_2-DCFDA staining using microplate reader

NMuMG cells were seeded at a density of 6.0 x 10^4 cells/well and Caki2 cells were seeded at a density of 2.5X10^4 cells/well in a 96-well black tissue culture plates. The cells were cultured for 24 h, following which they were subjected to the following stress conditions: H_2O_2 treatment (0-200 µM for NMuMG and 0-800 µM for Caki2) for 1h followed by 10 min recovery in PBS, glucose starvation by culturing in various glucose concentrations for 16 h for NMuMG and culturing in glucose free media for the indicated time periods for Caki2, CoCl2 treatment (0-250µM) for 24h or doxorubicin treatment (0-10 µM) for 24h. At the end of the treatments, cells were washed once with PBS, and stained with freshly prepared 10 µM H_2-DCFDA (Invitrogen, Cat. # D399) in PBS for 30 min at 37 °C in dark. Cells were washed again 2x with PBS and fluorescence measurements were taken using a microplate reader at excitation/emission wavelengths of 485/530 nm. Unstained cells were used as the negative controls.

5.2.15 H_2O_2 detection assay

H_2O_2 levels were measured using Amplex® Red Hydrogen Peroxide/Peroxidase Assay kit (Invitrogen). The H_2O_2 levels were determined from whole cell lysates (in RIPA) according to manufacturer's instruction. The concentration of H_2O_2 was determined for lysates generated from

5,000 and 10,000 cells in 50 µL by plotting fluorescence levels against experimentally determined dose curves.

5.2.16 Viability assays using CellTiter-Glo®

Cells were plated in 96-well white tissue culture plates and cultured for the indicated time under the indicated conditions. Antioxidant rescue experiments were performed with fresh media daily containing 20 µg/mL Vitamin C or 250 µM N-acetylcysteine (NAC). CellTiter-Glo® assay reagent was added directly to cells as per manufacturer's instructions, incubated for 10 min, and the luminescence was measured on a GloMax® microplate reader.

5.2.17 LDH assays using LDH Cytotoxicity Assay Kit II (Abcam, ab65393)

NMuMG cells were seeded at a density of 6.0 x 10^4 cells/well and Caki2 cells were seeded at a density of 1.0 x 10^4 cells/well in 96-well tissue culture plates. The cells were cultured for 24 h, following which they were subjected to H_2O_2 treatment (0-300 µM for NMuMG) for 6h or 24h and 200 µM H_2O_2 for Caki2 for the indicated time periods. Media was harvested from wells (10 µL) and transferred to a separate 96-well assay plate along with negative control (media alone) and positive control (lysed cells). LDH Reaction Mix (100 µl) was added to each well, mixed and incubated for 30 min at room temperature. The absorbance at 490 nm was measured on the GloMax® microplate reader.

5.2.18 H_2-DCFDA staining for MCF10A and MCF10A-T1K followed by flow cytometry

MCF10A and MCF10A-T1K cells were seeded in 60mm dishes in MCF10A media and cultured for 48 h such that they reach 50-80 % confluency at the day of the experiment. The cells were then harvested using trypsin, washed once using serum-free and phenol red-free media and stained for intracellular ROS with freshly prepared 10 µM H_2-DCFDA in PBS-Glucose (1X PBS supplemented with 25 mM glucose) as described before. The cells were immediately examined by flow cytometry and the results were analyzed using FlowJo software.

5.2.19 RNA-seq

RNA isolation, library construction, sequencing and transcriptome analysis was performed as described in our previous publication[26]. Sequencing was performed in biological triplicates. RNA-seq of NMuMG epithelial cell lines was performed at the Purdue Genomics Core using

Illumina HiSeq technology. The resulting reads were trimmed using Trimmomatic utility[126] and mapped to mm9 using STAR[46] using default parameters. Read counts were obtained using HTSeq-count[47] in conjunction with a standard gene annotation files from UCSC (University of California Santa Cruz; http://genome.ucsc.edu) and differential expression was determined using DESeq2 pipeline[48]. Differentially expressed genes were filtered using a false discovery rate threshold of < 0.05 and a fold change threshold of > 1.3-fold relative to the reference sample. Gene ontology and transcription factor prediction analyses were performed using GeneCodis[50] iCisTarget[127], and ToppCluster[128]. Data sets generated in these experiments are available at the Gene Expression Omnibus under accession number GSE113606.

5.2.20 ATAC-seq

The ATAC-seq protocol originally described[129] was adapted as follows for HK2 and NMuMG isogenic lines: 50,000 cells were resuspended in Nuclei Lysis buffer containing 0.05% IGEPAL CA-630, incubated for 5 minutes on ice and centrifuged for 10 minutes at 500xg at 4°C. Nuclei extraction was confirmed by microscopic inspection and the nuclei pellet was resuspended in transposition master mix. Tagmentation, cleanup of tagmented DNA, and PCR enrichment was performed as per original description. High throughput sequencing was performed by HiSeq2500 using 50 bp paired-end at the Purdue Genomics Core. Sequenced reads were mapped by the Bowtie2 aligner[130] using hg19 or mm10 reference genome, respectively. Reads mapping to the mitochondrial genome were discarded. Bigwig files were generated for visual inspection of tracks using the bamCoverage utility of deepTools[131]. Peaks of differential accessibility were identified using the SICER-df-rb utility[132] with a false discovery rate threshold of < 0.05 and a fold change threshold of > 1.5-fold difference in accessibility. Scaled heat maps were generated for the peak regions using the computeMatrix and plotHeatmap utilities of deepTools. Peak regions were analyzed for enrichment of sequence motifs and association with genomic elements using the findMotifs and annotatePeaks utilities of HOMER[133]. Data sets generated in these experiments are available at the Gene Expression Omnibus under accession number GSE113606.

5.2.21 qRT-PCR

RNA was isolated from cells using Trizol (Ambion, Thermofisher). Total RNA was converted to cDNA with Verso cDNA Synthesis Kit according to manufacturer's instructions

(Thermo Scientific). Real-time PCR was performed using a Bio-Rad CFX Connect Real-Time system and Thermo Scientific Maxima SYBR Green qPCR Master Mix (Thermo Scientific). The results were analyzed using the Pfaffl method[134].

Gene	Forward Primer	Reverse Primer
c-Jun	ACTCGGACCTTCTCACGTC	GGTCGGTGTAGTGGTGATGT
BCL2L1	GACAAGGAGATGCAGGTATTGG	TCCCGTAGAGATCCACAAAAGT
HK2	TGATCGCCTGCTTATTCACGG	AACCGCCTAGAAATCTCCAGA
IL1RL1	ACGCTCGACTTATCCTGTGG	CAGGTCAATTGTTGGACACG
NRF2	GATCCGCCAGCTACTCCCAGGTTG	CAGGGCAAGCGACTCATGGTCATC
HMOX1	GCCGAGAATGCTGAGTTCATG	TGGTACAAGGAAGCCATCACC
NQO1	CGCCTGAGCCCAGATATTGT	GCACTCTCTCAAACCAGCCT
BMF	GTGGCAACATCAAGCAGAGG	CGGTGGAACTGGTCTGCAA
ATF3	CTGCAGAAAGAGTCGGAG	TGAGCCCGGACAATACAC
IGFBP4	CTCTTCCGGTGCTGACCTCT	GGTGCTCCGGTCTCGAAT
BCL2	CTGCACCTGACGCCCTTCACC	CACATGACCCCACCGAACTCAAAGA

5.2.22 TCGA analysis

TCGA data analysis was performed as described in Chowdhury et al. 2016.

5.3 Results

5.3.1 Knockdown of PBRM1 in normal epithelium promotes growth and a loss of epithelial cell maintenance

Since mutation of PBRM1 in epithelial cells is an early event in tumorigenesis[93] we set out to understand the tumor suppressive role PBRM1 plays in the context of normal epithelial cells. We depleted PBRM1 using lentiviral shRNA in several epithelial cell lines including the immortalized human kidney epithelial cell line HK-2, the canine kidney epithelial cell line MDCK, and the mouse mammary epithelial cell line NMuMG (S1A). In addition to its role in renal cancer, PBRM1 acts as a tumor suppressor in mammary epithelium derived cancers as observed in PBRM1 mutated [56] and PBRM1-downregulated breast cancers (S1B)[135]. The loss of PBRM1 resulted in an increase in proliferation in all of these cell lines (Fig 5.1A). Since NMuMG is the most commonly used epithelial cell line model, we used it for further analysis and validated the PBRM1 knockdown phenotype using CRISPR-mediated knockout of PBRM1 (Fig 5.1A, S1C). In NMuMG cells, knockdown of PBRM1 decreases protein levels of E-cadherin, a marker of

epithelial cells, and increases vimentin, a marker of mesenchymal cells (Fig 5.1B)[136]. A decrease in E-cadherin at adherens junctions results in a weakening of cell-cell adhesion and also results in the release of bound β-catenin, which normally anchors E-cadherin to the actin cytoskeleton[136]. In agreement with this, we observed an increase in nuclear β-catenin signaling upon PBRM1 knockdown (Fig 5.1C). The complete loss of E-cadherin expression and cellular morphology characteristic of a robust epithelial-to-mesenchymal transition (EMT) was not observed; instead, the observed phenotypes reflect a partial EMT or a reduction in epithelial maintenance. The same phenotypes were also observed upon knockdown of BRD7, another PBAF-specific subunit[114], although these findings are complicated by a decrease in PBRM1 upon BRD7 knockdown (S1D). Consistent with the documented role for the BAF complex in maintaining human mammary epithelial proliferation[137], knockdown of BAF subunits ARID1A or BRG1 resulted in cell arrest and death (data not shown).

A decrease in E-cadherin in epithelial cells during EMT results in a weakening of cell-cell contacts resulting in an increase in migration rates, which was observed in the PBRM1 knockdown (Fig 5.1D) and PBRM1 knockout (S1E). A decrease in E-cadherin also results in a decrease in cellular polarity, a feature central to epithelial function. To investigate the contribution of PBRM1 to the maintenance of epithelial cell polarity we plated NMuMG cells in Matrigel-based 3D culture where they self-assemble into luminal structures consisting of hollow acini displaying apical-basal polarity[138]. Upon PBRM1 knockdown, the spheres fail to establish hollow lumen and lose both ZO-1 at apical tight junctions and basal/lateral staining of alpha 6 integrin (Figure 5.1E, S1F). This phenotype is consistent with that observed in NMuMG epithelial cells with PTEN deletion or PI3K activating mutation[139].

5.3.2 PBRM1 regulates genes involved in cell adhesion, signaling, stress response, and apoptosis.

To identify genes regulated by PBRM1 in epithelial cells, we performed RNA-Seq from control and PBRM1 knockdown NMuMG cells. In total, we identified 2467 genes with significantly increased transcript levels and 1927 genes with significantly decreased transcript levels upon *PBRM1* knockdown. Gene ontology (GO) analysis identified numerous pathways significantly enriched in genes downregulated upon shPBRM1, including cell movement, cell structure, development, and signaling (Fig 5.2A), as would be expected based on the loss of epithelial characteristics in the PBRM1 knockdown (Fig 5.1). In addition, there were numerous

enriched biological pathways involved in stress response, cellular homeostasis, translational elongation, and apoptosis. In contrast, there were few significantly enriched biological pathways for genes upregulated upon PBRM1 knockdown, however, these pathways included microtubule-based processes (Fig 5.2B).

Figure 5-1 Knockdown of PBRM1 in normal epithelium promotes growth and a loss of epithelial cell maintenance.

A) Epithelial cell lines HK-2 (human kidney), MDCK (canine kidney) and NMuMG (mouse mammary), were counted after 72h growth and cell number are presented as mean ± SD. n = 3-5. B) Immunoblot analysis of whole cell lysates from NMuMG cells indicates that PBRM1 knockdown results in decreased E-cadherin expression and increased vimentin expression. Quantification represented as percent of shPBRM1 over vector. C) β-catenin signaling, as measured using TopFlash reporter assay in NMuMG cells with vector control or shPBRM1. Individual replicates are presented as mean ± SD n = 8. D) Migration differences determined by measuring the cell-free area at 40x magnification at 0h and 8h after scratching with standard pipette tip. The data from twelve independent images were statistically analyzed and presented as mean ± SD n = 12. ** = $p < 0.01$ E) Acini with hollow lumen from NMuMG cells grown in 3D culture for 10 days were counted in a blinded manner and the frequency was calculated from total acini in a field of image (average of 5-6 acini per field). The data from eleven independent images were statistically analyzed (Student t-test) and presented as mean ± SD n = 11. Representative image of acini grown for 14 days were analyzed using immunofluorescence staining with anti-ZO1 (red) and anti-alpha-6-integrin (green). Nuclei (blue) were visualized by DAPI. *=$p < 0.05$, ** = $p < 0.01$, *** = $p < 0.001$, **** = $p < 0.0001$ (paired Student's t test). ns, not significant. Error bars represent S.D. Also see Figure S1.

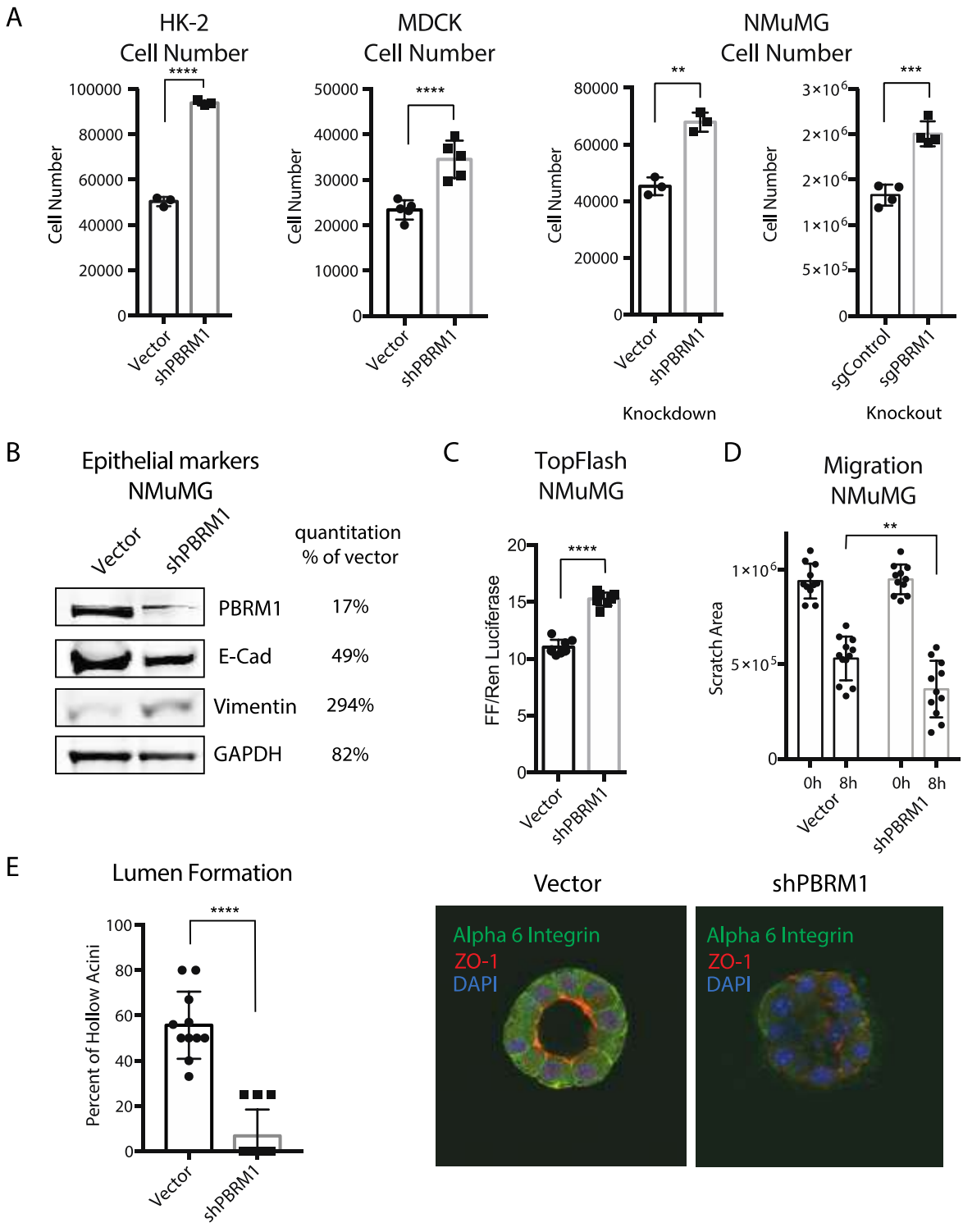
A
HK-2
Cell Number
MDCK
Cell Number
NMuMG
Cell Number
Cell Number
Vector
shPBRM1
sgControl
sgPBRM1
Knockdown
Knockout
B
Epithelial markers
NMuMG
quantitation
% of vector
PBRM1
17%
E-Cad
49%
Vimentin
294%
GAPDH
82%
C
TopFlash
NMuMG
FF/Ren Luciferase
D
Migration
NMuMG
Scratch Area
0h
8h
E
Lumen Formation
Percent of Hollow Acini
Vector
shPBRM1
Alpha 6 Integrin
ZO-1
DAPI

Figure 5-2 PBRM1 regulates genes involved in cell adhesion, signaling, stress response, and apoptosis and is predicted to cooperate with transcription factors involved in response to stress.

A) Top overrepresented biological process GO terms (p values<10^{-10}) for differentially expressed genes that are downregulated in NMuMG cells with shPBRM1. B) Top overrepresented biological process GO terms (p values<10^{-10}) for differentially expressed genes that are upregulated in NMuMG cells with shPBRM1. C) Putative transcription factors were identified for genes exhibiting differential expression in NMuMG cells with shPBRM1. D) Heat maps of regions identified as differentially accessible with PBRM1 knockdown using ATAC-Seq analysis of NMuMG cells. Regions of at least 1.5-fold differential accessibility were calculated between pooled samples of three biological replicates. E) Metagene plots of the regions identified as differentially accessible with PBRM1 knockdown using ATAC-Seq analysis of NMuMG cells. F) Genomic elements associated with the differentially accessible peaks. The overall distribution was calculated as a percentage of the total differentially accessible regions for each condition. G) Motif analysis was performed using HOMER for the differentially accessible peaks. Statistically significant motifs were identified based on relative enrichment over genomic areas with similar AT content. H) The contribution of PBRM1 to the transcriptional regulation of NRF2 (left) or c-Jun (right) target genes using qRT-PCR and *OAZ1* as the housekeeping gene. n = 3. *=p <0.05, ** = p <0.01, *** = p < 0.001, **** = p < 0.0001 (paired Student's t test). Error bars represent S.D. Also see Figure S2.

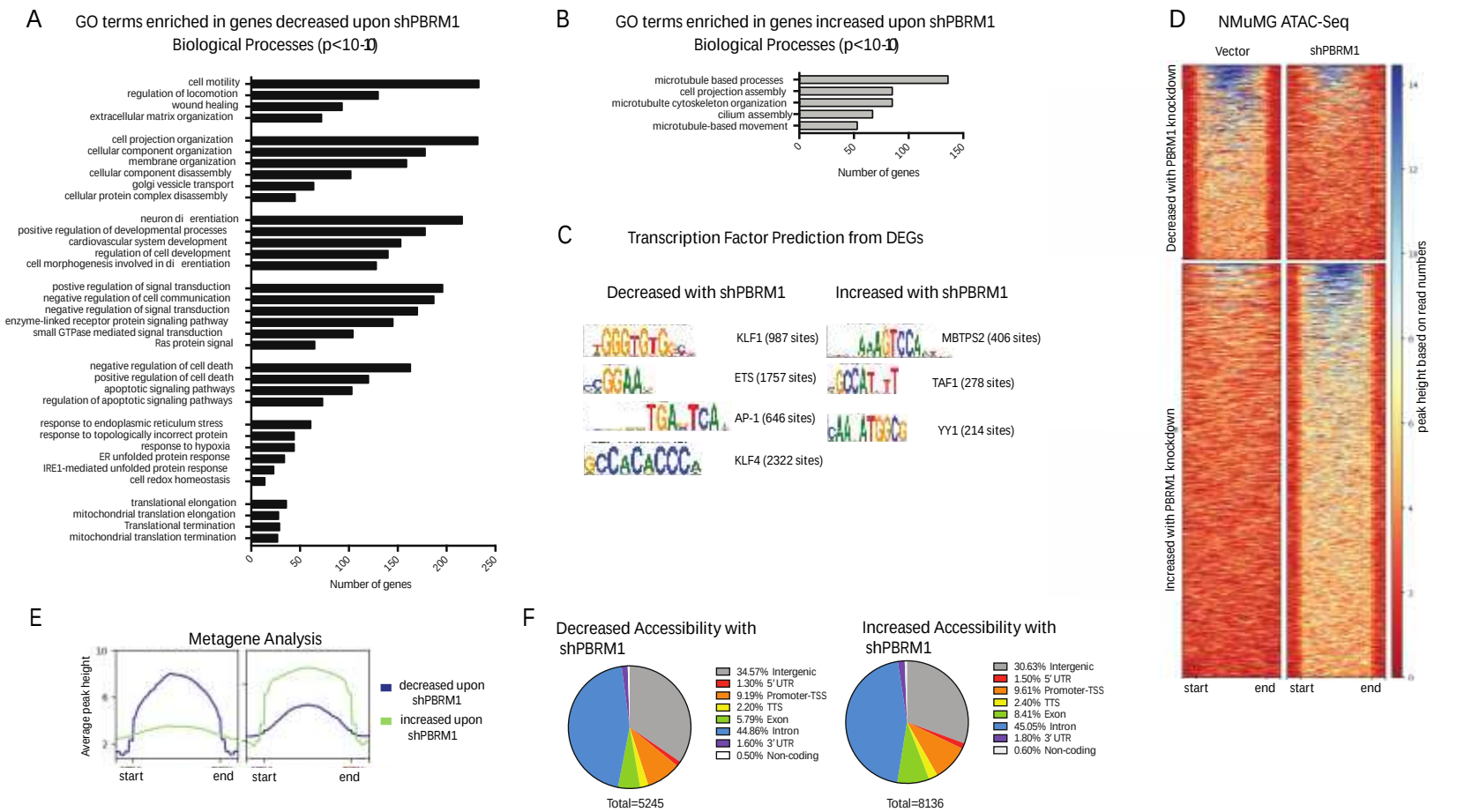
A
GO terms enriched in genes decreased upon shPBRM1
Biological Processes (p<10-10)
cell motility
regulation of locomotion
wound healing
extracellular matrix organization
cell projection organization
cellular component organization
membrane organization
cellular component disassembly
golgi vessicle transport
cellular protein complex disassembly
neuron di erentiation
positive regulation of developmental processes
cardiovascular system development
regulation of cell development
cell morphogenesis involved in di erentiation
postive regulation of signal transduction
negative regulation of cell communication
negative regulation of signal transduction
enzyme-linked receptor protein signaling pathway
small GTPase mediated signal transduction
Ras protein signal
negative regulation of cell death
positive regulation of cell death
apoptotic signaling pathways
regulation of apoptotic signaling pathways
response to endoplasmic reticulum stress
response to topologically incorrect protein
response to hypoxia
ER unfolded protein response
IRE1-mediated unfolded protein response
cell redox homeostasis
translational elongation
mitochondrial translation elongation
Translational termination
mitochondrial translation termination
0
50
100
150
200
250
Number of genes
B
GO terms enriched in genes increased upon shPBRM1
Biological Processes (p<10-10)
microtubule based processes
cell projection assembly
microtubulte cytoskeleton organization
cilium assembly
microtubule-based movement
0
50
100
150
Number of genes
C
Transcription Factor Prediction from DEGs
Decreased with shPBRM1
Increased with shPBRM1
KLF1 (987 sites)
MBTPS2 (406 sites)
ETS (1757 sites)
TAF1 (278 sites)
AP-1 (646 sites)
YY1 (214 sites)
KLF4 (2322 sites)
D
NMuMG ATAC-Seq
Vector
shPBRM1
Decreased with PBRM1 knockdown
Increased with PBRM1 knockdown
peak height based on read numbers
start
end
start
end
E
Metagene Analysis
Average peak height
decreased upon shPBRM1
increased upon shPBRM1
start
end
start
end
F
Decreased Accessibility with shPBRM1
34.57% Intergenic
1.30% 5' UTR
9.19% Promoter-TSS
2.20% TTS
5.79% Exon
44.86% Intron
1.60% 3' UTR
0.50% Non-coding
Total=5245
Increased Accessibility with shPBRM1
30.63% Intergenic
1.50% 5' UTR
9.61% Promoter-TSS
2.40% TTS
8.41% Exon
45.05% Intron
1.80% 3' UTR
0.60% Non-coding
Total=8136
G
Motifs enriched in peaks with decreased accessibility in shPBRM1
KLF6/KLF1 (2507)
ETS/GABPA/ELF1 (1989)
AP1 (1969)
FOXO (1440)
KLF3/KLF4/SP1 (1438)
NFkB (134)
Motifs enriched in peaks with increased accessibility in shPBRM1
AP1 (2565)
ETS (1610)
SP1 (1543)
KLF1 (1424)
TR4 (745)
HNF1B (241)
H
NRF2 targets
Vector
sgPBRM1
shNRF2
sgPBRM1 + shNRF2
Fold change over vector
NRF2
HMOX1
NQO1
c-Jun targets
Vector
sgPBRM1
sh c-Jun
sgPBRM1 + sh c-Jun
Fold change over control
cJUN
BCL2L1
HK2
IL1RL1

5.3.3 PBRM1 is predicted to cooperate with transcription factors involved in response to stress.

We further utilized the RNA-Seq datasets to predict upstream regulators that might cooperate with PBRM1 in transcription of target genes. For genes decreased with shPBRM1, several enriched consensus sequences were identified, with the most robust identified for KLF transcription factors, including KLF4, which is required for epithelial cell homeostasis[140,141]. In fact, the KLF4 knockdown in NMuMG cells has a similar phenotype to the PBRM1 knockdown[142]. In addition, there was significant enrichment for genes with consensus sequences for ETS transcription factors, which are primarily thought of as oncogenic, but are involved in a variety of processes like cell cycle, differentiation, and apoptosis[143]. Lastly, there was significant enrichment for genes with consensus sequences for AP-1 transcription factors, such as JUN/FOS and NRF2, which are upregulated during stress[144,145]. Similar to the RNA-Seq analysis, very few TF consensus sequences were enriched in the promoters of genes upregulated upon shPBRM1, but the main consensus sequences enriched were associated with MBTPS2, a protease that activates transcription factors involved in cholesterol synthesis and ER stress response[146], and YY1, a structural protein involved in promoter-enhancer associations[147].

To further define whether these putative transcription factors are directly regulated by PBRM1's chromatin remodeling function, we next turned to ATAC-Seq to identify sites of PBRM1-dependent chromatin accessibility. As observed elsewhere[121], PBRM1 knockdown did not have dramatic effects on global chromatin accessibility. It did, however, result in a significant decrease in accessibility (at least 1.5-fold) at 5,245 sites and increased accessibility at 6,790 in NMuMG cells (Fig 5.2D, E) with similar genomic distributions (Fig 5.2F). Similar results were obtained using PBRM1 knockdown in HK-2 epithelial cells (S2A, B). To identify transcription factors (TFs) that are potentially dependent on PBRM1 for chromatin binding, we calculated the enrichment of TF consensus binding sequences at sites with differential accessibility upon PBRM1 knockdown (Fig 5.2G, S2C). Several TF consensus sequences were significantly enriched compared to background at sites of increased as well as at sites of decreased accessibility upon shPBRM1. Consensus sequences for KLF, AP-1, ETS, FOXO, and NFkB transcription factors were highly enriched in regions with decreased accessibility upon shPBRM1, which correlates with the predicted regulators based on RNA-seq data (Fig 5.2D). In addition, there was a significant overlap between genes downregulated upon shPBRM1 and genes with an associated

region of decreased accessibility (536 genes, p = 4.5x10-83) and these regions displayed enrichment for KLF, AP-1, ETS, and FOXO consensus sequences. While we observed similar enrichment of consensus sequence binding sites in the regions with increased accessibility upon shPBRM1, the regions of accessibility didn't correlate to genes upregulated upon shPBRM (144 genes, p = 0.455). Since many of the biological pathways identified were related to apoptosis and stress response, we investigated the cooperation between PBRM1 and c-Jun and NRF2, two transcription factors that are activated during stress[144,145] (Fig 5.2H). Using lentiviral mediated shRNA knockdown, we found that similar to the PBRM1 knockout, knockdown of c-Jun (but not NRF2) increased proliferation (S2D). Using a publicly available dataset of NRF2 bound and regulated genes in A549 lung cancer cell lines (GSE113497), we identified 36 NRF2 targets that are also differentially expressed in the PBRM1 knockdown and have associated sites of decreased chromatin accessibility in the shPBRM1 ATAC-seq. Intriguingly, these included canonical NRF2 target antioxidant genes HMOX1 and NQO1[148]. Using qRT-PCR we confirmed NRF2 knockdown and evaluated the requirement for PBRM1 on expression of these genes (Fig 2H-left). In contrast to many published reports, HMOX1 did not show a dependence on NRF2 for expression, although it was dependent on PBRM1. As expected, NQO1 was dependent on both NRF2 and PBRM1 for expression. In the absence of comprehensive c-Jun datasets, we selected several putative c-Jun targets from c-Jun N terminal kinase (JNK)-dependent genes identified in previous studies. These include BCL2L1, an antiapoptotic regulator[149], HK2, a metabolic enzyme and antiapoptotic regulator[150], and IL1RL1, an anti-inflammatory IL33 receptor[123]. We confirmed c-Jun knockdown in NMuMG cells using qRTPCR and validated that these genes are regulated by both PBRM1 and c-Jun (Fig 5.2H-right). In summary, genes affected by PBRM1 knockdown are targets of transcription factors involved in response to stress.

5.3.4 Knockdown of PBRM1 results in elevated ROS under cellular stress conditions.

Due to the transcriptional signature indicating an increased importance for PBRM1 in regulating genes involved in stress response, we next examined how depletion of PBRM1 affects reactive oxygen species (ROS), which are generated by cells under a variety of cellular stresses[151]. NMuMG cells have low endogenous ROS levels and PBRM1 knockdown results in a small but significant increase in ROS under normal cell culture conditions (Fig 5.3A), as measured by conversion of 2',7'-dichlorodihydrofluorescein diacetate (H_2DCFDA) to the highly fluorescent

2',7'-dichlorofluorescein (DCF) by intracellular ROS. To understand the effects of PBRM1 on ROS under high cellular stress, we looked at ROS levels after recovery from hydrogen peroxide treatment (Fig 5.3B), glucose deprivation (Fig 5.3C), hypoxia-inducing $CoCl_2$ treatment (Fig 5.3D), and DNA-damaging doxorubicin treatment (Fig 5.3E). Under all of these stress conditions, cells lacking PBRM1 expression displayed increased levels of ROS.

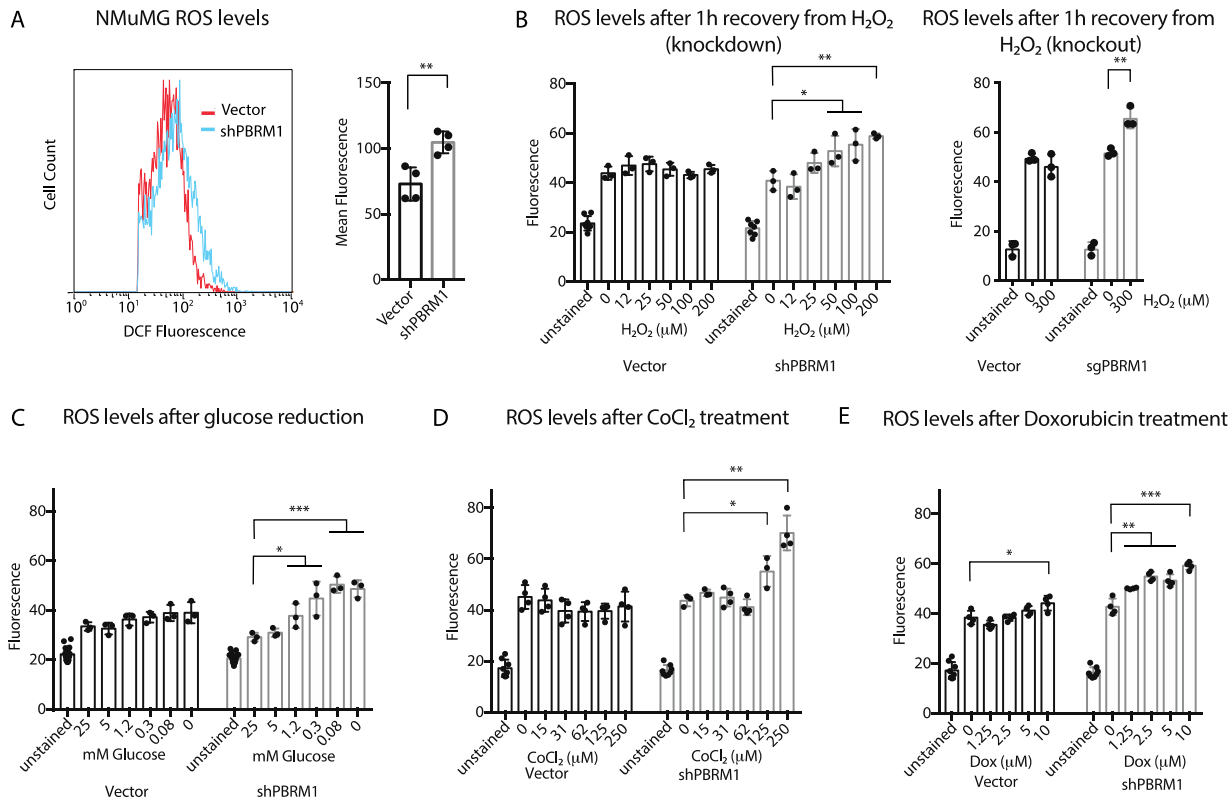

Figure 5-3 Knockdown of PBRM1 results in elevated ROS under cellular stress conditions.

A) NMuMG cells were trypsinized and stained for 30 min with H_2-DCFDA, washed with PBS, and analyzed using flow cytometry. The mean fluorescence value for 10,000 cells was calculated from four independent experiments. B) NMuMG cells grown in 96-well plates were treated with increasing concentrations of H_2O_2 for 1 h, washed with PBS, and incubated with H_2-DCFDA for 30 min. Reagent was washed away and the DCF fluorescence was measured in live cells. C) NMuMG cells grown in 96-well plates were treated with media containing varying concentrations of glucose (normal media = 25 mM) for 16 h, washed with PBS, and incubated with H_2-DCFDA for 30 min. Reagent was washed away and the DCF fluorescence was measured in live cells. D) NMuMG cells grown in 96-well plates were treated with media containing varying concentrations of $CoCl_2$ for 24 h, washed with PBS, and incubated with H_2-DCFDA for 30 min. Reagent was washed away and the DCF fluorescence was measured in live cells. E) NMuMG cells grown in 96-well plates were treated with media containing varying concentrations of doxorubicin for 24h, washed with PBS, and incubated with H_2-DCFDA for 30 min. Reagent was washed away and the DCF fluorescence was measured in live cells. *=p <0.05, ** = p <0.01, *** = p < 0.001, **** = p < 0.0001 (paired Student's t test). ns, not significant. Error bars represent S.D.

5.3.5 PBRM1 expression is cytoprotective under high stress conditions

A low level increase in ROS production promotes cancer progression by stimulating signaling, and facilitating transformation through increasing genomic instability and inflammation (Fig 5.4A)[151]. In addition, ROS can increase AKT phosphorylation and induce changes in cell adhesion molecules to increase motility[151], both of which we observed previously in Caki2 renal cancer cells without PBRM1[26] and in epithelial cells lacking PBRM1 (S1A). While increases in ROS are characteristic in cancer and contribute to transformation and oncogenesis, cancer cells need to avoid extremely high levels of ROS due to cytotoxicity (Fig 5.4A)[151].To understand how PBRM1-regulated ROS levels under high stress conditions affect cellular viability, we measured cell survival after high concentrations of hydrogen peroxide for 16h. We found that PBRM1 knockdown decreased viability under these high stress conditions in the NMuMG (Fig 5.4C) and MDCK epithelial cells (S3A), an effect observed similarly with the NRF2 knockdown (Fig 5.4B). This was not due to increased apoptosis in the PBRM1 knockdown, and in fact, cells lacking PBRM1 displayed a deficiency in Annexin V (Fig 5.4D) and cleaved PARP (Fig 5.4E, S3C) under stress conditions. This is in line with the transcriptional role for PBRM1 in regulating pro-apoptotic genes (Fig 5.2A). While it seems counterintuitive that PBRM1-expressing cells have both increased apoptosis and increased cell survival under high stress conditions, it is consistent with a role for PBRM1 in the stress response, which often results in apoptosis if cellular stresses are not resolved. In contrast, cells lacking PBRM1 are unable to mount a proper response to external stress, leading to high ROS levels and cell death through other means, such as necrosis (Fulda et al., 2010), which is supported by the increase in necrosis marker lactate dehydrogenase (LDH) in the NMuMG cells lacking PBRM1 (Fig 5.4F).

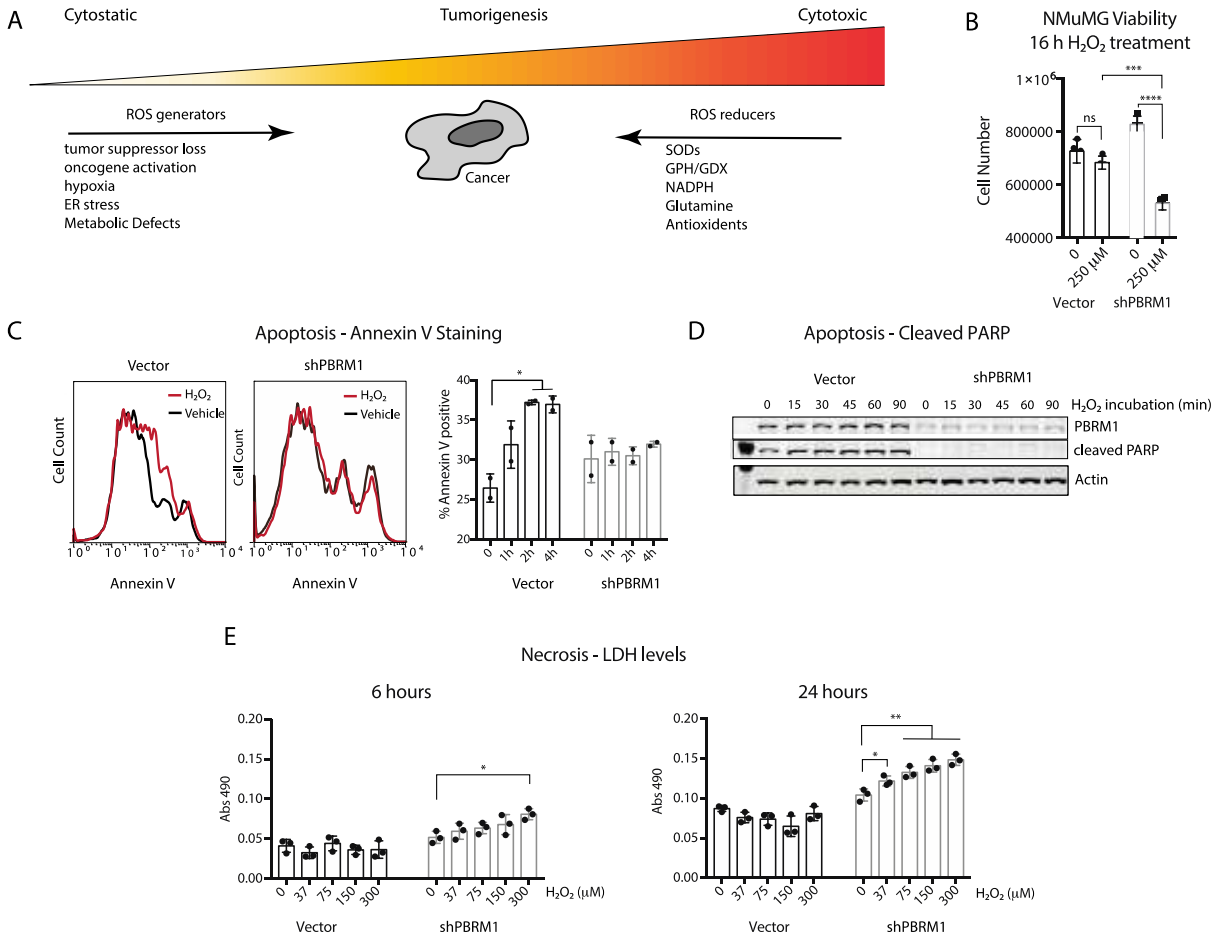

Figure 5-4 PBRM1 expression is cytoprotective under high stress conditions.

PBRM1 induces apoptotic pathways and increases cellular viability under high cellular stress conditions. A) Depiction of the multifaceted role ROS regulators play in cancer B) NMuMG cells were cultured in normal cell media or 250 μM H_2O_2 for 16 h and the number of live cells were counted using trypan blue. C) Annexin V staining was measured in NMuMG cells treated with 200 μM H_2O_2 for the indicated times. The percentage of Annexin V positive cells was calculated for two independent experiments. D) Whole cell lysates were prepared from NMuMG cells treated with 200 μM H_2O_2 for the indicated times and probed for the indicated proteins using immunoblot analysis. E) LDH release was measured from 10 μL of media using LDH Cytotoxicity Assay Kit II (Abcam). *=p <0.05, ** = p <0.01, *** = p < 0.001, **** = p < 0.0001 (paired Student's t test). ns, not significant. Error bars represent S.D. Also see Figure S3.

5.3.6 PBRM1-regulated transcriptional effects under cellular stress conditions

To determine if the dependency on PBRM1 expression for viability under stress conditions is due to the PBRM1's regulation of different genes under stress conditions, we characterized the transcriptional profile of NMuMG cells with and without PBRM1 knockdown, grown in H_2O_2 (200 μM) for 2h or low glucose media for 6h. There were between 1000-2000 DEGs identified in cells grown in H_2O_2 or low glucose growth conditions for both vector control and shPBRM1 cells; however, the impact of PBRM1 knockdown on overall gene expression was more significant than the impact of either stress condition (Fig 5.5A). We observed a significant correlation between gene expression changes induced by PBRM1 knockdown in different stress conditions (S4A), and a significant correlation between gene expression changes induced by stress conditions in the two cell lines (vector and shPBRM1) (S4B) indicating that many genes altered by stress are not dependent on PBRM1 and many genes dependent on PBRM1 are not altered by stress (S4C). In addition, we observed a significant correlation between gene expression changes induced by the two different stress conditions (S4C). As expected, the significantly enriched GO terms were similar for genes regulated by PBRM1 under stress treatment compared to untreated cells; however, more genes from pathways involved in cell adhesion, signaling, and apoptosis were altered upon shPBRM1 under stress treatments (Fig 5.5B). Further, we observed several GO terms that were significantly enriched only for genes downregulated with shPBRM1 under either stress treatment, including cell cycle, protein metabolic processes, and cellular response to stress, and for genes downregulated upon shPBRM1 only under H_2O_2 treatment, such as RNA processing and DNA-damage response (Fig 5.5C). Accordingly, there were many genes dependent on PBRM1 expression for induction under H_2O_2 stress (Fig 5.5D), many of which are involved in cell adhesion, apoptosis, ER stress, and antioxidant response. We used this dataset to identify the NRF2 and c-Jun targets from Figure 2 that were induced under H_2O_2 stress. c-Jun target, *IL1RL1*, an IL-33 receptor involved in protection from stress[152], requires both PBRM1 and c-Jun for induction upon H_2O_2 treatment (Fig 5.5E). Similarly, the antioxidant NRF2 targets, *HMOX1* and *NQO1*, are induced upon H_2O_2 treatment and require PBRM1 and/or NRF2 for full gene induction. (Fig 5.5F) In conclusion, the RNA-Seq analysis of PBRM1-dependent gene expression under stress conditions supports a role for PBRM1 in inducing a subset of stress response genes to promote cell survival under conditions of high stress.

Figure 5-5 PBRM1-regulated transcriptional effects under cellular stress conditions

A) RNA-Seq was performed on NMuMG cells grown in 200 μM H_2O_2 for 2h or glucose-free media for 6h. B) Top overrepresented biological process GO terms ($p < 10^{-10}$) for genes differentially expressed upon shPBRM1 in all cell culture conditions. C) Overrepresented biological process GO terms ($p < 10^{-10}$) for differentially expressed genes downregulated with shPBRM1 only under H_2O_2 or low glucose cell culture conditions. D) Representation of the RNA-seq data for a subset of differentially expressed genes that require PBRM1 for upregulation during H_2O_2 stress. E) The contribution of PBRM1 to the transcriptional regulation of c-Jun target gene *IL1RL1* under normal cell culture or 4 h H_2O_2 (250 μM) using qRT-PCR and *OAZ1* as the housekeeping gene. n = 3. *=p <0.05, ** = p <0.01, *** = p < 0.001, **** = p < 0.0001 (paired Student's t test). ns, not significant. Error bars represent S.D. F) The contribution of PBRM1 to the transcriptional regulation of NRF2 target genes *NQO1* (left) and *HMOX* (right) under normal cell culture or 4 h H_2O_2 (250 μM) using qRT-PCR and *OAZ1* as the housekeeping gene. n = 3. *=p <0.05, ** = p <0.01, *** = p < 0.001, **** = p < 0.0001 (paired Student's t test). ns, not significant. Error bars represent S.D. Also see Figure S4.

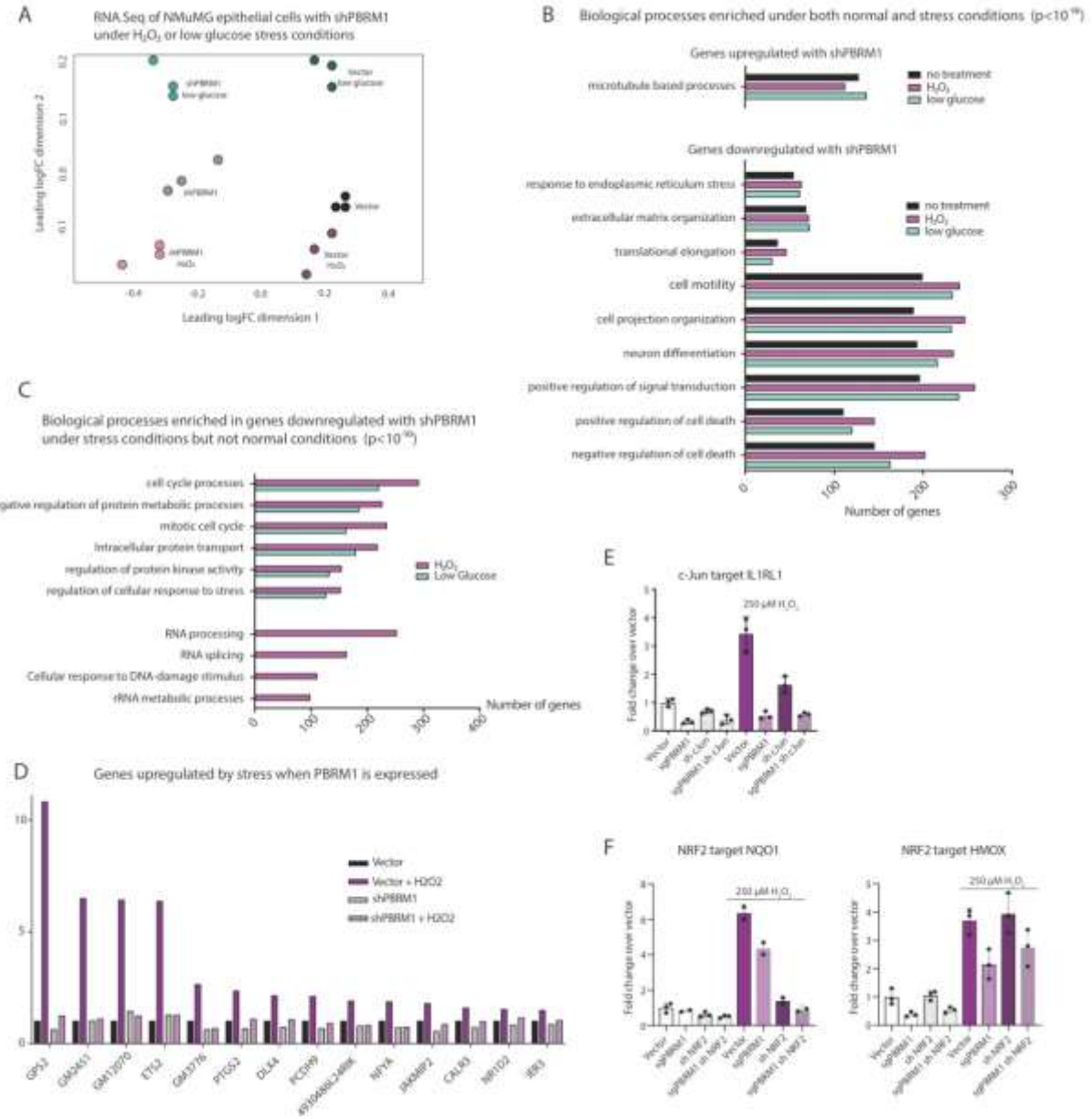
A
RNA Seq of NMuMG epithelial cells with shPBRM1 under H_2O_2 or low glucose stress conditions
Leading logFC dimension 2
Leading logFC dimension 1
B
Biological processes enriched under both normal and stress conditions ($p<10^{-19}$)
Genes upregulated with shPBRM1
microtubule based processes
no treatment
H_2O_2
low glucose
Genes downregulated with shPBRM1
response to endoplasmic reticulum stress
extracellular matrix organization
translational elongation
cell motility
cell projection organization
neuron differentiation
positive regulation of signal transduction
positive regulation of cell death
negative regulation of cell death
Number of genes
C
Biological processes enriched in genes downregulated with shPBRM1 under stress conditions but not normal conditions ($p<10^{-30}$)
cell cycle processes
negative regulation of protein metabolic processes
mitotic cell cycle
Intracellular protein transport
regulation of protein kinase activity
regulation of cellular response to stress
RNA processing
RNA splicing
Cellular response to DNA damage stimulus
rRNA metabolic processes
H_2O_2
Low Glucose
Number of genes
D
Genes upregulated by stress when PBRM1 is expressed
Vector
Vector + H2O2
shPBRM1
shPBRM1 + H2O2
GPX3
GM2431
GM12070
ETS2
GM3776
PTGS2
DLK4
PCSK9
4910486L24Rik
NFYA
2K04RP2
CALR3
NR1D2
IER3
E
c-Jun target IL1RL1
250 μM H_2O_2
Fold change over vector
F
NRF2 target NQO1
NRF2 target HMOX
250 μM H_2O_2
Fold change over vector

5.3.7 PBRM1 has cell-type specific roles on viability:

Since establishing that PBRM1 knockdown can have different effects on viability depending on the stress environment, we re-evaluated the premature senescence phenotype previously described for PBRM1 knockout in mouse embryonic fibroblasts (MEFs)[31]. We confirmed that PBRM1 knockdown (S5A) results in a loss in the proliferative capacity of MEFs (Fig 5.6A) similar to published findings with the PBRM1 conditional knockout[31]. We next observed a significant increase in ROS levels and H_2O_2 levels in MEFs upon PBRM1 knockdown (Fig5. 6B, S5B), which was most similar to the robust increase in ROS levels observed in shPBRM1 NMuMG cells grown under high stress conditions. This particular sensitivity of MEFs to PBRM1 knockdown is most likely due to the unique susceptibility of MEFs to oxidative stress from high oxygen content in air[122]. To support this, we found that exogenous antioxidants such as Vitamin C (Fig 5.6C) or N acetyl cysteine (NAC) (S5C) were able to reverse the viability defect induced by PBRM1 knockdown in MEFs.

We next sought to examine how intrinsic genetic changes could alter dependency on PBRM1. To do this we employed the MCF10A human mammary epithelial cell line[153], and the MCF10A-T1k cell line, which has been transformed with T24-HRas and passaged in a mouse[154]. We knocked down PBRM1 in both of these cell lines (S6A) and found dramatically different effects on viability. Similar to other epithelial cell lines, PBRM1 knockdown in MCF10A results in an increase in proliferation and a slight increase in ROS (Fig 5.6D), with some, but not all, of the same changes in gene expression compared to PBRM1 knockdown in NMuMG cells (S6B), In contrast, PBRM1 knockdown in the MCF10A-T1k cell line is highly deleterious to viability, causing cells to cease proliferation altogether within 3-4 passages (Fig 5.6E, left). Similar to MEFs, PBRM1 knockdown in this line induces a highly significant increase in ROS levels, (Fig 5.6E, right) and similar to MEFs, Vitamin C administration can partially restore proliferative capacity in the PBRM1 knockdown (Fig 5.6F). The oncogene-induced stress in the MCF10A-T1k cell line promotes dependency on PBRM1 for viability, which may be reflected in its increased level of ROS at baseline compared to MCF10A cells (S6C). In summary, our data up to this point establish that PBRM1 knockdown can have different effects on viability in the same cell line due to different external stress environments, or in two different cell lines due to cell-type susceptibilities to stress.

Figure 5-6 PBRM1 has cell-type specific roles on viability.

A) Mouse embryonic fibroblasts (MEFs) were counted after 72h growth using trypan blue and data presented as mean ± SD. n = 3. B) Equal numbers of MEFs were plated in 96-well format. After 24h the cells were washed with PBS, incubated with H2-DCFDA for 1h and the DCF fluorescence was measured in live cells. Data presented as mean ± SD. n = 5. C) MEFs were cultured for 8 days in normal media or media supplemented with 20 µg/mL Vitamin C. Luminescence was measured using CellTiter-Glo® assay system and data presented as mean ± SD. n = 7. *=p <0.05, ** = p <0.01, *** = p < 0.001, **** = p < 0.0001 (paired Student's t test). ns, not significant. Error bars represent S.D. D) Human mammary epithelial cell line MCF10A was counted after 72h growth using trypan blue to eliminate dead cells, and data presented as mean ± SD. n = 3. * p <0.05 (left). MCF10A cells were trypsinized and stained for 30 min with H_2-DCFDA, washed with PBS, and 100,000 cells were analyzed using flow cytometry (right). E) Transformed human mammary cell line MCF10A-T1k was counted after 72h growth using trypan blue to eliminate dead cells, and data presented as mean ± SD. n = 3. *** p<0.001 (left). MCF10A-T1k cells were trypsinized and stained for 30 min with H_2-DCFDA, washed with PBS, and 100,000 cells were analyzed using flow cytometry (right). F) MCF10A-T1k cells were cultured for 7 days in normal media or media supplemented with 20 µg Vitamin C (left). Luminescence was measured using CellTiter-Glo® assay system (right) and data presented as mean ± SD. n = 3. *p<0.05 ** p<0.01. Also see Figure S5 and Figure S6.

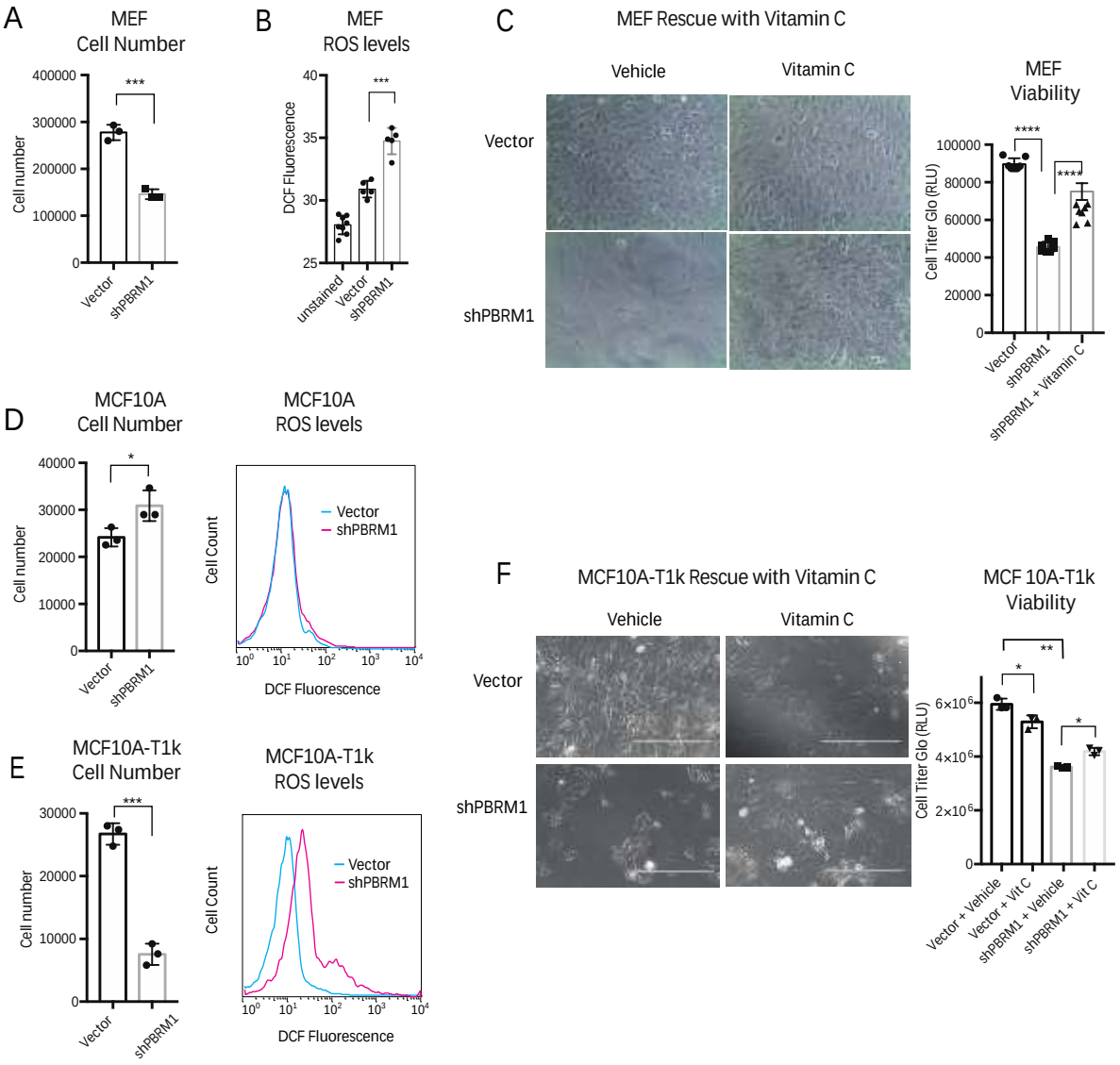
A
MEF
Cell Number
Cell number
400000
300000
200000
100000
0
***
Vector
shPBRM1
B
MEF
ROS levels
DCF Fluorescence
40
35
30
25
***
unstained
Vector
shPBRM1
C
MEF Rescue with Vitamin C
Vehicle
Vitamin C
Vector
shPBRM1
MEF
Viability
Cell Titer Glo (RLU)
100000
80000
60000
40000
20000
0
****
****
Vector
shPBRM1
shPBRM1 + Vitamin C
D
MCF10A
Cell Number
Cell number
40000
30000
20000
10000
0
*
Vector
shPBRM1
MCF10A
ROS levels
Cell Count
Vector
shPBRM1
DCF Fluorescence
E
MCF10A-T1k
Cell Number
Cell number
30000
20000
10000
0
***
Vector
shPBRM1
MCF10A-T1k
ROS levels
Cell Count
Vector
shPBRM1
DCF Fluorescence
F
MCF10A-T1k Rescue with Vitamin C
Vehicle
Vitamin C
Vector
shPBRM1
MCF 10A-T1k
Viability
Cell Titer Glo (RLU)
6x10^6
4x10^6
2x10^6
0
**
*
*
Vector + Vehicle
Vector + Vit C
shPBRM1 + Vehicle
shPBRM1 + Vit C

5.3.8 PBRM1 displays stress response phenotype in renal cancer cells:

To begin to decipher how the stress response functions observed for PBRM1 in epithelial cells might relate to its role in renal carcinoma, we first determined the enriched GO terms for the genes with decreased expression in patients with PBRM1 mutations, which were similar to the pathways observed in the NMuMG cells, including cell adhesion, neuronal processes, apoptosis and ER stress/proteolysis (S7A). Further we compared the differentially regulated genes and observed the most significant gene overlap between genes with decreased expression in patients with PBRM1 mutations and genes with decreased expression in the PBRM1 knockdown (S7B), similar to the overlaps we observed with Caki2 cells, a renal carcinoma cell line with loss of function mutations in PBRM1[26]. Therefore, we used Caki2 ccRCC cell lines with PBRM1 re-expression to determine if the same phenotypes are observed in the renal cancer setting. Previously we have shown that re-expression of PBRM1 decreases growth and migration of Caki2 cells[26]. When we used DCF staining to determine ROS levels, we observed highly elevated ROS compared to the epithelial cells, which is consistent with previous observations about high ROS in cancer cell lines[151](Fig 5.3A, 5.7A). However, the re-expression of PBRM1 only reduced ROS levels to a very slight degree under normal cell culture conditions (Fig 5.7A). In contrast to the NMuMG cells, high stress conditions in Caki2 cells did not result in an increase in ROS levels in the absence of PBRM1; however, in the presence of PBRM1, high stress conditions induced a dramatic decrease in ROS levels (Fig 5.7B, 5.7C). Further, PBRM1 re-expression promoted cell survival (Fig 5.7D) as well as increased cleaved PARP (Fig 7E) under hydrogen peroxide treatment conditions, consistent with a role for PBRM1 in activating apoptosis pathways under high cellular stress. In contrast, Caki2 cells lacking PBRM1 display an increase in necrosis marker lactate dehydrogenase (LDH) when exposed to H_2O_2 stress (Fig 5.7F).

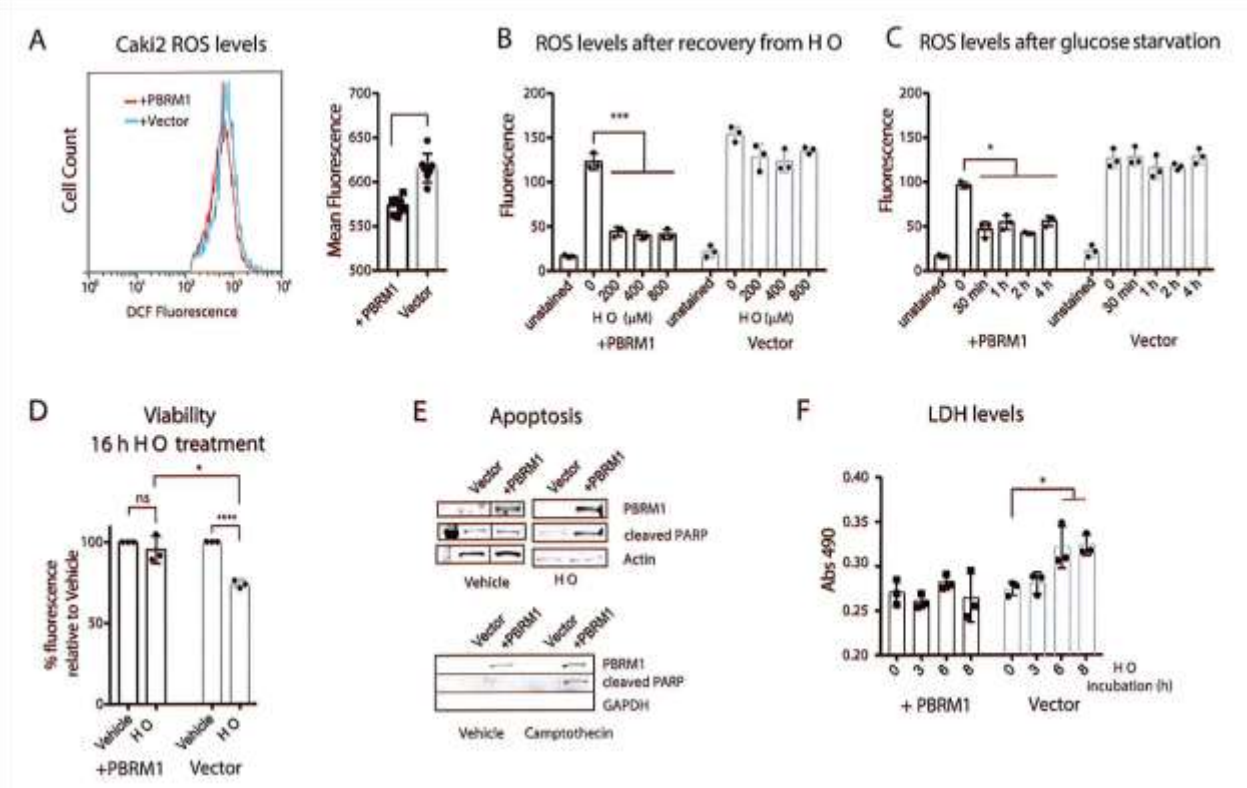

Figure 5-7 PBRM1 displays stress response phenotype in renal cancer cells.

PBRM1 regulates stress response in renal carcinoma cells. A) Caki2 cells were trypsinized and stained for 30 min with H_2-DCFDA, washed with PBS, and analyzed using flow cytometry. The mean fluorescence value for 10,000 cells was calculated from seven independent experiments. B) Caki2 cells grown in 96-well plates were treated with increasing concentrations of H_2O_2 for 1 h, washed with PBS, and incubated with H_2-DCFDA for 30 min. Reagent was washed away and the DCF fluorescence was measured in live cells. C) Caki2 cells grown in 96-well plates were treated with glucose-free media for varying time periods, washed with PBS, and incubated with H_2-DCFDA for 30 min. Reagent was washed away and the DCF fluorescence was measured in live cells. *=p <0.05, ** = p <0.01, *** = p < 0.001, **** = p < 0.0001 (paired Student's t test). ns, not significant. Error bars represent S.D. D) Caki2 cells were cultured in normal cell media or 200 μM H_2O_2 for 16 h and the cell viability was estimated using crystal violet staining. E) Whole cell lysates were prepared from Caki2 cells treated with 200 μM H_2O_2 or 100 μM camptothecin for 2h and relative levels of indicated proteins were probed using immunoblot analysis. Irrelevant lane spliced out. F) LDH release was measured from 10 μL of media using LDH Cytotoxicity Assay Kit II (Abcam). *=p <0.05, ** = p <0.01, *** = p < 0.001, **** = p < 0.0001 (paired Student's t test). ns, not significant. Error bars represent S.D. Also see Figure S7.

5.4 Discussion

Chromatin regulators are frequently misregulated in cancer with resulting alterations in gene transcription; however, many of these regulators alter a large number of genes to a small degree and can regulate very different sets of genes in different cell lines. An additional challenge resides in the fact that many chromatin regulators modulate transcription differently depending on environmental inputs[155]. Thus, it has been incredibly challenging to decipher how the transcriptional effects of chromatin regulators observed in a particular cell line relates to its general biochemical function or its phenotype *in vivo*. Traditional cell culture models are often devoid of the environmental stimuli chromatin regulators normally sense, making it a significant challenge to develop a relevant cell culture model for accurately studying these regulators. Here, we have used transcriptional analysis of epithelial cells with PBRM1 knockdown to identify pathways involved in epithelial cell maintenance and stress response. In addition, we have validated a role for PBRM1 in the maintenance of epithelial cell identity and identified KLF, AP-1 and ETS transcription factors consensus sequences in both genes downregulated upon shPBRM1, as well as regions with decreased chromatin accessibility upon shPBRM1. From this, we have validated a role for PBRM1 in facilitating the transcription of c-Jun and NRF2 target genes, restraining ROS production and inducing both apoptotic and cell survival pathways under high stress conditions[156,157].

In addition to changes in transcription factor expression and localization during cellular stress, oxidative stress and metabolic stress are known to specifically upregulate H3K14Ac at stress response genes[158], a histone mark specifically recognized by PBRM1[27]. While H3K14Ac is generally found at active promoters with H3K9Ac, it is found without H3K9Ac at inducible genes[100] and is specifically increased in gene bodies during stress[159]. H3K14Ac is also a mark associated with renal epithelium adaption to oxidative stress[160,161], high-fat diet induced inflammation in rodents[162], endoplasmic reticulum stress[163], and sites of DNA-damage [164], a process for which PBRM1 has a well-established role[32]. Therefore, specific patterns of histone acetylation likely delineate a subset of stress-response genes targeted by PBRM1, which is likely to be unique for a particular cell type, as well as a particular stressor.

A role for PBRM1 in stress response is in agreement with recent findings that PBRM1 deletion alone is not sufficient for transformation but acts to facilitate oncogenesis in cooperation with VHL deletion[35,122,123]. PBRM1 deletion allows for an amplification of oncogenic signaling[35,121], as well as a bypass of checkpoints induced by replication stress after VHL deletion[122]. This could be in part due to PBRM1's role in regulating the hypoxia stress response in cooperation with HIF1a, which allows for the reduction of ROS and induction of apoptosis in response to hypoxia [165].

Not only is a role in stress response likely part of PBRM1's function as a tumor suppressor during cancer initiation, it may also be involved in PBRM1's protective function against cancer therapeutics, similar to the protective role PBRM1 plays under high stress conditions. ccRCC patients with PBRM1 mutations tend to have favorable prognosis [166] and recent studies indicate that PBRM1 mutant tumors respond particularly well to sunitinib [167] and PD-1 inhibitors [38]In support of this, a recent CRISPR-Cas9 screen identified PBRM1, along with other PBAF-specific subunits, as resistance factors against T-cell mediated killing [39]. This is related to a general role for PBRM1 in suppressing the inflammatory response, as PBRM1 deletion also increases innate immunity hyperinflammation in the gut [168,169]. The general role for PBRM1 in the stress response could relate to PBRM1's role in suppressing inflammation (and T-cell mediated toxicity) through the regulation of homeostasis [170], although that connection will need to be explored further.

CHAPTER 6. FUTURE DIRECTIONS

6.1 Introduction

Polybromo1 (PBRM1) is a member of the PBRM1-BRG1 Association Factors (PBAF) chromatin remodeling complex. PBRM1 contains six bromodomains (acetyl-lysine binders), two bromo-adjacent homologs (protein-protein domains) and a high mobility group (DNA interacting motif)[15] and is the defining feature of this complex compared to BAF. Due to the large number of reader domains, PBRM1 is predicted to allow for altered targeting of PBAF compared to BAF. Though frequently mutated in renal clear cell carcinoma (ccRCC), defining the function of PBRM1 has been challenging. Depletion of PBRM1 in most cell lines and in adult mice causes little to no phenotypical change[26,30,41]. Recent mouse studies have validated PBRM1 as a tumor suppressor, however loss of PBRM1 alone is not sufficient for oncogenesis. When *PBRM1* is knocked out in the kidneys in combination with *Von-Hippel Lindau (VHL),* the most commonly mutated gene in ccRCC, tumors form[35]. As described earlier, VHL is a E3 ubiquitin ligase that regulates hypoxia inducible factors (HIF). These transcription factors activate genes that allow cells to adapt to low oxygen levels. In cells without VHL, HIF factors are no longer being regulated and are able to reprogram the cells metabolism and promote angiogenesis, which is beneficial to cancer growth. It is unclear how the loss of PBRM1 promotes tumorigenesis in VHL-negative cells. We predict PBRM1 is acting to protect cells after loss of VHL and its protective mechanism is only necessary when the cellular environment is experiencing elevated stress. To examine this hypothesis, we explored how PBRM1 expression affected cells under different stressors. We identified a general role of PBRM1 in protecting cells from stress[171]. We observed that cells without PBRM1 have elevated reactive oxygen species compared to cells expressing PBRM1. Furthermore, PBRM1-negative cells showed a sensitivity to addition of external stress, indicating under normal conditions, PBRM1 is dispensable for cell survival, however it is necessary under stress. From our transcriptional analysis we have found PBRM1 is regulating pathways that are activated under elevated levels of ROS. Under external stress PBRM1 increases the expression of genes in these stress response pathways. PBRM1 appears to be acting as a stress sensor and working to protect cells through upregulating genes important for protecting the cell. However, we have not fully elucidated how PBRM1 is protecting cells from stress. PBRM1 is the only known

protein with six consecutive bromodomains, indicating that the function of this protein is due to its ability to read epigenetic modifications. Our preliminary work indicates that PBRM1 preferentially binds the combination of histone 3 lysine 14 acetylation (H3K14Ac) and H3K18Ac. Our proposed mechanism is that the pattern of these two histone acetylation marks are altered when cells experience stress, recruiting PBAF through the PBRM1 bromodomains, allowing for remodeling of stress gene promoters allowing for transcription factor binding and transcriptional activation of these genes. Here we discuss our preliminary data for this hypothesis and discuss how we plan to further examine the mechanism of PBRM1 under stress.

6.2 PBRM1-regulated transcriptional effects are amplified under stress

From our work in NMuMG cells, we have found that PBRM1 is regulating genes involved in pathways such as hypoxia, apoptosis, and cell adhesion[171]. We wanted to examine if PBRM1 is regulating the same set of genes across multiple cell lines. We performed RNA-seq in both cancer lines: Caki2, ccRCC with PBRM1 re-expression, Caki1, ccRCC with PBRM1knockdown, NMuMG, mouse mammary epithelial with PBRM knockdown, and HK2, human renal epithelial cells with PBRM1 knockdown[26,171]. Through these studies, we have found comparing genes that are upregulated by PBRM1 showed poor overlap, however, there is significant overlap gene ontology (GO) terms for all four cell lines with pathways including hypoxia, apoptosis, and cell adhesion (Fig 6.1A). These pathways are all associated with response to changes in environment and elevated stress. Evaluation of transcription factor consensus sequences in the promoters of genes upregulated by PBRM1 in all four cell lines revealed significant enrichment of FOXO, E12, LEF1, AP1, AP4, MAZ, NFAT, and MYOD consensus sequences (Fig 6.1B). Due to NFAT and LEF1 being similarly enriched at PBRM1 down-regulated genes, the consensus sequences that are uniquely enriched in PBRM1-upregulated genes are bound by FOXO, AP1, AP4, MAZ, E12, and MYOD TFs. These transcription factors implicated in the transcription of genes involved in cell type identity (MYOD, E12), proliferation and migration (AP4, MAZ) and stress-response (FOXO, AP1).

To further examine PBRM1 transcriptional effect on gene expression, we cultured Caki2 cells in an organotypic 3D culture hydrogel system. This method mimics the extracellular matrix environment as well as constraining nutrient and oxygen availability[67]. We found that culturing Caki2 cells under 3D conditions enhanced the growth suppressive effect of PBRM1 re-expression

compared to standard 2D culture (Fig 6.2A). To define a mechanistic basis for these observations, we characterized the transcriptional profile of Caki2 cells derived from 3D culture and compared it to the RNA-Seq from Caki2 cells grown in standard 2D (Fig 6.2B). Comparison of differentially expressed genes (DEGs) by PBRM1 showed significant overlap in both 2D and 3D growth conditions, although more genes were both significantly upregulated and significantly downregulated upon PBRM1 re-expression in 3D culture compared to 2D culture. Accordingly, the correlation between datasets was quite high ($R^2 = 0.41$), with many of the same genes similarly regulated in both conditions (Fig 6.2B). The biggest difference was that genes tended to exhibit a greater fold change in transcript levels with PBRM1 re-expression in 3D culture than 2D culture (slope = 0.36, almost 3-fold higher fold change on average).

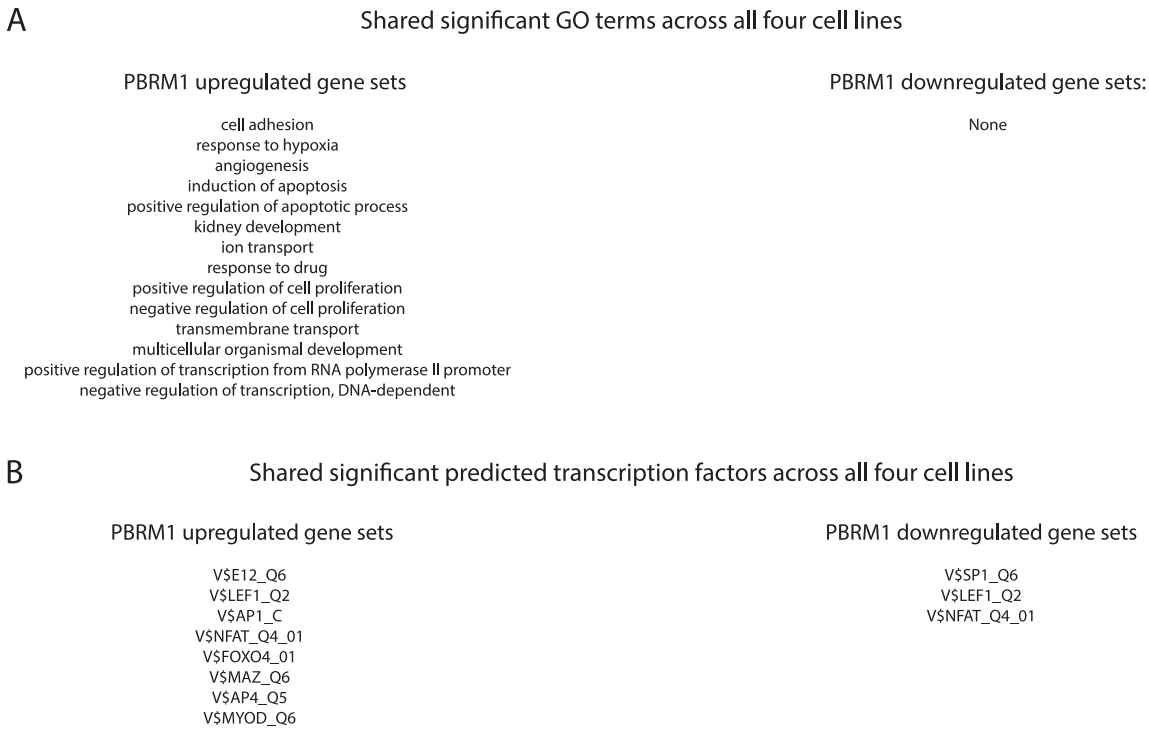

Figure 6-1 Shared gene ontology and predicted transcription factor binding

A. Biological process GO terms enriched among differentially expressed genes from all four cell lines. left) The significantly enriched terms shared between PBRM1 upregulated genes in all four cell lines. right) The significantly enriched terms shared between PBRM1 downregulated genes in all four cell lines. B. Putative transcription factors (based on consensus binding sequences in promoters) were identified for genes exhibiting differential expression. The top 20 significantly enriched transcription factors identified from each set of genes were compared. left) The significantly enriched transcription factors shared between PBRM1-upregulated genes in all four cell lines. right) The significantly enriched transcription factors shared between PBRM1-downregulated genes in all four cell lines.

To understand how the 3D culture environment can amplify the transcriptional role of PBRM1, we examined the gene expression differences between Caki2 cells grown in 3D culture relative to 2D culture, both with and without PBRM1 re-expression. We observed that the majority of DEGs in 3D conditions were identified in both Caki2 with vector control, and Caki2 with PBRM1 re-expression. Gene expression differences in 3D culture compared to their 2D culture were highly correlated ($R^2 = 0.74$) between control cells (*x*-axis) and cells re-expressing PBRM1 *y*-axis) (Fig 2C). In addition, shared genes were generally regulated to the same degree (slope = 0.90) indicating that gene expression differences between 2D and 3D culture are due to the change

in growth environment and are mainly PBRM1 independent (Fig 2C). Indeed, the biological pathways regulated in the two cell lines were similar, although cell cycle GO terms were more enriched for the genes downregulated in Caki2+PBRM1 cells, potentially reflecting the observed viability difference (Fig 2A). For genes upregulated in 3D culture, the predominant biological processes involved transcriptional regulation, so we looked more closely at how 3D cell culture conditions upregulate the expression of the transcription factors predicted to cooperate with PBRM1. We found that many of them are transcriptionally upregulated in 3D culture, including selected AP-1 monomers (*JunD*, *JunB*, *Jun*, *c-Fos*)[172], AP-1 co-regulator *Elk1*, forkhead transcription factors (*FOXO4*, *FOXA2*), NFAT variants (*NFATC1*, *NFAT5*), and *MAZ* (Fig 2C). All of these transcription factors have previously been reported as being transcriptionally upregulated under metabolic stress conditions[144]. Of particular note is *FOXO4*, which was transcriptionally upregulated in 3D culture (Fig 2C) and has consensus binding sequences enriched in the promoters of PBRM1 upregulated genes (Fig 1B). FOXO TFs are regulators of hypoxia response, metabolism, and inflammation,[173] and are excluded from the nucleus under low stress conditions by posttranslational modification such as AKT phosphorylation[174,175]. During periods of nutrient deprivation or oxidative stress, FOXOs are shuttled into the nucleus[176] where they upregulate the expression of genes involved in survival, apoptosis, and autophagy[84,157]. While PBRM1 likely regulates the function of numerous different transcription factors, we focused on FOXO targets to understand the role PBRM1 plays in the regulation of these canonical stress response genes.

Figure 6-2 PBRM1 transcriptional regulation is amplified under conditions of cellular stress.

A. The reduction in cellular proliferation upon PBRM1 re-expression in Caki2 cells is amplified when the cells are grown 10 days in 3D culture conditions. Cell growth was quantitated using the CellTiter-Glo® assay added directly to Caki2 cells in matrigel cultures. n=2. B. RNA-Seq was performed on Caki2 cells grown in 3D matrigel based cell culture. Each data point represents a single gene, *x axis*: differential expression in 3D culture upon re-expression of PBRM1, *y axis*: differential expression in 2D culture upon re-expression of PBRM1. The degree of correlation as well as the slope were calculated using all differentially expressed genes. A heat map was generated for the 100 most highly upregulated genes upon PBRM1 re-expression in 3D culture using R where every replicate is normalized to the average Vector sample expression (right). C. Scatterplot of genes identified as differentially expressed upon transition of cells from 2D culture to 3D culture, *x axis*: differential expression upon transition of Caki2-Vector cells to 3D culture, *y axis*: differential expression upon transition of Caki2-PBRM1 cells to 3D culture. The degree of correlation as well as the slope were calculated using all differentially expressed genes. The transcriptional upregulation of several relevant transcription factors upon transition into 3D culture is consistent between Caki2-Vector and Caki2-PBRM1 cells The $\log_2$ fold change and standard deviation values were acquired from RNA-Seq datasets. D. Canonical FOXO4 target genes are more robustly upregulated by PBRM1 in 3D culture compared to 2D culture. The $\log_2$ fold change and standard deviation values were acquired from RNA-Seq datasets

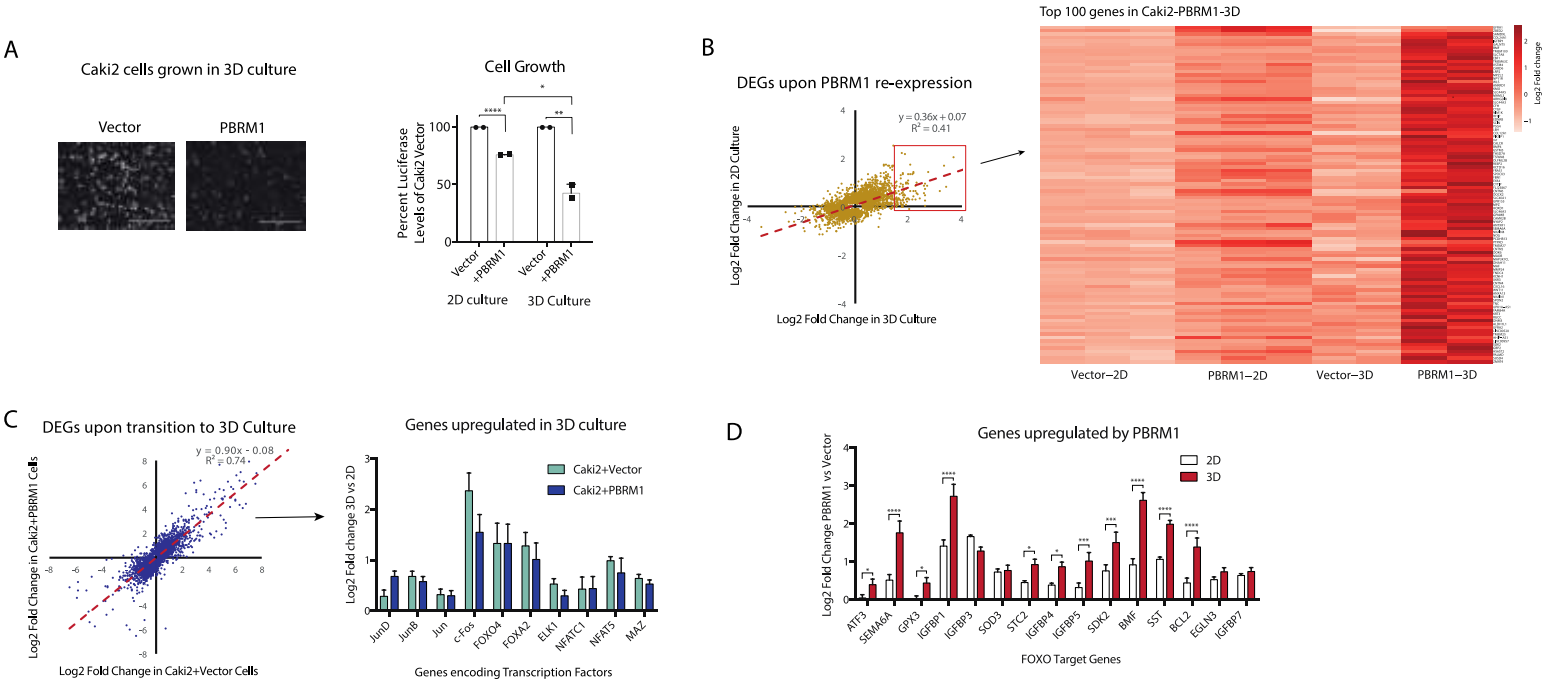
A
Caki2 cells grown in 3D culture
Vector
PBRM1
Cell Growth
Percent Luciferase Levels of Caki2 Vector
2D culture
3D Culture
B
DEGs upon PBRM1 re-expression
Log2 Fold Change in 2D Culture
Log2 Fold Change in 3D Culture
Top 100 genes in Caki2-PBRM1-3D
Vector–2D
PBRM1–2D
Vector–3D
PBRM1–3D
C
DEGs upon transition to 3D Culture
Log2 Fold Change in Caki2+PBRM1 Cells
Log2 Fold Change in Caki2+Vector Cells
Genes upregulated in 3D culture
Caki2+Vector
Caki2+PBRM1
Log2 Fold change 3D vs 2D
JunD
JunB
Jun
c-Fos
FOXO4
FOXA2
ELK1
NFATC1
NFAT5
MAZ
Genes encoding Transcription Factors
D
Genes upregulated by PBRM1
2D
3D
Log2 Fold Change PBRM1 vs Vector
ATF3
SEMA6A
GPX3
IGFBP1
IGFBP3
SOD3
STC2
IGFBP4
IGFBP5
SDK2
BMF
SST
BCL2
EGLN3
IGFBP7
FOXO Target Genes

6.3 PBRM1 regulates FOXO target genes in a stress dependent manner

Using the RNA-Seq data, we identified a subset of FOXO target genes that are upregulated by PBRM1 (Fig 6.3A). Many of them are upregulated in both 2D and 3D culture, but upregulated to a greater degree in 3D culture, which is in line with the general trend for PBRM1-regulated genes (Fig 4B). In addition, a few are only upregulated by PBRM1 in 3D culture, such as glutathione peroxidase GPX3 and stress response transcription factor ATF3. As 3D culture encapsulates a variety of stress conditions compared to 2D culture, we further analyzed the upregulation of the same genes with more defined stressors under standard cell culture conditions. Under glucose deprivation, FOXO4 is upregulated in both Caki2+Vector and Caki2+PBRM1 (Fig 6.3B), but PBRM1 only upregulates a subset of relevant FOXO targets for this particular stress condition, including IGFBP4 and IGFBP5, which are involved in regulating insulin growth factor function (Fig 6.3A)[177]. A similar upregulation of FOXO4 was found with H2O2 treatment (Fig 6.3A), although under this condition PBRM1 upregulated a different subset of relevant FOXO targets, including ATF3 and *GPX3,* which are involved in neutralizing reactive oxygen species (Fig 6.3B)[178,179]. Based on these results, PBRM1 transcriptional targets are dependent on the transcription factor profile of the cell as well as the particular environmental stress conditions the cell experiences.

6.4 PBRM1 regulates ROS levels in cancer

As mentioned previously we examined how PBRM1 effects ROS levels in cancers. We evaluated how Caki2+Vector and Caki2+PBRM1 cells handle stress. Treatment with 200 mM H_2O_2 for 16 hours showed that Caki2+Vector cells were more sensitive to treatment than Caki2+PBRM1. When we examined baseline ROS levels in the Caki2 cells we found that they were elevated compared to epithelial cells. This was not surprising as ROS levels are inherently elevated in cancer cells. Re-expression of PBRM1 alone did not significantly reduce ROS, however, when Caki2+PBRM1 were treated with increasing amounts of H_2O_2 and allowed the cells to recover for an hour, ROS levels decreased below baseline. Caki2+Vector cells remained high. We observed similar results under glucose deprivation. We predict this phenomenon is seen because cancer cells have adapted to high ROS and though elevated it is not detected as a stress

when PBRM1 is re-expressed, although once cells experience stress of H_2O_2 or glucose starvation, the stress response system is activated and PBRM1 is signaled to handle the elevated ROS.

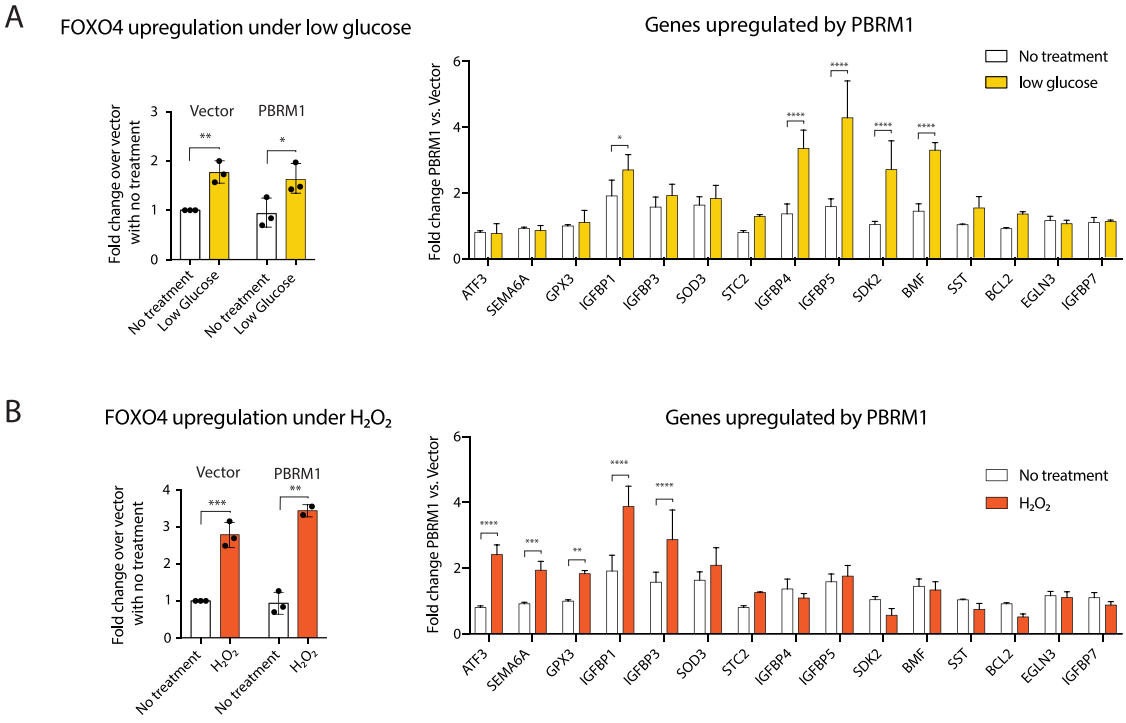

Figure 6-3 Regulation of FOXO4 targets by PBRM1

A) *FOXO4* is transcriptionally upregulated upon glucose starvation in 2D culture using qRT-PCR analysis and *GAPDH* as the housekeeping gene. n = 3 B) The contribution of PBRM1 to the transcriptional regulation of FOXO target genes under normal cell culture or 3 h glucose starvation using qRT-PCR and *GAPDH* as the housekeeping gene. n = 3. F) *FOXO4* is transcriptionally upregulated upon 3 h H_2O_2 (200 µM) treatment in 2D culture using qRT-PCR analysis and *GAPDH* as the housekeeping gene. n = 3. The contribution of PBRM1 to the transcriptional regulation of FOXO target genes under normal cell culture or 3 h H_2O_2 (200 µM) using qRT-PCR and *GAPDH* as the housekeeping gene. n = 3. A designation of *=p <0.05, ** = p <0.01, *** = p < 0.001, **** = p < 0.0001 (paired Student's t test). ns, not significant. Error bars represent S.D.

6.5 PBRM1 binds to H3K14/18Ac *in vitro*

The next question is how does PBRM1 sense stress and how it is targeted to facilitate the up-regulation of stress genes. From our work with PBRM1 mutants, we know the bromodomains are essential for PBRM1 function, we predict PBRM1 is targeted to specific regions of the genome through changes in the epigenetic landscape after stress. We have found that full length PBRM1

preferentially binds to histone 3 lysine 14 acetylation (H3K14Ac) over any other single acetylation mark on the H3 tail[27]. However, with six consecutive binding domains, it is unlikely PBRM1 only binds to one PTM. We acquired a set of peptides that contained combinations of H3K14Ac with other H3 marks: H3K9/14Ac, H3K14/18Ac, H3K14/23Ac, and H3K14/27Ac. Intriguingly, peptide pulldown assays demonstrated that PBRM1 specifically interacted with H3K14/18Ac over any other combination (Fig 6.4A). When we examined if a quadruple acetylated peptide (H3K14,18 23,27) had stronger affinity than H3K14/18Ac, we were surprised to find that PBRM1 remained bound to H3K14/18Ac peptide up to 550 mM NaCl and interaction was not enhanced by the addition of H3K23/27Ac (Fig 6.4B). Finally, we examined if PBRM1 preferential binding to H3K14/18Ac is due the spacing of the acetylation marks or preference of these particular marks on the H3 tail. We used a H4K12/16Ac peptide as these marks are spaced the same distance as H3K14/18Ac. We observed a very slight increase in binding of PBRM1 for H4K12/16Ac compared to H4 unmodified and H4K12Ac (Fig 6.4C). This indicated that PBRM1 is preferentially binding H3K14/18Ac and this interaction is not only due to preferential spacing of these marks.

6.6 Proposed mechanism of PBRM1 regulation of stress response genes

Our *in vitro* studies indicate that PBRM1 binds the combination of H3K14/18Ac. We first want to validate this observation *in vivo* and work to understand how these marks work in combination to recruit PBRM1. Our knowledge of these two marks is limited. However we know H3K14Ac is associated with DNA damage and the recruitment of RSC, the PBAF homolog in yeast[117]. It is also found at inducible promoters in embryonic stem cells[100].H3K18Ac levels are increased under heat shock stress in *c. elegans*[180] and at promoter of inducible genes after stress treatment with diamine in yeast[181]. The fact that both of these marks are associated with inducible gene expression and stress response is in line with our model of PBRM1 acting at stress response elements. Our hypothesis is that under stress, H3K14/18Ac marks are enriched at promoters of stress genes, and these marks recruits PBAF to remodel the nucleosomes, allowing binding of transcription factors, promoting expression of gene expression. It is important to note PBRM1 upregulates genes under none stress condition, however, their expression is increased under stress. This indicates that PBRM1, in concert with PBAF, is not acting as a master regulator. Rather PBRM1 is targeting PBAF in order to fine tune expression in response to changes in the cellular environment.

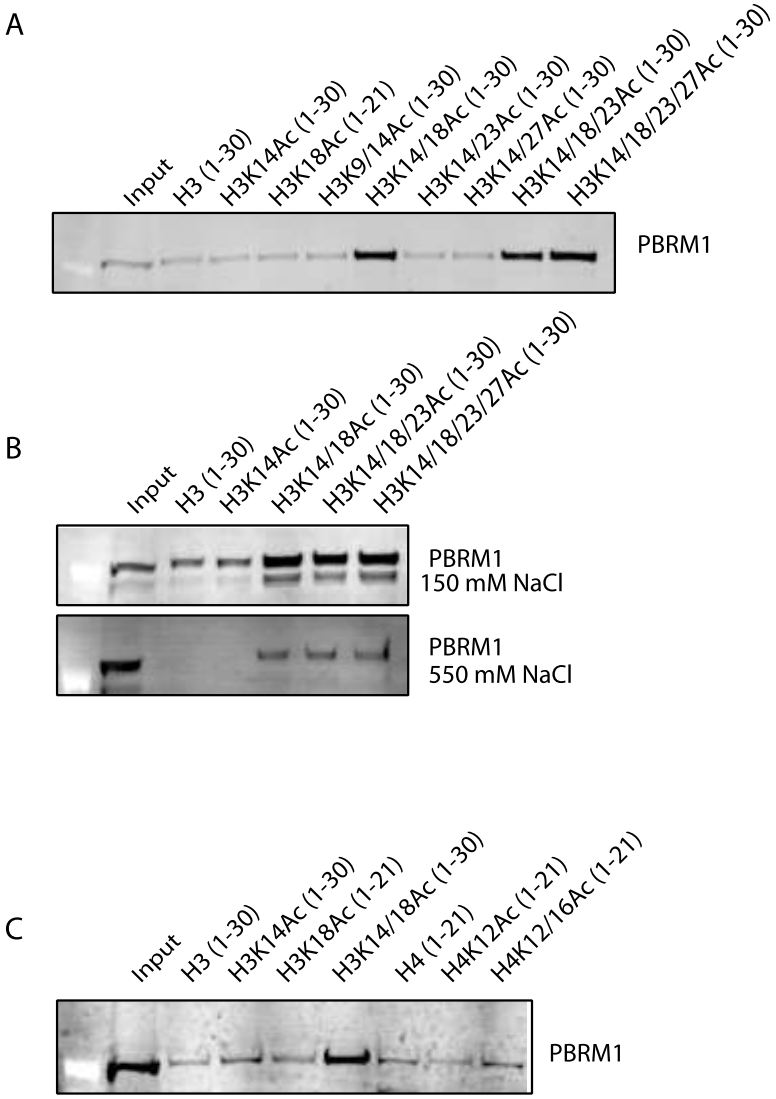

Figure 6-4 Peptide pull down assay with nuclear lysate from human cell lines

A) PBRM1 enrichment for multiple acetylated peptides. **B)** Evaluating the binding affinity of PBRM1 to peptides by increasing NaCl concentrations. **C)** Evaluation of PBRM1 binding to peptides with similarly spaced acetylation marks.

Though we have demonstrated loss of PBRM1 sensitizes cells to increases in ROS by glucose starvation and or addition of H_2O_2, however, we want to identify a more defined stress. We have repeatedly observed PBRM1 upregulates genes involved in endoplasmic reticulum (ER) stress. The ER is involved in proper protein folding. Under conditions like viral infection, hypoxia,

and oxidative stress, proteins can become unfolded and accumulate in the ER [182]The buildup of unfolded proteins activates the unfolded protein response (UPR). We have found PBRM1 expression effects cell proliferation when ER stress is induced by Brefeldin A, a drug that prevents protein transportation. out of the ER. In evaluating PBRM1 expression on ER stress response, we found Caki2+vector cells show a 30% decrease in growth with 6.25 ng/ml Brefeldin A compared to DMSO after 48 hours of treatment. Caki2+PBRM1 cells, in contrast, only had a 10% decrease in growth. (Fig 6.5A). We also found that this treatment with Brefeldin A for 72 h promoted the cleavage of PARP, a signal of DNA damage, in cells with PBRM1 (Fig 6.5B). In contrast only full length PARP was observed in the Caki2 vector cells. This indicates that even though both cell lines are experiencing the same stress, PBRM1 is activating a different stress pathway than the cells without PBRM1 expression.

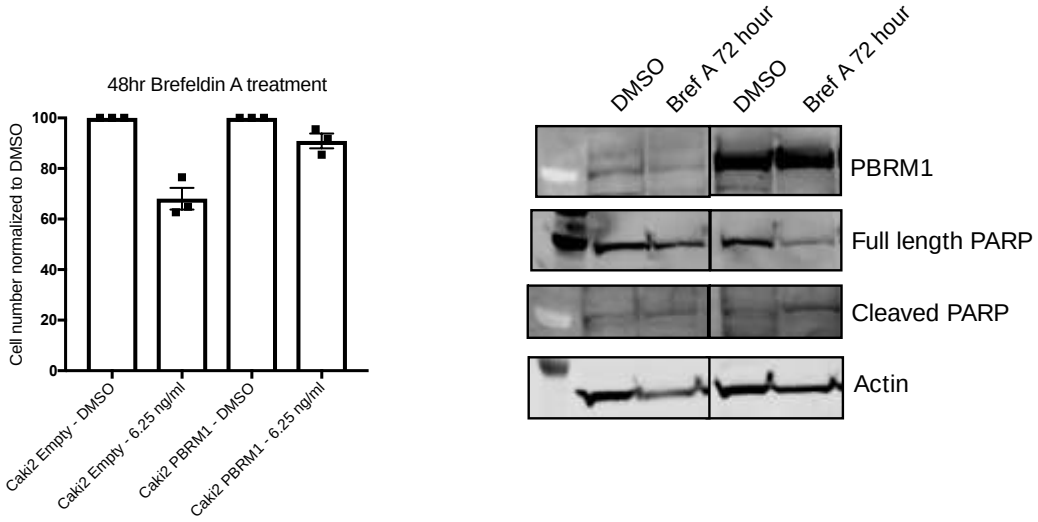

Figure 6-5 ER Stress response

A) Growth curves of Caki2 Empty and Caki2 PBRM1 cells in response to Brefeldin A treatment.

B) Immunoblot of Caki2 Empty and Caki2 PBRM1 cells in response to Brefeldin A treatment.

6.7 Future directions

Once we have characterized a robust ER phenotype, we will use optimized conditions to examine how H3K14Ac and H3K18Ac deposition changes over the genome after induction of ER stress and if those marks influence the localization of PBRM1. This will be accomplished with chromatin immunoprecipitation followed by sequencing (ChIP-seq). In conjunction, we will perform RNA-seq and ATAC-seq under the same treatment. Together this will allow us to correlate PBAF localization with gene expression changed and genome accessibility. From our 3D RNA-seq data, we saw that transcription factors associated with stress response are upregulated by stress independent of PBRM1. We hypothesize that PBAF is necessary for remodeling promoters to allow these transcription factors to bind. Previous ATAC-seq experiments in our lab and others have shown only minor changes in genome accessibility by PBRM1. We anticipate that repeating the ATAC-seq under these stress conditions in conjunction with ChIP-seq will demonstrate that remodeling correlates with changes in H3K14/18Ac levels and PBRM1 localization and determine how this effects gene expression. Taken together, we will have sites where PBRM1 functions under stress. Using these sites, we will be able to use ChIP-qPCR and qRTPCR to perform an extensive time course experiment to determine how quickly histone modifications change at these stress response promoters and determine how rapidly PBRM1 is recruited to influence gene expression. Additionally, we can use our bromodomain mutant lines to further examine how the individual domains contribute at these sites. In our previous work, we saw that loss of activity of certain bromodomains impaired gene expression of CNTN6 and IGFBP4 differently[27]. We are not sure if these genes are direct targets of PBRM1 or regulated by a downstream effect of PBRM1. Once we have sites of direct PBRM1 activity, we will be able to determine if the domains act in a similar method at all genes, or if the activity of individual bromodomains is site specific.

Finally, using these sites, we can use ChIP-qPCR to evaluate transcription factor binding and how PBRM1 remodeling effects their ability interacts with these regions of the genome. We predict that without PBRM1, the consensus binding sites are inaccessible. However, it will be intriguing to evaluate how these transcription factor binding changes under stress.

6.8 Conclusions

Though we are just starting to understand the role of PBRM1, our work has helped propel our understanding the role of the individual roles of the bromodomains and identified how PBRM1 regulates stress in cells. We have demonstrated the importance of studying chromatin binding domains in the context of the full-length protein and how a mutation in a single domain can compromise the function of a whole complex. We have optimized the sequential salt extraction method to evaluating how tightly proteins associate with chromatin. Additionally, we have not only shed light on how PBRM1 protects cells from stress, but we have exhibited that cells without PBRM1 have an increased sensitivity to external stresses. Elucidating the role of PBRM1 in stress response can help us understand why patients with loss of PBRM1 mutations have an increased response to immunotherapy. As oncology moves into more personalized treatments, expanding our knowledge of tumor suppressors like PBRM1 will allow clinicians to predict better treatment for cancer patients.

APPENDIX A. SUPPLEMENTAL MATERIAL FOR CHAPTER 2

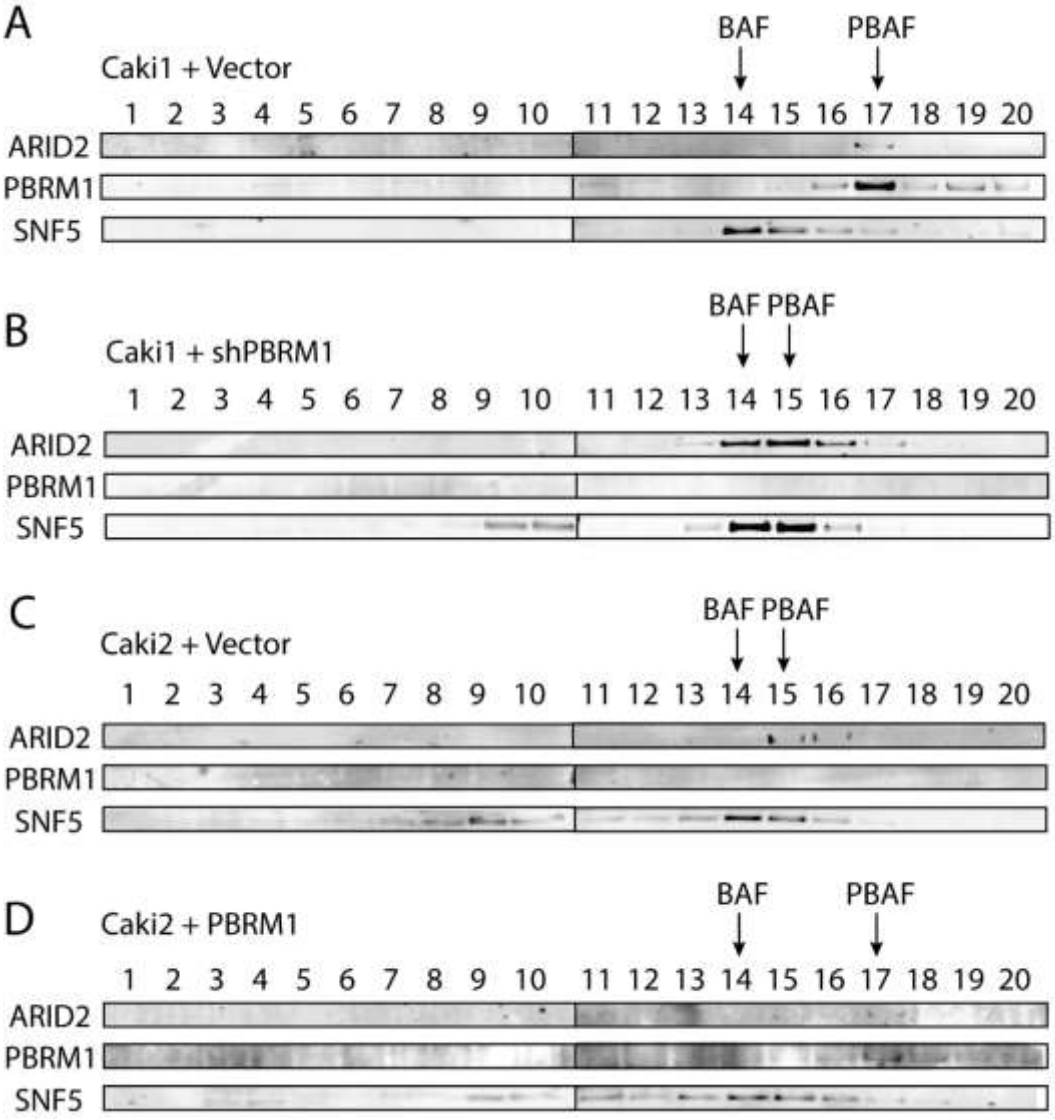

Fig S1. Glycerol gradient analysis of BAF/PBAF complexes in Caki1 and Caki2 cell lines. (A) In Caki1 cells PBAF (represented by PBRM1 and ARID2) elutes in higher fractions of a glycerol gradient indicating a larger size than BAF (represented by SNF5, which exists in both BAF and the less abundant PBAF), (B) Upon PBRM1 knockdown, the size of PBAF decreases, as represented by a shift in ARID2 staining to earlier fractions (C) In Caki2 cells with PBRM1 mutation, ARID2 staining is detected in an earlier fraction. (D) Upon the re-expression of PBRM1, the size of PBAF (represented by ARID2 staining) increases and elutes in later fractions, mimicking the staining profile observed for Caki1 cells.

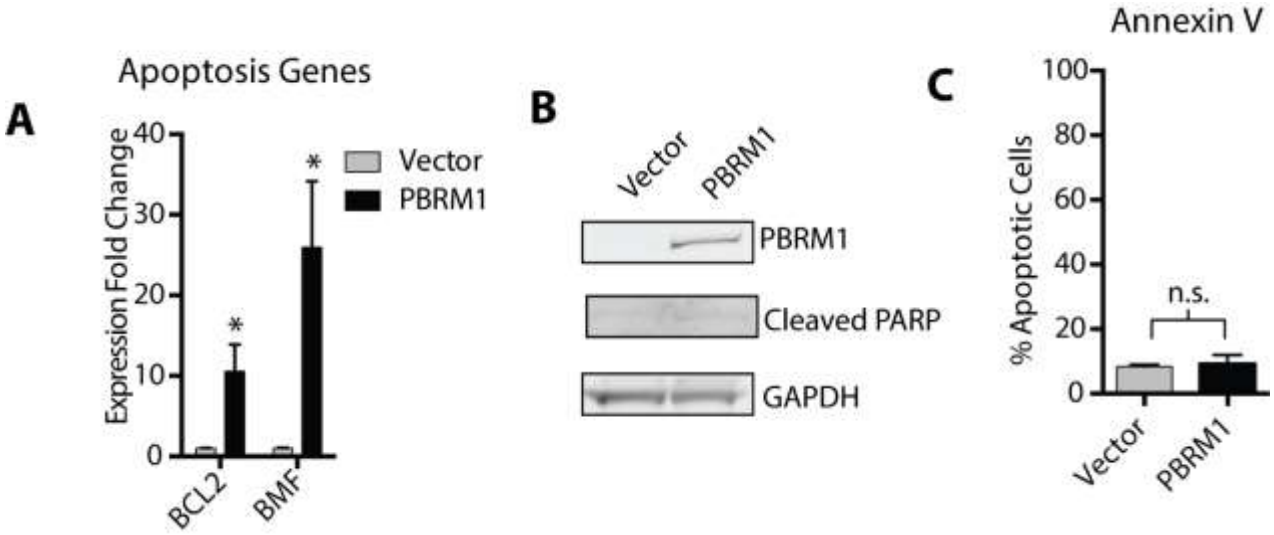

S2 Fig4. (A) Validating relative expression of genes regulating apoptosis (identified in RNA_seq data) in Caki2+Vector and Caki2+PBRM1 cells by qRTPCR. A designation of * indicates $p < 0.05$ (Student *t*-test). n = 3 independent biological replicate experiments. Error bars represent s.e.m. (B) Blot of cleaved PARP (apoptotic marker) and (C) Percentage of apoptotic cells determined by flow cytometric analysis on Caki2+Vectorand Caki2+PBRM1 cells. n = 3 independent biological replicates. Error bars represent s.e.m.

	Ave Log2FC	SEM	p value (T-test)	
CE20:3	0.17264237	0.015461901	0.00000360762	
CE16:0	0.20664802	0.042148497	0.000159941	
CE22:5	0.23773636	0.044166088	0.000205819	
CE18:1	-0.07742901	0.018279374	0.000509685	
CE22:6	0.43833536	0.08869657	0.0007808	
CE20:5	0.39527845	0.09065654	0.001093932	
CE24:0	0.58566475	0.12204117	0.003800019	$p < 0.05$
CE22:0	0.3561029	0.090167575	0.026642418	
CE20:4	0.13451694	0.05077553	0.02999903	
CE20:1	-0.15811884	0.0568701	0.03986379	
CE22:4	0.13237497	0.046222325	0.046906997	
CE18:0	0.13249697	0.040642347	0.047301915	
CE 18:2	0.11329424	0.03576691	0.047883056	
CE14:0	0.1427059	0.07847399	0.1171248	
CE22:1	-0.13035157	0.04358268	0.1621179	
CE18:3	0.096495815	0.06802414	0.19667952	
CE20:0	0.14445157	0.057293862	0.2368875	$p > 0.05$
CE22:2	-0.051018685	0.033964958	0.31052327	
CE12:0	0.1845361	0.09970774	0.33404738	
CE16:1	0.061216477	0.05355749	0.40208453	
CE 14:1	-0.08918863	0.09432081	0.4112673	
CE20:2	0.019586628	0.034403097	0.5309483	

S3 Fig. Semi-quantitative analysis of CE alterations upon PBRM1 re-expression
The log2 Fold change, SEM and p value (Student's T-test) of the analyzed CEs. n = 3 biological replicates.

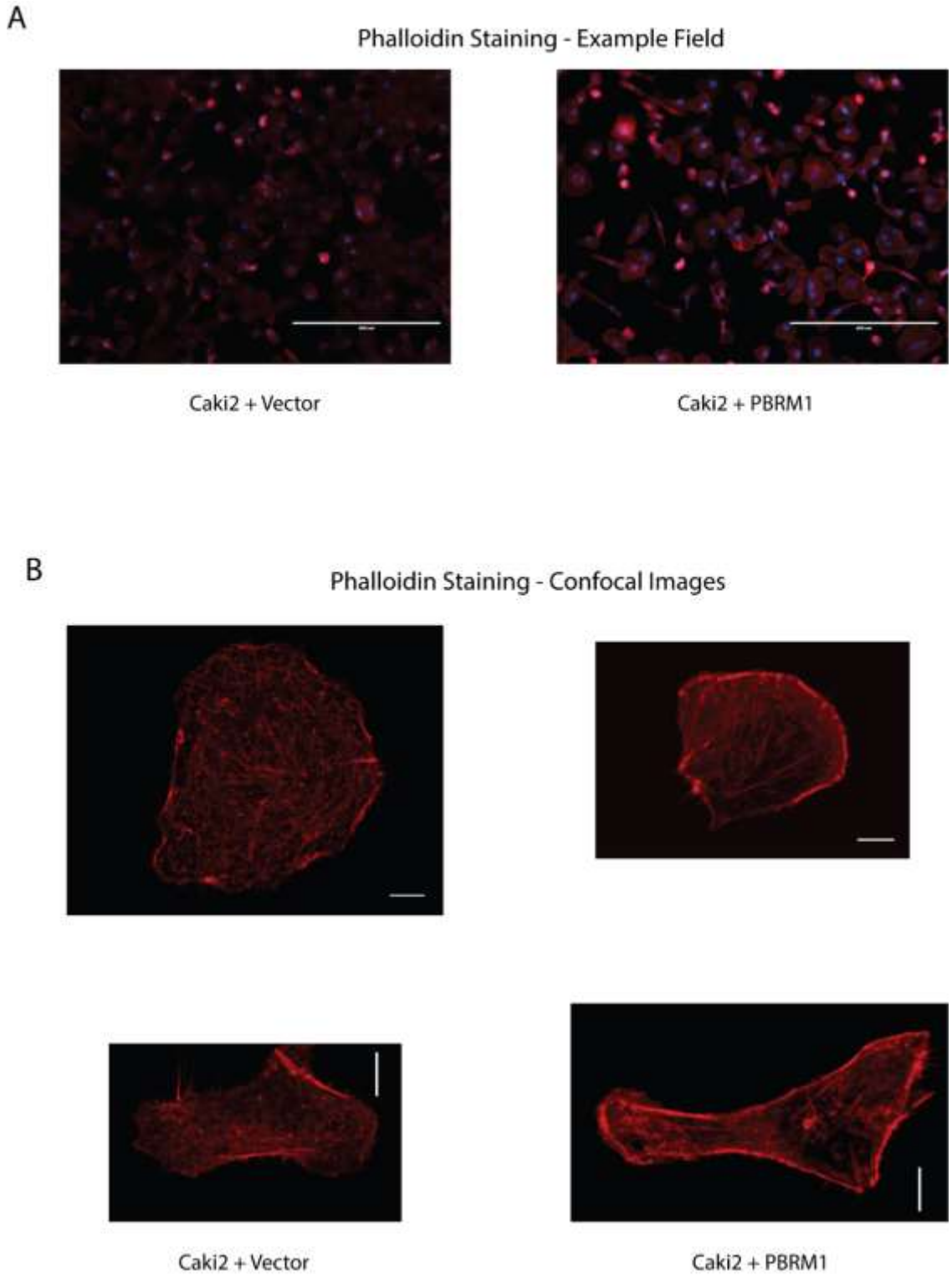

S4 Fig. Alteration of actin cytoskeleton reorganization upon PBRM1 re-expression (A) Representative Field showing Phalloidin (F-actin) and DAPI (nucleus) staining in Caki2+Vector and Caki2+PBRM1 cells used for unbiased quantification of cells with high cortical actin. 4X magnified image of this is shown in Fig 6B. (B) Examples of confocal images of Caki2+Vector and Caki2+PBRM1 cells stained with Phalloidin.

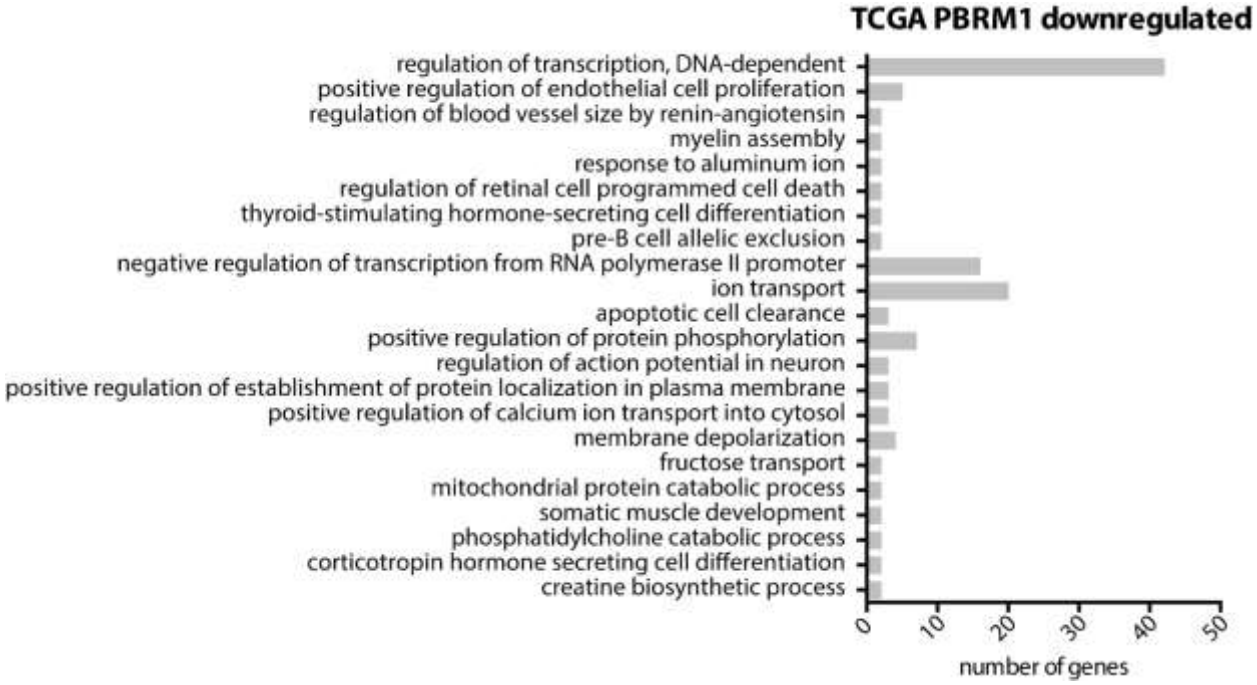

S5 Fig. Biological Pathways enriched by down regulated genes in the presence of wt PBRM1 in ccRCC tumor samples GO Biological Processes enriched by genes downregulated in TCGA ccRCC biospecimen with no PBRM1 mutation compared to ccRCC biospecimen with PBRM1 mutations.

APPENDIX B. SUPPLEMENTAL MATERIAL CHAPTER 5

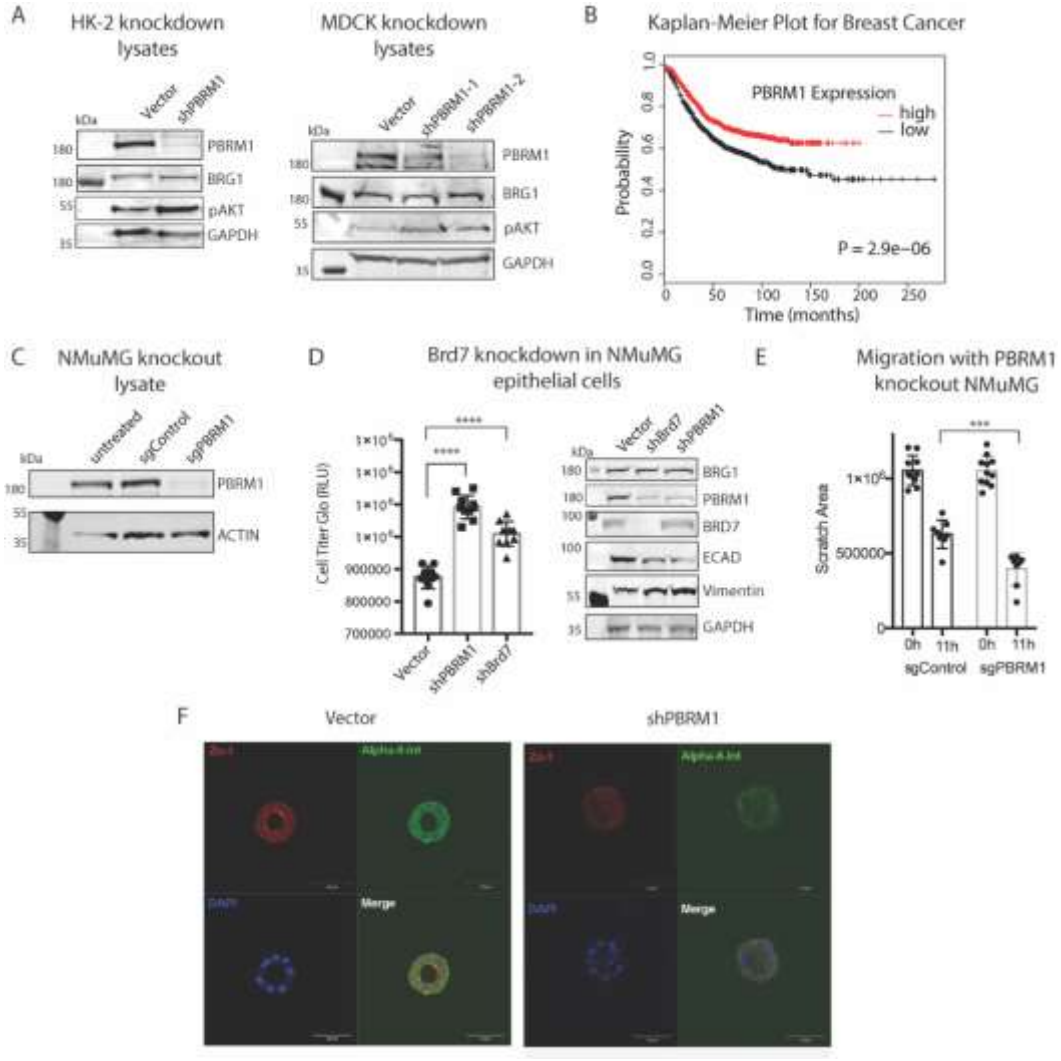

S1: Knockdown of PBRM1 in normal epithelium promotes growth and a loss of epithelial cell maintenance.

Related to Figure 1. **A.** Immunoblots of whole cell lysates of epithelial cell lines HK-2 and MDCK with PBRM1 knockdown. **B.** Microarray analysis of breast cancer patients and PBRM1 expression in tumors predicts survival. **C.** Immunoblots of whole cell lysates of epithelial cell line NMuMG with PBRM1 knockout. **D.** NMuMG cells with PBRM1 or BRD7 knockdown were counted after 72h growth and presented as mean ± SD. n = 10. Immunoblot analysis of whole cell lysates from NMuMG cells indicates that PBRM1 or BRD7 knockdown results in decreased E-cadherin expression and increased vimentin expression. **E.** Migration differences between NMuMG control and PBRM1 knockout lines at 0h and 11h. **F.** Representative image of acini from Fig 1E, analyzed using immunofluorescence staining with anti-ZO1 (red) and anti-alpha-6-integrin (green). Nuclei (blue) were visualized by DAPI. *=p <0.05, ** = p <0.01, *** = p < 0.001, **** = p < 0.0001 (paired Student's t test). ns, not significant. Error bars represent S.D

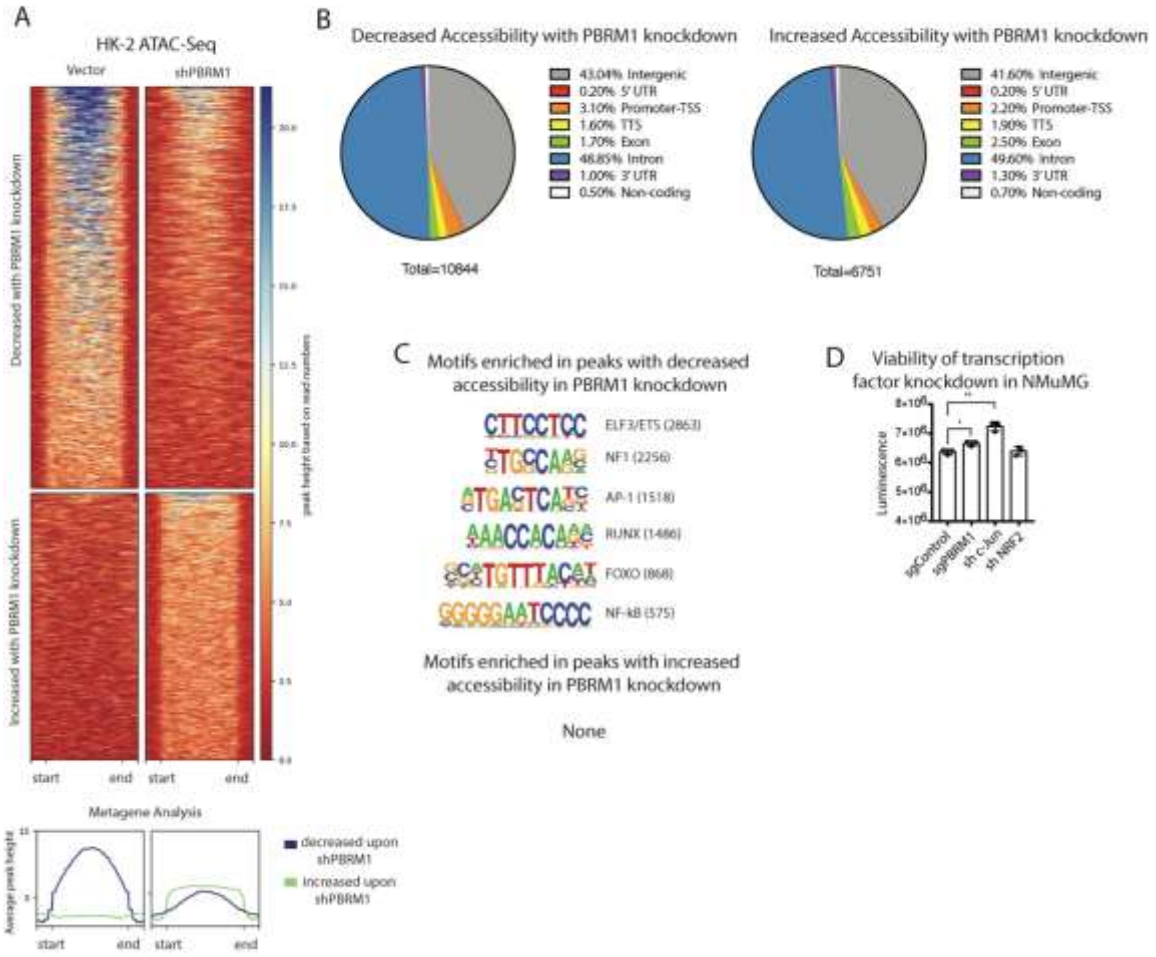

S2: PBRM1 is predicted to cooperate with transcription factors involved in response to stress Related to Figure 2. **A.** Heat maps and metagene plots of regions identified as differentially accessible upon PBRM1 knockdown by ATAC-Seq analysis of HK-2 cells. Regions of at least 1.5-fold differential accessibility were calculated between pooled samples of three biological replicates. **B.** Genomic elements associated with the differentially accessible peaks. The overall distribution was calculated as a percentage of the total differentially accessible regions for each condition. **C.** Motif analysis was performed using HOMER for the differentially accessible peaks. Statistically significant motifs were identified based on relative enrichment over genomic areas with similar AT content. **D.** NMuMG sgcontrol, sgPBRM1, shc-JUN and shNRF2 were cultured and counted after 48h growth. *=p <0.05, ** = p <0.01, *** = p < 0.001, **** = p < 0.0001 (paired Student's t test). Error bars represent S.D. n=3.

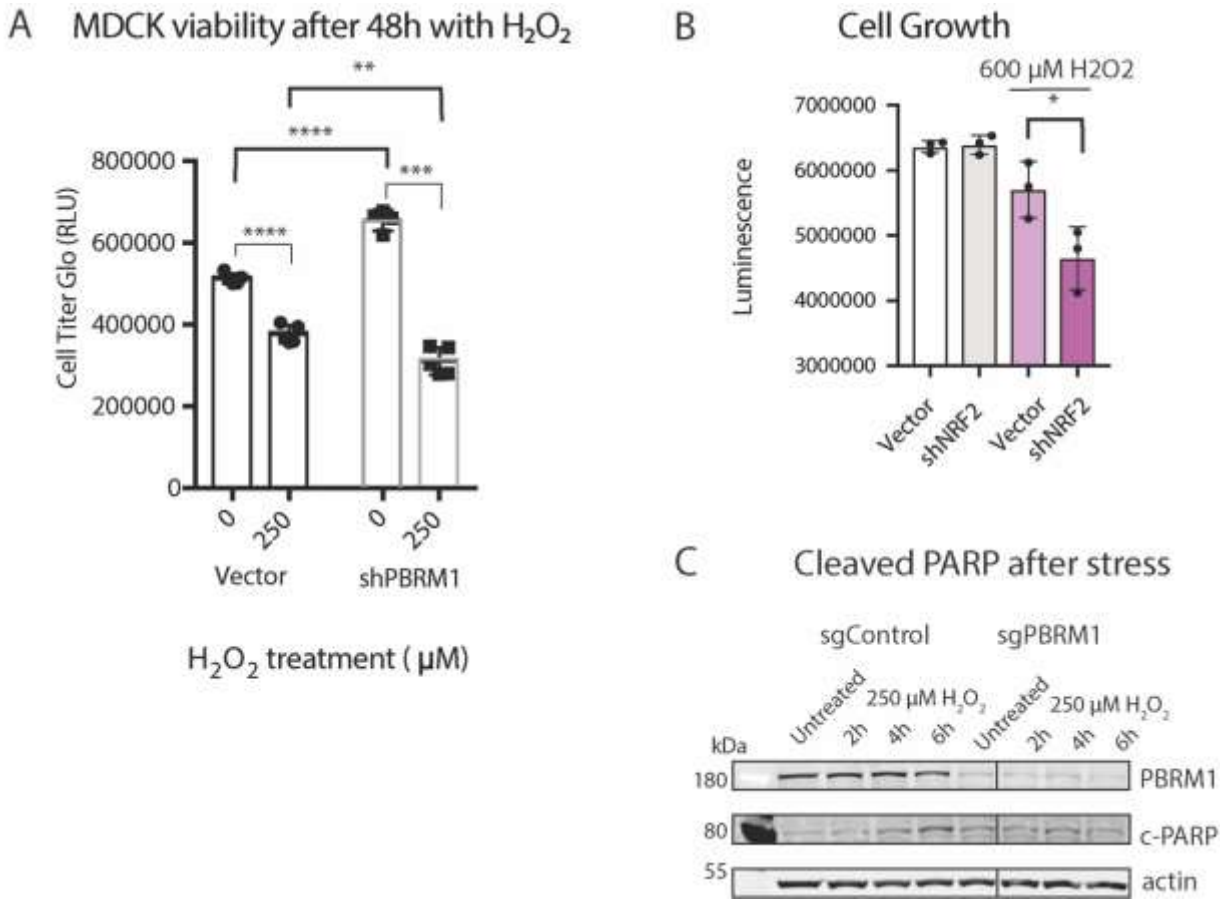

S3: PBRM1 expression is cytoprotective under high stress conditions.
Related to Figure 4. A. MDCK cells were cultured in normal cell media or 250 µM H_2O_2 for 48 h and luminescence was measured using CellTiter-Glo® assay system and data presented as mean ± SD. n = 4. B. NMuMG cells were cultured in normal cell media or 600 µM H_2O_2 for 5 h and luminescence was measured. Data presented as mean ± SD. n = 3. *=p <0.05, ** = p <0.01, *** = p < 0.001, **** = p < 0.0001 (paired Student's t test). ns, not significant. Error bars represent S.D. C. Immunoblots of whole cell lysates from NMuMG cells treated with 250 µM H_2O_2 for 2h, 4h or 6h. All lanes are from same blot with one irrelevant lane spliced out.

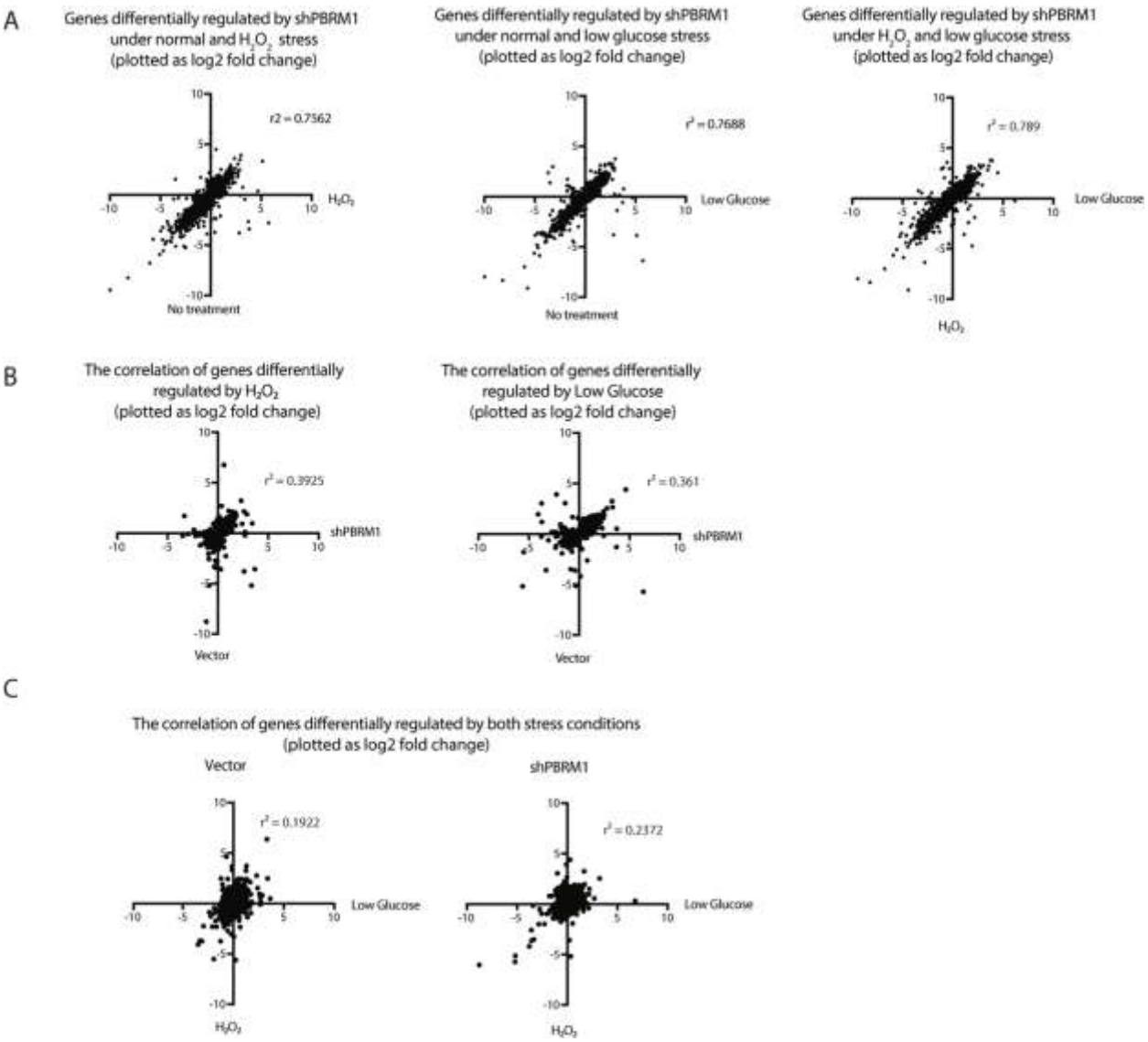

S4: PBRM1-regulated transcriptional effects under cellular stress conditions. Related to Figure 5. A. Each data point represents the log2 fold change expression value of a single gene, Left and Center plots- *x axis*: differential expression in H_2O_2 treated cells (left) or low glucose treated cells (center) upon shPBRM1, *y axis*: differential expression in normal cell culture conditions upon shPBRM1 (left and center); Right plot- *x axis:* differential expression under low glucose stress, *y axis:* differential expression under H_2O_2 stress. The degree of correlation was calculated using all differentially expressed genes. B. Each data point represents the log2 fold change expression value of a single gene upon 2h H_2O_2 treatment (left) or 6h low glucose treatment (right), *x axis*: differential expression in shPBRM1, *y axis*: differential expression in vector control cells. The degree of correlation was calculated using all differentially expressed genes. C. Each data point represents the log2 fold change expression value of a single gene upon 2h H_2O_2 treatment (y axis) or 6h low glucose treatment (x axis) of vector control cells (left) or shPBRM1 cells (right).

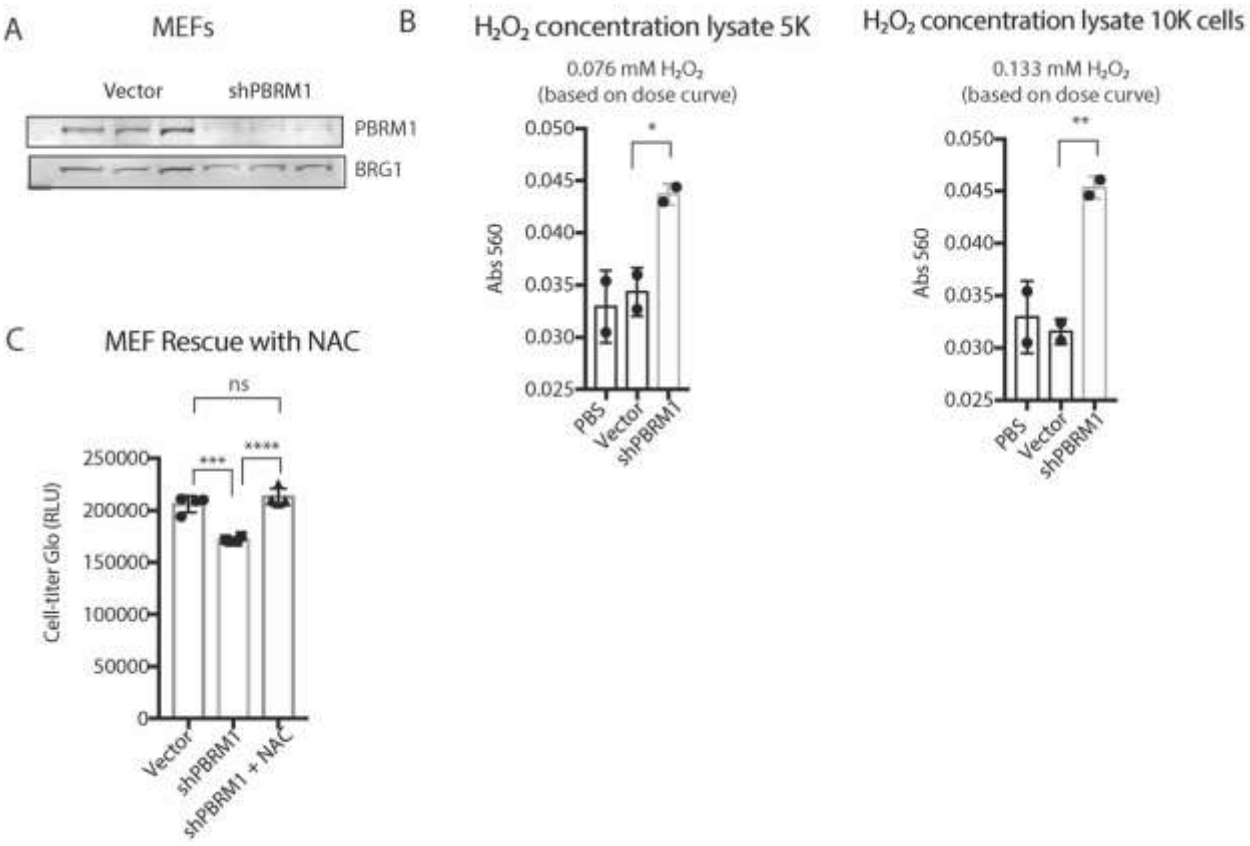

S5: PBRM1 has cell-type specific roles on viability. Related to Figure 6.
A. PBRM1 knockdown in MEFs was analyzed using immunoblot analysis of nuclear lysates. B. Hydrogen peroxide levels were quantitated in MEFs using Amplex® Red Hydrogen Peroxide/Peroxidase Assay Kit. Whole cell lysates were generated from the indicated number of cells in 50 µL RIPA. C. MEFs were cultured for 3 days in normal media or media supplemented with 500 µM NAC. Luminescence was measured using CellTiter-Glo® assay system and data presented as mean ± SD. n = 4. *=p <0.05, ** = p <0.01, *** = p < 0.001, **** = p < 0.0001 (paired Student's t test). ns, not significant. Error bars represent S.D.

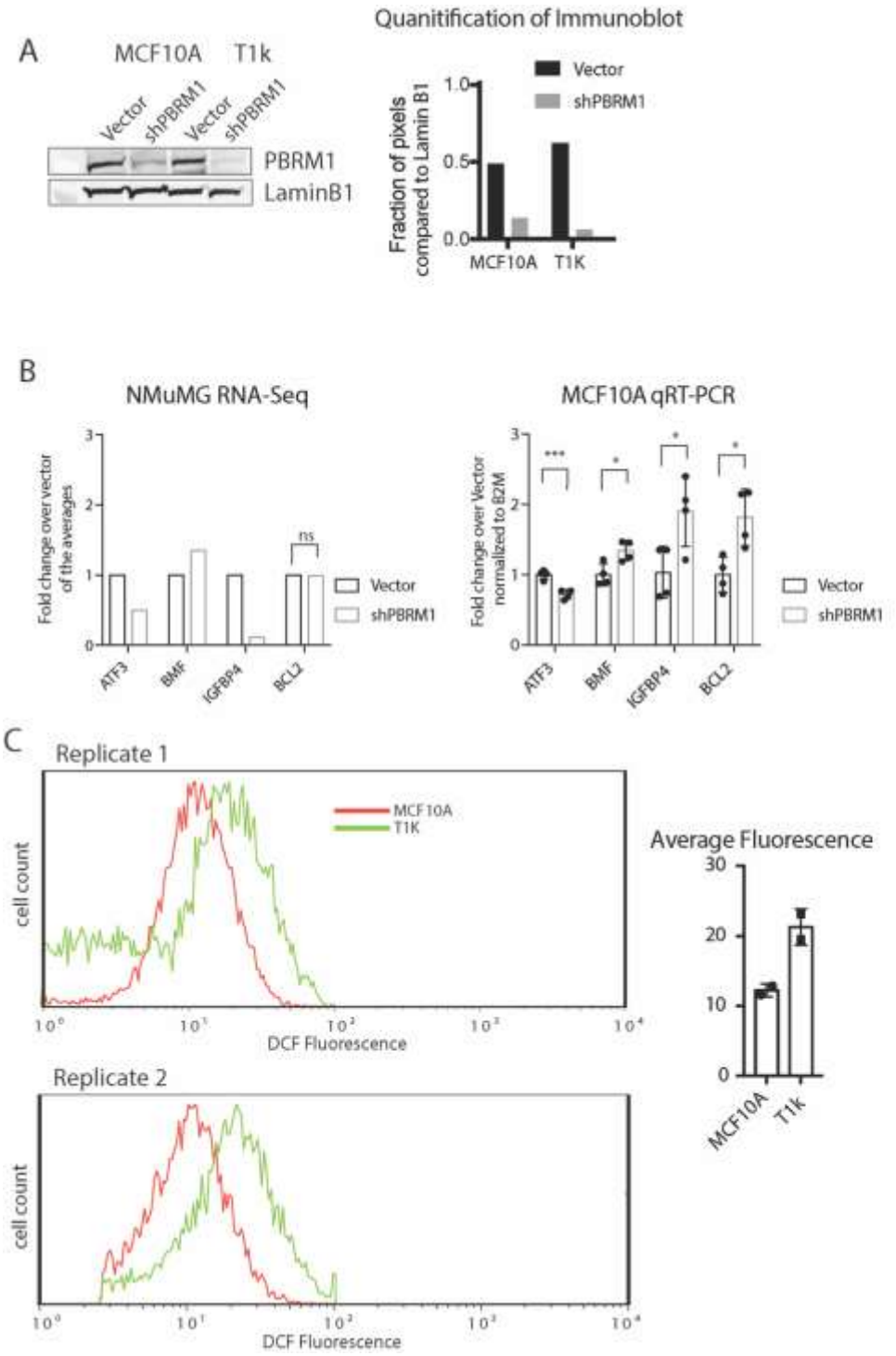

S6: PBRM1 has cell-type specific roles on viability. Related to Figure 6.
A. PBRM1 knockdown in MCF10A and MCF10A-T1k cell lines was analyzed using immunoblot analysis of nuclear lysates. Quantification indicates the intensity of PBRM1 staining over LaminB1. B. Comparison of the expression changes of ATF3, BMF, IGFBP4 and BCL2 in PBRM1 knockdown in mouse mammary epithelial cells (NMuMG: RNA-seq) with human mammary epithelial cells (MCF10A: qPCR). C. ROS levels for MCF10A and MCF10A-T1k cells were determined using H_2-DCFDA by flow cytometry.

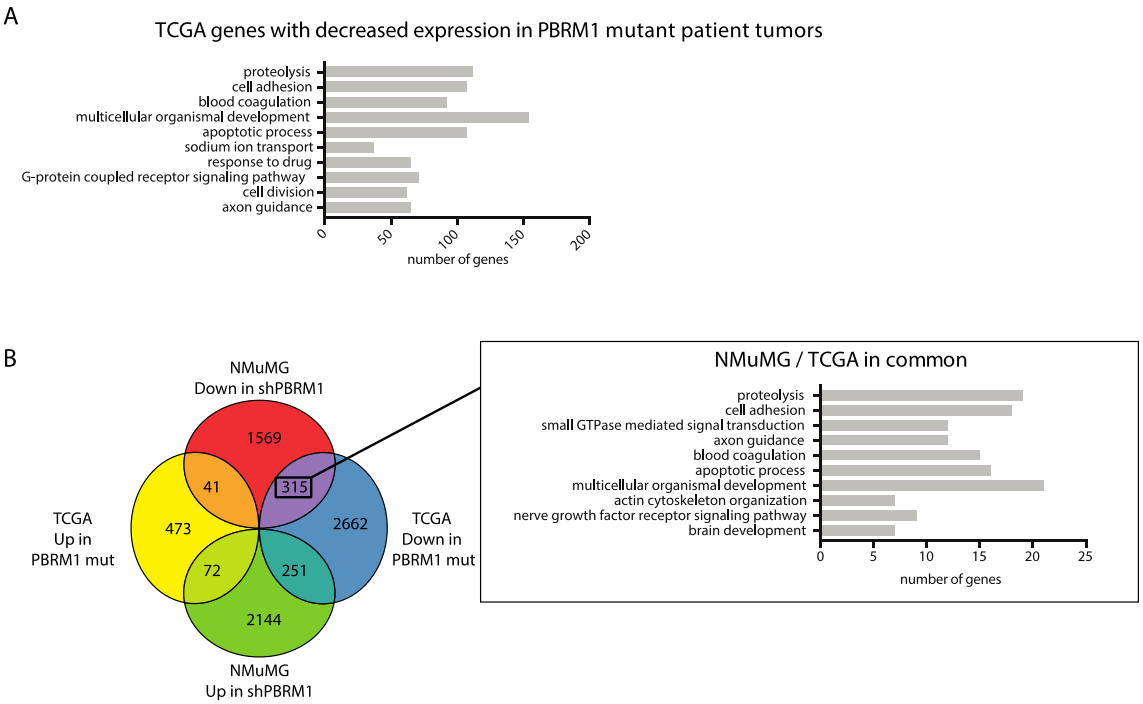

SI7: Pathways deregulated upon PBRM1 knockdown in NMuMG cells correlate with TCGA patient dataset. Related to Figure 7.

A. Summary of genes with decreased expression in renal clear cell carcinoma patients with PBRM1 mutations from The Cancer Genome Atlas (TCGA). B. Overlap of differentially regulated genes in NMuMG cells and TCGA patient data. Summary of genes with decreased expression in both NMuMG shPBRM1 and patients with PBRM1 mutations.

REFERENCES

1. Lander, E. S. *et al.* Initial sequencing and analysis of the human genome. *Nature* (2001). doi:10.1038/35057062

2. Luger, K., Mäder, A. W., Richmond, R. K., Sargent, D. F. & Richmond, T. J. Crystal structure of the nucleosome core particle at 2.8 Å resolution. *Nature* (1997). doi:10.1038/38444

3. Bannister, A. J. & Kouzarides, T. Regulation of chromatin by histone modifications. *Cell Res.* **21,** 381–395 (2011).

4. Strahl, B. D. & Allis, C. D. The language of covalent histone modifications. *Nature* (2000). doi:10.1038/47412

5. Connelly, K. E. & Dykhuizen, E. C. Compositional and functional diversity of canonical PRC1 complexes in mammals. *Biochimica et Biophysica Acta - Gene Regulatory Mechanisms* (2017). doi:10.1016/j.bbagrm.2016.12.006

6. Shain, A. H. & Pollack, J. R. The Spectrum of SWI/SNF Mutations, Ubiquitous in Human Cancers. *PLoS One* (2013). doi:10.1371/journal.pone.0055119

7. Kadoch, C. *et al.* Proteomic and bioinformatic analysis of mammalian SWI/SNF complexes identifies extensive roles in human malignancy. *Nat. Genet.* (2013). doi:10.1038/ng.2628

8. Hohmann, A. F. & Vakoc, C. R. A rationale to target the SWI/SNF complex for cancer therapy. *Trends in Genetics* (2014). doi:10.1016/j.tig.2014.05.001

9. Medina, P. P. *et al.* Frequent BRG1/SMARCA4-Inactivating mutations in human lung cancer cell lines. *Hum. Mutat.* (2008). doi:10.1002/humu.20730

10. Jones, S. *et al.* Frequent mutations of chromatin remodeling gene ARID1A in ovarian clear cell carcinoma. *Science (80-.).* (2010). doi:10.1126/science.1196333

11. Creighton, C. J. *et al.* Comprehensivemolecular characterization of clear cell renal cell carcinoma. *Nature* (2013). doi:10.1038/nature12222

12. Neigeborn, L. & Carlson, M. Genes affecting the regulation of SUC2 gene expression by glucose repression in Saccharomyces cerevisiae. *Genetics* (1984).

13. Stern, M., Jensen, R. & Herskowitz, I. Five SWI genes are required for expression of the HO gene in yeast. *J. Mol. Biol.* (1984). doi:10.1016/0022-2836(84)90315-2

14. Breeden, L. & Nasmyth, K. Regulation of the yeast HO gene. *Cold Spring Harb. Symp. Quant. Biol.* (1985). doi:10.1101/SQB.1985.050.01.078

15. Wang, W. *et al.* Purification and biochemical heterogeneity of the mammalian SWI-SNF complex. *EMBO J.* (1996). doi:10.1002/anie.200805483

16. Smith, C. L. & Peterson, C. L. A Conserved Swi2/Snf2 ATPase Motif Couples ATP Hydrolysis to Chromatin Remodeling. *Mol. Cell. Biol.* (2005). doi:10.1128/MCB.25.14.5880-5892.2005

17. Xue, Y. *et al.* The human SWI/SNF-B chromatin-remodeling complex is related to yeast Rsc and localizes at kinetochores of mitotic chromosomes. *Proc. Natl. Acad. Sci.* (2000). doi:10.1073/pnas.240208597

18. Phelan, M. L., Sif, S., Narlikar, G. J. & Kingston, R. E. Reconstitution of a core chromatin remodeling complex from SWI/SNF subunits. *Mol. Cell* (1999). doi:10.1016/S1097-2765(00)80315-9

19. Alpsoy, A. & Dykhuizen, E. C. Glioma tumor suppressor candidate region gene 1 (GLTSCR1) and its paralog GLTSCR1-like form SWI/SNF chromatin remodeling subcomplexes. *J. Biol. Chem.* (2018). doi:10.1074/jbc.RA117.001065

20. Niimi, A., Chambers, A. L., Downs, J. A. & Lehmann, A. R. A role for chromatin remodellers in replication of damaged DNA. *Nucleic Acids Res.* (2012). doi:10.1093/nar/gks453

21. Ntranos, A. & Casaccia, P. Bromodomains: Translating the words of lysine acetylation into myelin injury and repair. *Neuroscience Letters* (2016). doi:10.1016/j.neulet.2015.10.015

22. Filippakopoulos, P. *et al.* Histone recognition and large-scale structural analysis of the human bromodomain family. *Cell* **149,** 214–231 (2012).

23. Dhalluin, C. *et al.* Structure and ligand of a histone acetyltransferase bromodomain. *Nature* (1999). doi:10.1038/20974

24. Charlop-Powers, Z., Zeng, L., Zhang, Q. & Zhou, M. M. Structural insights into selective histone H3 recognition by the human Polybromo bromodomain 2. *Cell Res.* (2010). doi:10.1038/cr.2010.43

25. Chandrasekaran, R. & Thompson, M. Polybromo-1-bromodomains bind histone H3 at specific acetyl-lysine positions. *Biochem. Biophys. Res. Commun.* (2007). doi:10.1016/j.bbrc.2007.01.193

26. Chowdhury, B. *et al.* PBRM1 regulates the expression of genes involved in metabolism and cell adhesion in renal clear cell carcinoma. *PLoS One* (2016). doi:10.1371/journal.pone.0153718

27. Porter, E. G. & Dykhuizen, E. C. Individual bromodomains of Polybromo-1 contribute to chromatin association and tumor suppression in clear cell renal carcinoma. *J. Biol. Chem.* **292,** 2601–2610 (2017).

28. Lemon, B., Inouye, C., King, D. S. & Tjian, R. Selectivity of chromatin-remodelling cofactors for ligand-activated transcription. *Nature* (2001). doi:10.1038/414924a

29. Bultman, S. *et al.* A Brg1 null mutation in the mouse reveals functional differences among mammalian SWI/SNF complexes. *Mol. Cell* (2000). doi:10.1016/S1097-2765(00)00127-1

30. Wang, Z. *et al.* Polybromo protein BAF180 functions in mammalian cardiac chamber maturation. *Genes Dev.* (2004). doi:10.1101/gad.1238104

31. Lee, H. *et al.* BAF180 regulates cellular senescence and hematopoietic stem cell homeostasis through p21. *Oncotarget* (2016). doi:10.18632/oncotarget.8102

32. Kakarougkas, A. *et al.* Requirement for PBAF in Transcriptional Repression and Repair at DNA Breaks in Actively Transcribed Regions of Chromatin. *Mol. Cell* **55,** 723–732 (2014).

33. Brugarolas, J. Molecular genetics of clear-cell renal cell carcinoma. *J. Clin. Oncol.* (2014). doi:10.1200/JCO.2012.45.2003

34. Motzer, J. *et al.* Kidney cancer, version 3.2015. *J. Natl. Compr. Canc. Netw.* (2015). doi:10.6004/JNCCN.2015.0022

35. Nargund, A. M. *et al.* The SWI/SNF Protein PBRM1 Restrains VHL-Loss-Driven Clear Cell Renal Cell Carcinoma. *Cell Rep.* (2017). doi:10.1016/j.celrep.2017.02.074

36. Gossage, L., Eisen, T. & Maher, E. R. VHL, the story of a tumour suppressor gene. *Nature Reviews Cancer* (2015). doi:10.1038/nrc3844

37. Batie, M., Peso, L. del & Rocha, S. Hypoxia and Chromatin, a Focus on Transcriptional Repression Mechanisms. (2018). doi:10.20944/PREPRINTS201803.0004.V1

38. Miao, D. *et al.* Genomic correlates of response to immune checkpoint therapies in clear cell renal cell carcinoma. *Science (80-.).* (2018). doi:10.1126/science.aan5951

39. Pan, D. *et al.* A major chromatin regulator determines resistance of tumor cells to T cell-mediated killing. *Science (80-.).* (2018). doi:10.1126/science.aao1710

40. Duns, G. *et al.* Targeted exome sequencing in clear cell renal cell carcinoma tumors suggests aberrant chromatin regulation as a crucial step in ccRCC development. *Hum. Mutat.* (2012). doi:10.1002/humu.22090

41. Varela, I. *et al.* Exome sequencing identifies frequent mutation of the SWI/SNF complex gene PBRM1 in renal carcinoma. *Nature* (2011). doi:10.1038/nature09639

42. Dalgliesh, G. L. *et al.* Systematic sequencing of renal carcinoma reveals inactivation of histone modifying genes. *Nature* (2010). doi:10.1038/nature08672

43. Peña-Llopis, S. *et al.* BAP1 loss defines a new class of renal cell carcinoma. *Nat. Genet.* (2012). doi:10.1038/ng.2323

44. Pawłowski, R. *et al.* Loss of PBRM1 expression is associated with renal cell carcinoma progression. *Int. J. Cancer* (2013). doi:10.1002/ijc.27822

45. Sato, Y. *et al.* Integrated molecular analysis of clear-cell renal cell carcinoma. *Nat. Genet.* (2013). doi:10.1038/ng.2699

46. Dobin, A. *et al.* STAR: Ultrafast universal RNA-seq aligner. *Bioinformatics* (2013). doi:10.1093/bioinformatics/bts635

47. Anders, S., Pyl, P. T. & Huber, W. HTSeq-A Python framework to work with high-throughput sequencing data. *Bioinformatics* (2015). doi:10.1093/bioinformatics/btu638

48. Love, M. I., Huber, W. & Anders, S. Moderated estimation of fold change and dispersion for RNA-seq data with DESeq2. *Genome Biol.* (2014). doi:10.1186/s13059-014-0550-8

49. Carmona-Saez, P., Chagoyen, M., Tirado, F., Carazo, J. M. & Pascual-Montano, A. GENECODIS: A web-based tool for finding significant concurrent annotations in gene lists. *Genome Biol.* (2007). doi:10.1186/gb-2007-8-1-r3

50. Nogales-Cadenas, R. *et al.* GeneCodis: Interpreting gene lists through enrichment analysis and integration of diverse biological information. *Nucleic Acids Res.* (2009). doi:10.1093/nar/gkp416

51. Tabas-Madrid, D., Nogales-Cadenas, R. & Pascual-Montano, A. GeneCodis3: A non-redundant and modular enrichment analysis tool for functional genomics. *Nucleic Acids Res.* (2012). doi:10.1093/nar/gks402

52. Subramanian, A. *et al.* Gene set enrichment analysis: A knowledge-based approach for interpreting genome-wide expression profiles. *Proc. Natl. Acad. Sci.* (2005). doi:10.1073/pnas.0506580102

53. Bligh, E. G. & Dyer, W. J. A RAPID METHOD OF TOTAL LIPID EXTRACTION AND PURIFICATION. *Can. J. Physiol. Pharmacol.* (1959). doi:10.1139/y59-099

54. Ferreira, C. R. *et al.* Ambient ionisation mass spectrometry for lipid profiling and structural analysis of mammalian oocytes, preimplantation embryos and stem cells. *Reproduction, Fertility and Development* (2015). doi:10.1071/RD14310

55. Forbes, S. A. *et al.* COSMIC: Mining complete cancer genomes in the catalogue of somatic mutations in cancer. *Nucleic Acids Res.* (2011). doi:10.1093/nar/gkq929

56. Xia, W. *et al.* BAF180 is a critical regulator of p21 induction and a tumor suppressor mutated in breast cancer. *Cancer Res.* (2008). doi:10.1158/0008-5472.CAN-07-5276

57. Lazebnik, Y. A., Kaufmann, S. H., Desnoyers, S., Poirier, G. G. & Earnshaw, W. C. Cleavage of poly(ADP-ribose) polymerase by a proteinase with properties like ICE. *Nature* (1994). doi:10.1038/371346a0

58. Shen, C. & Kaelin, W. G. The VHL/HIF axis in clear cell renal carcinoma. *Seminars in Cancer Biology* (2013). doi:10.1016/j.semcancer.2012.06.001

59. Kenneth, N. S., Mudie, S., van Uden, P. & Rocha, S. SWI/SNF regulates the cellular response to hypoxia. *J. Biol. Chem.* (2009). doi:10.1074/jbc.M808491200

60. Sena, J. A., Wang, L. & Hu, C.-J. BRG1 and BRM Chromatin-Remodeling Complexes Regulate the Hypoxia Response by Acting as Coactivators for a Subset of Hypoxia-Inducible Transcription Factor Target Genes. *Mol. Cell. Biol.* (2013). doi:10.1128/MCB.00731-13

61. Goda, N. *et al.* Hypoxia-Inducible Factor 1 Is Essential for Cell Cycle Arrest during Hypoxia. *Mol. Cell. Biol.* (2003). doi:10.1128/MCB.23.1.359-369.2003

62. Shen, C. *et al.* Genetic and functional studies implicate HIF1a as a 14q kidney cancer suppressor gene. *Cancer Discov.* (2011). doi:10.1158/2159-8290.CD-11-0098

63. Raval, R. R. *et al.* Contrasting Properties of Hypoxia-Inducible Factor 1 (HIF-1) and HIF-2 in von Hippel-Lindau-Associated Renal Cell Carcinoma. *Mol. Cell. Biol.* (2005). doi:10.1128/MCB.25.13.5675-5686.2005

64. Gebhard, R. L. *et al.* Abnormal cholesterol metabolism in renal clear cell carcinoma. *J. Lipid Res.* (1987).

65. Clayman, R. V., Gonzalez, R., Elliott, A. Y., Gleason, D. E. & Dempsey, M. E. Cholesterol accumulation in heterotransplanted renal cell cancer. *J. Urol.* (1983). doi:10.1016/S0022-5347(17)52265-X

66. Sundelin, J. P. *et al.* Increased Expression of the Very Low-Density Lipoprotein Receptor Mediates Lipid Accumulation in Clear-Cell Renal Cell Carcinoma. *PLoS One* (2012). doi:10.1371/journal.pone.0048694

67. Harunaga, J. S. & Yamada, K. M. Cell-matrix adhesions in 3D. *Matrix Biology* (2011). doi:10.1016/j.matbio.2011.06.001

68. Korhonen, M., Sariola, H., Gould, V. E., Kangas, L. & Virtanen, I. Integrins and Laminins in Human Renal Carcinoma Cells and Tumors Grown in Nude Mice. *Cancer Res.* (1994). doi:10.1162/jocn.2007.19.11.1776

69. Parsons, J. T., Horwitz, A. R. & Schwartz, M. A. Cell adhesion: Integrating cytoskeletal dynamics and cellular tension. *Nature Reviews Molecular Cell Biology* (2010). doi:10.1038/nrm2957

70. Shankar, J. & Nabi, I. R. Actin cytoskeleton regulation of epithelial mesenchymal transition in metastatic cancer cells. *PLoS One* (2015). doi:10.1371/journal.pone.0119954

71. Haynes, J., Srivastava, J., Madson, N., Wittmann, T. & Barber, D. L. Dynamic actin remodeling during epithelial-mesenchymal transition depends on increased moesin expression. *Mol. Biol. Cell* (2011). doi:10.1091/mbc.E11-02-0119

72. Klingner, C. *et al.* Isotropic actomyosin dynamics promote organization of the apical cell cortex in epithelial cells. *J. Cell Biol.* (2014). doi:10.1083/jcb.201402037

73. Thiery, J. P. & Sleeman, J. P. Complex networks orchestrate epithelial-mesenchymal transitions. *Nature Reviews Molecular Cell Biology* (2006). doi:10.1038/nrm1835

74. Ilatovskaya, D. V. *et al.* Arp2/3 complex inhibitors adversely affect actin cytoskeleton remodeling in the cultured murine kidney collecting duct M-1 cells. *Cell Tissue Res.* (2013). doi:10.1007/s00441-013-1710-y

75. Lamouille, S., Xu, J. & Derynck, R. Molecular mechanisms of epithelial-mesenchymal transition. *Nature Reviews Molecular Cell Biology* (2014). doi:10.1038/nrm3758

76. Morita, T., Mayanagi, T. & Sobue, K. Dual roles of myocardin-related transcription factors in epithelial-mesenchymal transition via slug induction and actin remodeling. *J. Cell Biol.* (2007). doi:10.1083/jcb.200708174

77. Thiery, J. P., Acloque, H., Huang, R. Y. J. & Nieto, M. A. Epithelial-Mesenchymal Transitions in Development and Disease. *Cell* (2009). doi:10.1016/j.cell.2009.11.007

78. Yilmaz, M. & Christofori, G. Mechanisms of Motility in Metastasizing Cells. *Mol. Cancer Res.* (2010). doi:10.1158/1541-7786.MCR-10-0139

79. Liang, C. C., Park, A. Y. & Guan, J. L. In vitro scratch assay: A convenient and inexpensive method for analysis of cell migration in vitro. *Nat. Protoc.* (2007). doi:10.1038/nprot.2007.30

80. Li, B. *et al.* Fructose-1,6-bisphosphatase opposes renal carcinoma progression. *Nature* (2014). doi:10.1515/ract-2016-2643

81. Zeng, Z., Que, T., Zhang, J. & Hu, Y. A study exploring critical pathways in clear cell renal cell carcinoma. *Exp. Ther. Med.* (2013). doi:10.3892/etm.2013.1392

82. Butz, H. *et al.* Integrative bioinformatics analysis reveals new prognostic biomarkers of clear cell renal cell carcinoma. *Clin. Chem.* (2014). doi:10.1373/clinchem.2014.225854

83. Gan, B. *et al.* FoxOs enforce a progression checkpoint to constrain mTORC1-Activated renal tumorigenesis. *Cancer Cell* (2010). doi:10.1016/j.ccr.2010.10.019

84. Lin, A. *et al.* The FoxO-BNIP3 axis exerts a unique regulation of mTORC1 and cell survival under energy stress. *Oncogene* (2014). doi:10.1038/onc.2013.273

85. Musselman, C. A., Lalonde, M. E., Côté, J. & Kutateladze, T. G. Perceiving the epigenetic landscape through histone readers. *Nature Structural and Molecular Biology* (2012). doi:10.1038/nsmb.2436

86. Yun, M., Wu, J., Workman, J. L. & Li, B. Readers of histone modifications. *Cell Research* (2011). doi:10.1038/cr.2011.42

87. Owen, D. J. The structural basis for the recognition of acetylated histone H4 by the bromodomain of histone acetyltransferase Gcn5p. *EMBO J.* (2000). doi:10.1093/emboj/19.22.6141

88. Yang, N. & Xu, R. M. Structure and function of the BAH domain in chromatin biology. *Critical Reviews in Biochemistry and Molecular Biology* (2013). doi:10.3109/10409238.2012.742035

89. Thompson, M. Polybromo-1: The chromatin targeting subunit of the PBAF complex. *Biochimie* (2009). doi:10.1016/j.biochi.2008.10.019

90. Narlikar, G. J., Sundaramoorthy, R. & Owen-Hughes, T. Mechanisms and functions of ATP-dependent chromatin-remodeling enzymes. *Cell* (2013). doi:10.1016/j.cell.2013.07.011

91. Hargreaves, D. C. & Crabtree, G. R. ATP-dependent chromatin remodeling: Genetics, genomics and mechanisms. *Cell Res.* (2011). doi:10.1038/cr.2011.32

92. Middeljans, E. *et al.* SS18 together with animal-specific factors defines human BAF-type SWI/SNF complexes. *PLoS One* (2012). doi:10.1371/journal.pone.0033834

93. Gerlinger, M. *et al.* Genomic architecture and evolution of clear cell renal cell carcinomas defined by multiregion sequencing. *Nat. Genet.* (2014). doi:10.1038/ng.2891

94. Brownlee, P. M., Chambers, A. L., Oliver, A. W. & Downs, J. A. Cancer and the bromodomains of BAF180. *Biochem. Soc. Trans.* (2012). doi:10.1042/BST20110754

95. Dephoure, N. *et al.* A quantitative atlas of mitotic phosphorylation. *Proc. Natl. Acad. Sci.* (2008). doi:10.1073/pnas.0805139105

96. Vivoli, M., Novak, H. R., Littlechild, J. A. & Harmer, N. J. Determination of Protein-ligand Interactions Using Differential Scanning Fluorimetry. *J. Vis. Exp.* (2014). doi:10.3791/51809

97. Jung, M. *et al.* Affinity map of bromodomain protein 4 (BRD4) interactions with the histone H4 tail and the small molecule inhibitor JQ1. *J. Biol. Chem.* (2014). doi:10.1074/jbc.M113.523019

98. Myrianthopoulos, V. *et al.* Discovery and Optimization of a Selective Ligand for the Switch/Sucrose Nonfermenting-Related Bromodomains of Polybromo Protein-1 by the Use of Virtual Screening and Hydration Analysis. *J. Med. Chem.* (2016). doi:10.1021/acs.jmedchem.6b00355

99. Sanchez, O. F., Williamson, D., Cai, L. & Yuan, C. A sensitive protein-based sensor for quantifying histone acetylation levels. *Talanta* (2015). doi:10.1016/j.talanta.2015.03.046

100. Karmodiya, K., Krebs, A. R., Oulad-Abdelghani, M., Kimura, H. & Tora, L. H3K9 and H3K14 acetylation co-occur at many gene regulatory elements, while H3K14ac marks a subset of inactive inducible promoters in mouse embryonic stem cells. *BMC Genomics* (2012). doi:10.1186/1471-2164-13-424

101. Bell, D. *et al.* Integrated genomic analyses of ovarian carcinoma. *Nature* (2011). doi:10.1038/nature10166

102. VanDemark, A. P. *et al.* Autoregulation of the Rsc4 Tandem Bromodomain by Gcn5 Acetylation. *Mol. Cell* (2007). doi:10.1016/j.molcel.2007.08.018

103. Sanchez, R. & Zhou, M.-M. The role of human bromodomains in chromatin biology and gene transcription. *Curr. Opin. Drug Discov. Devel.* **12,** 659–65 (2009).

104. Ji, X. *et al.* Chromatin proteomic profiling reveals novel proteins associated with histone-marked genomic regions. *Proc. Natl. Acad. Sci.* (2015). doi:10.1073/pnas.1502971112

105. Ramakrishnan, V. Histone structure and the organization of the nucleosome. *Annu. Rev. Biophys. Biomol. Struct.* **26,** 83–112 (1997).

106. Furey, T. S. ChIP–seq and beyond: new and improved methodologies to detect and characterize protein–DNA interactions. *Nat. Rev. Genet.* **13,** 840–852 (2012).

107. Skene, P. J. & Henikoff, S. An efficient targeted nuclease strategy for high-resolution mapping of DNA binding sites. *Elife* **6,** (2017).

108. Wu, S. Y., Lee, A. Y., Lai, H. T., Zhang, H. & Chiang, C. M. Phospho switch triggers brd4 chromatin binding and activator recruitment for gene-specific targeting. *Mol. Cell* **49,** 843–857 (2013).

109. Kerppola, T. K. Polycomb group complexes--many combinations, many functions. *Trends Cell Biol.* **19,** 692–704 (2009).

110. Filippakopoulos, P. *et al.* Selective inhibition of BET bromodomains. *Nature* **468,** 1067–1073 (2010).

111. Yang, F., Teves, S. S., Kemp, C. J. & Henikoff, S. Doxorubicin, DNA torsion, and chromatin dynamics. *Biochimica et Biophysica Acta - Reviews on Cancer* **1845,** 84–89 (2014).

112. Lee, S. Y. *et al. A proteomics approach for the identification of nucleophosmin and heterogeneous nuclear ribonucleoprotein C1/C2 as chromatin-binding proteins in response to DNA double-strand breaks. The Biochemical journal* **388,** (2005).

113. Donaldson, M. M., Boner, W. & Morgan, I. M. TopBP1 Regulates Human Papillomavirus Type 16 E2 Interaction with Chromatin. *J. Virol.* **81,** 4338–4342 (2007).

114. Kaeser, M. D., Aslanian, A., Dong, M. Q., Yates, J. R. & Emerson, B. M. BRD7, a novel PBAF-specific SWI/SNF subunit, is required for target gene activation and repression in embryonic stem cells. *J. Biol. Chem.* (2008). doi:10.1074/jbc.M806061200

115. Tatarskiy, V. V. *et al.* Stability of the PHF10 subunit of PBAF signature module is regulated by phosphorylation: Role of β-TrCP. *Sci. Rep.* (2017). doi:10.1038/s41598-017-05944-3

116. Duan, M. R. & Smerdon, M. J. Histone H3 lysine 14 (H3K14) acetylation facilitates DNA repair in a positioned nucleosome by stabilizing the binding of the chromatin remodeler RSC (Remodels Structure of Chromatin). *J. Biol. Chem.* (2014). doi:10.1074/jbc.M113.540732

117. Wang, Y. *et al.* Histone H3 lysine 14 acetylation is required for activation of a DNA damage checkpoint in fission yeast. *J. Biol. Chem.* (2012). doi:10.1074/jbc.M111.329417

118. Huang, X., Gao, X., Diaz-Trelles, R., Ruiz-Lozano, P. & Wang, Z. Coronary development is regulated by ATP-dependent SWI/SNF chromatin remodeling component BAF180. *Dev. Biol.* (2008). doi:10.1016/j.ydbio.2008.04.020

119. Brownlee, P. M., Chambers, A. L., Cloney, R., Bianchi, A. & Downs, J. A. BAF180 Promotes Cohesion and Prevents Genome Instability and Aneuploidy. *Cell Rep.* (2014). doi:10.1016/j.celrep.2014.02.012

120. Lee, H. S., Park, J. H., Kim, S. J., Kwon, S. J. & Kwon, J. A cooperative activation loop among SWI/SNF, γ-H2AX and H3 acetylation for DNA double-strand break repair. *EMBO J.* (2010). doi:10.1038/emboj.2010.27

121. Gao, W., Li, W., Xiao, T., Liu, X. S. & Kaelin, W. G. Inactivation of the PBRM1 tumor suppressor gene amplifies the HIF-response in VHL $^{-/-}$ clear cell renal carcinoma. *Proc. Natl. Acad. Sci.* (2017). doi:10.1073/pnas.1619726114

122. Espana-Agusti, J., Warren, A., Chew, S. K., Adams, D. J. & Matakidou, A. Loss of PBRM1 rescues VHL dependent replication stress to promote renal carcinogenesis. *Nat. Commun.* (2017). doi:10.1038/s41467-017-02245-1

123. Gu, Y. F. *et al.* Modeling renal cell carcinoma in mice: Bap1 and Pbrm1 inactivation drive tumor grade. *Cancer Discov.* (2017). doi:10.1158/2159-8290.CD-17-0292

124. Huang, L. *et al.* PBRM1 suppresses bladder cancer by cyclin B1 induced cell cycle arrest. *Oncotarget* (2015). doi:10.18632/oncotarget.3879

125. Murakami, A. *et al.* Context-dependent role for chromatin remodeling component PBRM1/BAF180 in clear cell renal cell carcinoma. *Oncogenesis* (2017). doi:10.1038/oncsis.2016.89

126. Bolger, A. M., Lohse, M. & Usadel, B. Trimmomatic: A flexible trimmer for Illumina sequence data. *Bioinformatics* (2014). doi:10.1093/bioinformatics/btu170

127. Herrmann, C., Van De Sande, B., Potier, D. & Aerts, S. i-cisTarget: An integrative genomics method for the prediction of regulatory features and cis-regulatory modules. *Nucleic Acids Res.* (2012). doi:10.1093/nar/gks543

128. Kaimal, V., Bardes, E. E., Tabar, S. C., Jegga, A. G. & Aronow, B. J. ToppCluster: A multiple gene list feature analyzer for comparative enrichment clustering and networkbased dissection of biological systems. *Nucleic Acids Res.* (2010). doi:10.1093/nar/gkq418

129. Buenrostro, J. D., Wu, B., Chang, H. Y. & Greenleaf, W. J. ATAC-seq: A method for assaying chromatin accessibility genome-wide. *Curr. Protoc. Mol. Biol.* (2015). doi:10.1002/0471142727.mb2129s109

130. Langmead, B., Trapnell, C., Pop, M. & Salzberg, S. L. Ultrafast and memory-efficient alignment of short DNA sequences to the human genome. *Genome Biol.* (2009). doi:10.1186/gb-2009-10-3-r25

131. Ramírez, F. *et al.* deepTools2: a next generation web server for deep-sequencing data analysis. *Nucleic Acids Res.* (2016). doi:10.1093/nar/gkw257

132. Xu, S., Grullon, S., Ge, K. & Peng, W. Spatial clustering for identification of chip-enriched regions (SICER) to map regions of histone methylation patterns in embryonic stem cells. *Methods Mol. Biol.* (2014). doi:10.1007/978-1-4939-0512-6_5

133. Heinz, S. *et al.* Simple Combinations of Lineage-Determining Transcription Factors Prime cis-Regulatory Elements Required for Macrophage and B Cell Identities. *Mol. Cell* (2010). doi:10.1016/j.molcel.2010.05.004

134. Pfaffl, M. W. A new mathematical model for relative quantification in real-time RT-PCR. *Nucleic Acids Res.* (2002). doi:10.1093/nar/29.9.e45

135. Mo, D. *et al.* Low PBRM1 identifies tumor progression and poor prognosis in breast cancer. *Int. J. Clin. Exp. Pathol.* **8,** 9307–9313 (2015).

136. Kalluri, R. & Weinberg, R. A. The basics of epithelial-mesenchymal transition. *Journal of Clinical Investigation* (2009). doi:10.1172/JCI39104

137. Cohet, N. *et al.* SWI/SNF chromatin remodeling enzyme ATPases promote cell proliferation in normal mammary epithelial cells. *J. Cell. Physiol.* (2010). doi:10.1002/jcp.22072

138. Hall, H. G., Farson, D. A. & Bissell, M. J. Lumen formation by epithelial cell lines in response to collagen overlay: a morphogenetic model in culture. *Proc. Natl. Acad. Sci.* (1982). doi:10.1073/pnas.79.15.4672

139. Berglund, F. M. *et al.* Disruption of epithelial architecture caused by loss of PTEN or by oncogenic mutant p110α/PIK3CA but not by HER2 or mutant AKT1. *Oncogene* (2013). doi:10.1038/onc.2012.459

140. Ghaleb, A. M., McConnell, B. B., Kaestner, K. H. & Yang, V. W. Altered intestinal epithelial homeostasis in mice with intestine-specific deletion of the Krüppel-like factor 4 gene. *Dev. Biol.* (2011). doi:10.1016/j.ydbio.2010.11.001

141. Yu, T. *et al.* Krüppel-like factor 4 regulates intestinal epithelial cell morphology and polarity. *PLoS One* (2012). doi:10.1371/journal.pone.0032492

142. Tiwari, N. *et al.* Klf4 Is a Transcriptional Regulator of Genes Critical for EMT, Including Jnk1 (Mapk8). *PLoS One* (2013). doi:10.1371/journal.pone.0057329

143. Sizemore, G. M., Pitarresi, J. R., Balakrishnan, S. & Ostrowski, M. C. The ETS family of oncogenic transcription factors in solid tumours. *Nature Reviews Cancer* (2017). doi:10.1038/nrc.2017.20

144. Jiang, S., Zhang, E., Zhang, R. & Li, X. Altered activity patterns of transcription factors induced by endoplasmic reticulum stress. *BMC Biochem.* (2016). doi:10.1186/s12858-016-0060-2

145. Rössler, O. G. & Thiel, G. Specificity of Stress-Responsive Transcription Factors Nrf2, ATF4, and AP-1. *J. Cell. Biochem.* (2017). doi:10.1002/jcb.25619

146. Rawson, R. B. The site-2 protease. *Biochimica et Biophysica Acta - Biomembranes* (2013). doi:10.1016/j.bbamem.2013.03.031

147. Beagan, J. A. *et al.* YY1 and CTCF orchestrate a 3D chromatin looping switch during early neural lineage commitment. *Genome Res.* (2017). doi:10.1101/gr.215160.116

148. Chorley, B. N. *et al.* Identification of novel NRF2-regulated genes by ChiP-Seq: Influence on retinoid X receptor alpha. *Nucleic Acids Res.* (2012). doi:10.1093/nar/gks409

149. Girnius, N. & Davis, R. J. JNK Promotes Epithelial Cell Anoikis by Transcriptional and Post-translational Regulation of BH3-Only Proteins. *Cell Rep.* (2017). doi:10.1016/j.celrep.2017.10.067

150. Insua-rodríguez, J. *et al.* Stress signaling in breast cancer cells induces matrix components that promote chemoresistant metastasis. *EMBO Mol. Med.* (2018). doi:10.15252/emmm.201809003

151. Liou, G. Y. & Storz, P. Reactive oxygen species in cancer. *Free Radical Research* (2010). doi:10.3109/10715761003667554

152. Kim, J. Y. *et al.* Interleukin-33/ST2 axis promotes epithelial cell transformation and breast tumorigenesis via upregulation of COT activity. *Oncogene* (2015). doi:10.1038/onc.2014.418

153. Soule, H. D. *et al.* Isolation and Characterization of a Spontaneously Immortalized Human Breast Epithelial Cell Line, MCF-10. *Cancer Res.* (1990). doi:10.1158/0008-5472.can-11-3095

154. Dawson, P. J., Wolman, S. R., Tait, L., Heppner, G. H. & Miller, F. R. MCF10AT: a model for the evolution of cancer from proliferative breast disease. *Am. J. Pathol.* (1996). doi:10.1002/hbm.10091

155. Johnson, D. G. & Dent, S. Y. R. Chromatin: Receiver and quarterback for cellular signals. *Cell* (2013). doi:10.1016/j.cell.2013.01.017

156. Roupé, K. M. *et al.* Transcription factor binding site analysis identifies FOXO transcription factors as regulators of the cutaneous wound healing process. *PLoS One* (2014). doi:10.1371/journal.pone.0089274

157. Wang, Y., Zhou, Y. & Graves, D. T. FOXO transcription factors: Their clinical significance and regulation. *BioMed Research International* (2014). doi:10.1155/2014/925350

158. Schram, A. W. *et al.* A Dual Role for SAGA-Associated Factor 29 (SGF29) in ER Stress Survival by Coordination of Both Histone H3 Acetylation and Histone H3 Lysine-4 Trimethylation. *PLoS One* (2013). doi:10.1371/journal.pone.0070035

159. Johnsson, A. *et al.* HAT-HDAC interplay modulates global histone H3K14 acetylation in gene-coding regions during stress. *EMBO Rep.* (2009). doi:10.1038/embor.2009.127

160. Mahalingaiah, P. K. S. *et al.* Oxidative stress-induced epigenetic changes associated with malignant transformation of human kidney epithelial cells. *Oncotarget* (2016). doi:10.18632/oncotarget.12091

161. Mahalingaiah, P. K. S., Ponnusamy, L. & Singh, K. P. Chronic oxidative stress leads to malignant transformation along with acquisition of stem cell characteristics, and epithelial to mesenchymal transition in human renal epithelial cells. *J. Cell. Physiol.* (2015). doi:10.1002/jcp.24922

162. Suter, M. A. *et al.* A maternal high-fat diet modulates fetal SIRT1 histone and protein deacetylase activity in nonhuman primates. *FASEB J.* (2012). doi:10.1096/fj.12-212878

163. Dicks, N., Gutierrez, K., Michalak, M., Bordignon, V. & Agellon, L. B. Endoplasmic Reticulum Stress, Genome Damage, and Cancer. *Front. Oncol.* (2015). doi:10.3389/fonc.2015.00011

164. Chiu, L. Y., Gong, F. & Miller, K. M. Bromodomain proteins: Repairing DNA damage within chromatin. *Philosophical Transactions of the Royal Society B: Biological Sciences* (2017). doi:10.1098/rstb.2016.0286

165. Kim, J. W., Tchernyshyov, I., Semenza, G. L. & Dang, C. V. HIF-1-mediated expression of pyruvate dehydrogenase kinase: A metabolic switch required for cellular adaptation to hypoxia. *Cell Metab.* (2006). doi:10.1016/j.cmet.2006.02.002

166. Piva, F. *et al.* BAP1, PBRM1 and SETD2 in clear-cell renal cell carcinoma: Molecular diagnostics and possible targets for personalized therapies. *Expert Review of Molecular Diagnostics* (2015). doi:10.1586/14737159.2015.1068122

167. Beuselinck, B. *et al.* Pro-angiogenic gene expression is associated with better outcome on sunitinib in metastatic clear-cell renal cell carcinoma. *Acta Oncol. (Madr).* (2018). doi:10.1080/0284186X.2017.1388927

168. He, X. *et al.* Bap180/Baf180 is required to maintain homeostasis of intestinal innate immune response in Drosophila and mice. *Nat. Microbiol.* (2017). doi:10.1038/nmicrobiol.2017.56

169. Shu, X. *et al.* PBRM1 restricts the basal activity of innate immune system through repressing RIG-I-like receptor signaling and is a potential prognostic biomarker for colon cancer. *J. Pathol.* (2017). doi:10.1002/path.4986

170. Chovatiya, R. & Medzhitov, R. Stress, inflammation, and defense of homeostasis. *Molecular Cell* (2014). doi:10.1016/j.molcel.2014.03.030

171. Porter, E. G. *et al.* PBRM1 regulates stress response in epithelial cells. *bioRxiv* (2018).

172. Shaulian, E. & Karin, M. AP-1 as a regulator of cell life and death. *Nature Cell Biology* (2002). doi:10.1038/ncb0502-e131

173. Calnan, D. R. & Brunet, A. The FoxO code. *Oncogene* (2008). doi:10.1038/onc.2008.21

174. Zhang, X., Tang, N., Hadden, T. J. & Rishi, A. K. Akt, FoxO and regulation of apoptosis. *Biochimica et Biophysica Acta - Molecular Cell Research* (2011). doi:10.1016/j.bbamcr.2011.03.010

175. Daitoku, H., Sakamaki, J. ichi & Fukamizu, A. Regulation of FoxO transcription factors by acetylation and protein-protein interactions. *Biochimica et Biophysica Acta - Molecular Cell Research* (2011). doi:10.1016/j.bbamcr.2011.03.001

176. van der HEIDE, L. P., HOEKMAN, M. F. M. & SMIDT, M. P. The ins and outs of FoxO shuttling: mechanisms of FoxO translocation and transcriptional regulation. *Biochem. J.* (2004). doi:10.1042/bj20040167

177. Kasprzak, A., Kwasniewski, W., Adamek, A. & Gozdzicka-Jozefiak, A. Insulin-like growth factor (IGF) axis in cancerogenesis. *Mutation Research - Reviews in Mutation Research* (2017). doi:10.1016/j.mrrev.2016.08.007

178. Hai, T., Wolford, C. C. & Chang, Y. S. ATF3, a hub of the cellular adaptive-response network, in the pathogenesis of diseases: Is modulation of inflammation a unifying component? *Gene Expression* (2010). doi:10.3727/105221610X12819686555015

179. Brigelius-Flohé, R. & Kipp, A. Glutathione peroxidases in different stages of carcinogenesis. *Biochimica et Biophysica Acta - General Subjects* (2009). doi:10.1016/j.bbagen.2009.03.006

180. Guertin, M. J. & Lis, J. T. Chromatin landscape dictates HSF binding to target DNA elements. *PLoS Genet.* (2010). doi:10.1371/journal.pgen.1001114

181. Weiner, A. *et al.* High-resolution chromatin dynamics during a yeast stress response. *Mol. Cell* (2015). doi:10.1016/j.molcel.2015.02.002

182. Pluquet, O., Pourtier, A. & Abbadie, C. The unfolded protein response and cellular senescence. A Review in the Theme: Cellular Mechanisms of Endoplasmic Reticulum Stress Signaling in Health and Disease. *Am. J. Physiol. - Cell Physiol.* (2015). doi:10.1152/ajpcell.00334.2014

PUBLICATIONS

Porter EG*, Dhiman A*, Chowhurdy B, Carter BC, Lin H, Stewart JC, Kazemian M, Wendt MK, Dykhuizen EC, PBRM1 Regulates Stress Response in Epithelial Cells. bioRxiv 408575; doi: https://doi.org/10.1101/408575 (Submitted iSceince September 2018.)

Porter EG, Connelly KE, Dykhuizen EC. Sequential Salt Extractions for the Analysis of Bulk Chromatin Binding Properties of Chromatin Modifying Complexes. *J. Vis Exp. (128),* e55369, doi:10.3791/55369 (2017).

Porter EG, Dykhuizen EC Individual Bromodomains of Polybromo-1 Contribute to Chromatin Association and Tumor Suppression in Clear Cell Renal Carcinoma. *Journal of Biological Chemistry.* 292:2601–2610.

Chowdhury B, **Porter EG**, Stewart JC, Ferreira CR, Schipma MIJ, Dykhuizen EC. PBRM1 Regulates the Expression of Genes Involved in Metabolism and Cell Adhesion in ccRCC. PLOS ONE. 11, e0153718